Zwitterionic Poly(carboxybetaine) Materials for Blood-Contacting Medical Devices and Nanoparticles

Wei Yang

A dissertation

Submitted in partial fulfillment of the

Requirements for the degree of

Doctor of Philosophy

University of Washington

2014

Reading Committee:

Shaoyi Jiang, Chair

Daniel M. Ratner

Cole A. DeForest

Program Authorized to Offer Degree:

Chemical Engineering

University of Washington

Abstract

Zwitterionic Poly(carboxybetaine) Materials for Blood-Contacting Medical Devices and Nanoparticles

Wei Yang
Chair of the Supervisory Committee:
Professor Shaoyi Jiang
Department of Chemical Engineering

Nonspecific protein adsorption in complex media is a crucial issue for biological applications. It degrades the performance of surface-based implanted devices and causes nanoparticles to be recognized by the immune system and rapidly eliminated from systemic circulation. The presented work is a compilation of efforts aimed at developing surface coating based on PCB materials for blood-contacting medical devices and nanoparticles. Surfaces with different packing densities were applied for various purposes.

An amperometric enzyme glucose sensor based on glucose oxidase, was used to demonstrate the extraordinary performance of a lightly crosslinked PCB hydrogel in whole blood. This hydrogel presents an ultra-low fouling background to maintain a stable long-term response, even in whole blood. In addition, gold nanoparticles were used as a model system to demonstrate that NPs protected by PCB materials with a high packing density elicit an extremely low immune response after repeated injections, along with having prolonged circulation time and low accumulation in organs *in vivo*. Finally,

ligands with only one CB group were developed to prepare thin surface coatings via self-assembled monolayers. The functional ligands are highly resistant to pH changes, as well as nonspecific protein adsorption.

Table of Contents

Table of Schemes

Table of Tables

Table of Figures

Acknowledgements

The author would like to acknowledge the Office of Naval Research (N000140910137), Defense Advanced Research Projects Agency (DARPA N66001-12-1-4263), Defense Threat Reduction Agency (HDTRA-1-13-1-0044), and National Science Foundation (CERT 1264470 and DMR 1307375) for financial support. The author would like to thank the members of the Jiang research group, especially Dr. Jean-Rene Ella-Menye, Dr. Hong Xue, Dr.Yuting Li, Dr. Norman D. Brault, and Dr. Qing Shao for their assistance with chemical synthesis and helpful discussions. For all the work presented here, the author thanks Professor Shaoyi Jiang for his discussion, advisement, and funding support. Finally, the author would like to express her special appreciation to her family for all of the support they provided.

Chapter 1 Introduction

Nonspecific protein adsorption is a crucial issue for many biomedical applications, such as medical implants, drug delivery vehicles, and biosensors[1-3]. At present, there is a very limited number of effective nonfouling biomaterials available to meet the challenges of practical applications[4]. One of the most widely studied nonfouling materials is poly(ethylene glycol) (PEG) or oligo(ethylene glycol) (OEG)[3]. However, there are several potentially unfavorable effects that might be caused by PEG[5]. For example, unexpected changes in the pharmacokinetic behavior can occur with PEG-based carriers. Also, PEG can decompose in the presence of oxygen and transitionmetal ions[6]. Recently, in our group, we have demonstrated that zwitterionic materials such as sulfobetaine methacrylate (SBMA)[7], carboxybetaine methacrylate (CBMA)[8], and mixed charge materials[9] are highly resistant to nonspecific protein adsorption. These zwitterionic materials bind water more strongly via electrostatically induced hydration than neutral and hydrophilic PEG does via hydrogen-binding hydration[10]. It has been shown that superhydrophilic poly(carboxybetaine) (PCB) is superior to PEG to maintain protein stability and bioactivity[11].

For medical implants and *in vivo* sensors, surface resistance to protein adsorption and cell adhesion from complex media are needed to prevent undesirable responses of the living system to a device or implant[12-14]. This creates the need for surface modifications that have low reactivity with bloodborne proteins, otherwise scar tissue formation accompanied by adhesion of bacteria and macrophage, physiological condition changes,

and sensitivity isolation resulting from fibrous capsules will occur[15, 16]. Hydrogels, considered to be low fouling, have been widely used for surface coatings for implantable sensors[17]. However, due to their low density, their use in whole blood is still questionable. The 10% serum concentration commonly used to test the performance of medical devices is not sufficient, and thus whole blood is used in this work to evaluate the long-term stability of implantable sensors.

Nanoparticle-based biotechnology is quickly heading to the forefront of drug delivery, diagnostics, and many other areas. Various strategies have been studied for immunosuppression, including manipulating nanoparticle physical properties or surface chemistry (e.g., PEGylation)[18, 19]. Although modification with PEG can reduce nonspecific protein adsorption which prevents flocculation, opsonization, and subsequent complement activation[20], the recent discovery of a PEG-specific immune response has triggered further investigation[5, 21, 22]. Another problem faced by nanoparticles (NPs) is their relatively short retention in circulation[23]. Longer circulating NPs are more likely to reach their target, allowing high therapeutic efficacy and/or imaging sensitivity, as well as reduced accumulation in normal tissues and avoidance of side effects[24-26]. Although numerous strategies involving PEG coatings have been applied to improve the circulation time of NPs, success has been limited to circulation times of 8 to 10 hours[27]. Materials that provide extended systemic circulation and are invisible to immune system are highly desired.

The "graft-from" method via atom transfer radical polymerization (ATRP) has been applied to prepare surfaces to resist nonspecific protein adsorption[28]. However, ATRP reactions require surface-grafted initiators, catalysts, and oxygen-free conditions which

limit its practical application[28]. To address this problem, an alternative strategy, the "graft-to" method is often employed to prepare thin coating, which is desirable for such applications as quantum dots. However, it is still very challenging to create thin coatings, for example with only one CB group, that are stable in complex media.

In this work, we demonstrate how to eliminate nonspecific protein adsorption by using ultra-low fouling zwitterionic PCB for blood-contacting devices and NPs. Surfaces with different packing densities was applied for various purposes. In Chapters 2 and 3, glucose biosensors will be used as a model system to show the effect of a lightly crosslinked PCB hydrogel coating on the performance of sensors in whole blood and in Chapters 4 and 5, GNPs will be used to demonstrate a platform with high packing density that minimizes the immunogenicity of NPs while maintaining long circulation and low accumulation in undesired organs, even after repeated injections. In Chapters 6 and 7, a new surface chemistry will be introduced to modify GNPs via self-assembled monolayers (SAMs). GNPs and quantum dots (QDs) will be used as examples to demonstrate the thin coating containing only one CB group.

Chapter 2 Zwitterionic Poly(carboxybetaine) Hydrogels for Glucose Biosensors in Complex Media

Zwitterionic hydrogels based on poly(carboxybetaine) methacrylate (polyCBMA) were developed to protect implantable electrochemical glucose biosensors from biofouling in complex media. To enhance the linearity and sensitivity of the sensing profile, both physical and chemical adsorption methods were developed. Results show that glucose sensors coated with polyCBMA hydrogels via the chemical method achieve very high sensitivity and good linearity in response to glucose in PBS, 10%, 50%, and 100% human blood serum. Essentially identical glucose signals were observed even after prolonged exposure to blood samples for over 12 days. The excellent performance of polyCBMA hydrogel coating offers great promise for designing biocompatible implantable glucose biosensorsin biological medium.

2.1 Introduction

Nonspecific protein adsorption is a crucial issue for many biomedical applications, such as medical implants[1], drug delivery vehicles[4], and biosensors[3]. At present, there are few effective nonfouling biomaterials available to meet the challenges of practical applications[3, 4, 29]. PEG and OEG have been widely used to resist nonspecific protein adsorption[30-32]. However, PEG and OEG are subject to oxidation in the presence of oxygen and transition metal ions[32-34]. Zwitterionic phosphorylcholine (PC)-based materials are another class of nonfouling materials, but their monomers are generally difficult to synthesize[35, 36]. Recently, other zwitterionic materials such as sulfobetaine

methacrylate (SBMA)[7], carboxybetaine methacrylate (CBMA)[37, 38] or mixed charge materials[9, 39] have been shown to exhibit ultra-low protein adsorption, which is defined as fibrinogen adsorption <5 ng/cm^2 [40]). Results demonstrated that zwitterionic-based materials are suitable for applications in complex blood media due to their highly effective nonfouling properties and efficient functional abilities. In the following sections we will demonstrate the ability of such antifouling zwitterionic materials to enhance the performance of electrochemical biosensors for blood glucose monitoring.

Amperometric enzyme glucose sensors, based on glucose oxidase (GOx), have played a leading role in the move towards continuous monitoring of blood glucose towards a tight glycemic control[16, 41]. Numerous efforts have been devoted towards the development of glucose sensing devices[42-47]. Such implantable devices should provide reliable real-time continuous monitoring of sharp fluctuations in blood glucose levels, with high selectivity, specificity and speed over extended periods (days to weeks) under harsh conditions[16]. However, undesirable interactions between the surface of the implanted probe and the biological medium have been proved to be the major barrier to the development of reliable *in vivo* glucose sensors[16]. In blood, these interactions strongly affect the short-term and long-term thrombotic response induced by the sensor materials[48], which will suppresses the glucose response. As a result, most glucose biosensors lack the biocompatibility needed for reliable prolonged operation in whole blood. Alternative sensing sites, particularly the subcutaneous tissue, have thus received growing attention. However, such subcutaneous implantation generates a wound site that experiences an intense local inflammatory reaction[16]. Recent approaches for designing more biocompatible *in vivo* glucose sensors focus on preparing interfaces that resist biofouling

in complex media such as heparin[49], copolymers containing phosphorylcholine[50, 51], lipid film[52], Nafion coating[53], hydrotalcites[54], and poly(1,2-phenylenediamine)[55, 56].

Hydrogels derived from both synthetic polymers and natural polymers have been widely used in medical devices, tissue engineering and drug delivery[57-59]. They can be designed and prepared to be biodegradable, stimuli-sensitive, and functionalizable[60-62]. In general, hydrogels are thought to be biocompatible due to their tissue-like mechanical properties, freedom from toxic leachables, hydrophilicity, and high water content[63]. Previous studies have shown that hydrogel coatings based on PEG[64, 65], polyaniline[66], palladium hexacyanoferrate[67], polyacrylamide[68, 69], or poly(2-hydroxyethyl methacrylate) (polyHEMA)[43, 70, 71] was applied to minimize non-specific protein adsorption. These materials, however, dramatically decrease the electrochemical signal of the sensor. Zwitterionic hydrogels promote healing and integration comparable to polyHEMA hydrogels, but with only 10% cell adhesion, as demonstrated by an *in vivo* implantation study based on polyCBMA zwitterionic hydrogels[72]. This new surface platform offers considerable promise as glucose sensor coatings.

Previously, we have shown zwitterionic materials and coatings for flat surfaces and nanoparticles are ultra-low fouling[38, 73]. Herein, we demonstrate that polyCBMA hydrogels on glucose sensor surfaces present an ultra-low fouling background to maintain a highly stable response even in a complex medium such as human blood serum. Furthermore, the polyCBMA hydrogel coating preserves excellent linearity and stability of the glucose sensors and retains very high sensitivity.

2.2 Materials and Methods

2.2.1 Chemicals

Pooled human blood serum was purchased from BioChemed Services (Winchester, VA). Teflon sheeting was purchased from McMaster-Carr (Cleveland, OH). Dulbecco's Modified Eagle Medium (DMEM), fetal bovine serum, nonessential amino acids, and penicillin-streptomycin were purchased from Invitrogen Corp (Carlsbad, CA). COS-7 cells (African Green Monkey fibroblast cells) were purchased from the American Tissue Culture Collection (Manassas, VA). CBMA monomer was synthesized as described previously [37, 48]. Glutaraldehyde (50%) was purchased from TED PELLA, Inc. (Pedding, CA). 2-hydroxyethyl methacrylate (HEMA) was purchased from Polysciences (Warrington, PA). Dextrose (D-glucose, 99.5%), (N,N'-dimethylamino)ethyl methacrylate (98%), β-propiolactone (95%), ethyleneglycol dimethacrylate (EGDMA), 2-hydroxy-2-methylpropiophenone (Benacure 1173), GOx (EC 1.1.3.4, type X-S, Aspergillus niger, 5,000 U/g), and bovine serum albumin (BSA) were purchased from Sigma-Aldrich (Milwaukee, WI). Phosphate buffer saline (PBS, 0.01 M phosphate, 0.138 M sodium chloride, 0.0027 M potassium chloride, pH 7.4) was purchased from Sigma Chemical Co (St. Louis, MO). Water used in experiments was purified using a Millipore water purification system with a minimum resistivity of 18.0 MΩ· cm.

Teflon-covered platinum-iridium wire (9:1 in weight) with diameter 0.125 mm was obtained from World Precision Instruments, Inc. (Sarasota, FL). Platinum wire counter electrodes and Ag/AgCl reference electrodes were purchased from CH Instruments, Inc. (Austin, TX).

2.2.2. Sensors preparation and GOx solution immobilization

Glucose sensors used for this study were based on the coil-type implantable sensor previously described[17, 43]. Briefly, the coil-type glucose biosensors were prepared by

winding the top 10 mm of a 40-50 mm long platinum wire along a cotton-coated 25-gauge needle to form a coil-like cylinder which was filled with cotton after removal from the needle. The enzyme layer over the cylinder was formed by coating it with 3 μL aqueous solution of 10 mg/mL GOx, 30-40 mg/mL BSA and 0.6% (v/v) glutaraldehyde. The sensors (referred to as Pt/GOx) were allowed to dry at 4 ℃ for 1 h.

2.2.3. Preparation of polyCBMA and polyHEMA hydrogels for characterization

0.5 mole of CBMA monomer was first mixed with water and the solution was sonicated for 1 minute to dissolve the monomer. EGDMA was added to the above solution and the mixture was sonicated for an additional minute to complete dissolution. The molar ratio of CBMA and EGDMA was 1000:1 and the final concentration of CBMA was 10 M. 1% (w/w) photoinitiator (Benacure 1173) was added and the solutions mixed at room temperature. The solutions were transferred into a cast composed of a pair of glass plates separated with a 0.4 mm teflon spacer. The photo-polymerization reaction was carried out at 25 ℃ for 30 minutes under 254 nm UV light to polymerize the hydrogels. Then, the hydrogels were removed from the plates and immersed in PBS. The PBS was changed daily for 5 days to remove residual chemicals before further use. The polyHEMA hydrogels were prepared by adding 8 M HEMA, 0.008 M EGDMA, and 1% (w/w) photoinitiator in a mixed solvent comprised of 1 part ethanol, 1.5 parts ethylene glycol, and 1.5 parts water. This hydrogel was also formed as above.

2.2.4. Analysis of mechanical and cell adhesion properties of hydrogels

Hydrogels were allowed to swell to equilibrium in PBS buffer for five days. The equilibrated hydrogels were then punched into disks with a diameter of 5 mm. The disks were weighed and then dehydrated under vacuum at 50 ℃ and 30 in. Hg vacuum for 3

days. Dried hydrogel disks were weighed and their diameter was measured with a caliper. The volume fraction (Φ) of polymer within a swollen hydrogel is given by:

$$\Phi = \left[\frac{D_0}{D}\right]^3 \quad (2\text{-}1)$$

where D_o and D are the diameters of dried and swollen disks, respectively. The volume fraction of polymer in the relaxed (unswollen) hydrogel, φ_o, was determined from the monomer/crosslinker solutions: The volume of the solution was compared to the volume of water added. The difference in volume was taken as the volume of monomer, which corresponds to the volume of polymer after polymerization[74].

The swelling ratios were determined by the ratio of the swollen hydrogels weight to the dry hydrogels weight and the equilibrium water content values were determined as:

$$EWC = 100(\%) * \frac{m_w - m_d}{m_w} \quad (2\text{-}2)$$

where m_w is the mass of the wet hydrogel and m_d is the mass of the dry hydrogels. All samples were measured in triplicate.

Three hydrogel disks of 5 mm diameter (0.5 mm thickness when cast) were placed individually in the wells of a 48-well plate with 500 µL PBS solution. To sterilize the hydrogels, they were refrigerated overnight in 1x Penicillin-streptomycin in PBS. COS-7 cells (p=7) were seeded onto the hydrogels at a concentration of 1x 10^4 cells/mL in supplemented DMEM. Cells were allowed to grow for 72 hours at 37 ℃, 5% CO_2, and 100% humidity, after which time the hydrogels were photographed at 10x magnification with a Nikon Eclipse TE2000-U microscope. Photographs were taken at five predetermined areas on the surface of the hydrogels, for a total of fifteen images per hydrogel formulation, and the number of adherent cells from each image was totaled and normalized to the number of cells adhered to polyHEMA gels.

2.2.5. PolyCBMA and polyHEMA hydrogels formation on the sensor surface via physical adsorption[43]

A hydrogel coating on the glucose sensor tip was formed by pipetting 1.2 μL of the mixed solution (HEMA or CBMA, EGDMA, and photoinitiator along with water) onto the sensor tip (**Scheme 2.1a**). The solution was allowed to spread evenly over the surface of the tip. After exposing the tip to 254 nm UV light for 30 min, the sensors (referred to as Pt/GOx/HEMA or Pt/GOx/CBMA) were stored in PBS until further use.

2.2.6. PolyCBMA hydrogels formation via chemical adsorption

To improve the adhesion of the polyCBMA hydrogels to the platinum coil, after the GOx immobilization, the surface of the coils was functionalized using a solution of 10% (trimethoxysilyl)propyl methacrylate and 0.5% water in toluene at 80 ℃[75], as indicated in Scheme 2.1b. Then, the outermost hydrogel coating was formed by applying 1.2 μL CBMA hydrogel solution to the sensors as described above.

2.2.7. Sensor evaluation *in vitro*

The *in vitro* performance of the sensors was examined in a glucose/PBS solution to determine their sensitivity and linear range. The sensitivity of the Pt/GOx/hydrogel sensors was first measured using 4 and 20 mM glucose/PBS solutions. The difference between the base current of PBS and the steady state current of glucose in the sample was used to obtain the calibration curve. Then, the sensors were tested with glucose solution dispersed in 10%, 50% (diluted with PBS), and 100% human blood serum. For the long-term sensor evaluation, the sensors were dipped into 100% human blood serum at 4 ℃ before the next test at different incubating days. When determining glucose concentration in a serum sample, the base current was taken in glucose-free serum and then the sensor

was transferred to the glucose-containing 100% serum sample to obtain a steady state current. All experiments were carried out at room temperature and all solutions were stirred continuously during the measurement. Amperometric measurements were performed at room temperature at +0.75 V vs. Ag/AgCl along with a platinum wire counter electrode and Princeton Applied Research Model PG580 electrochemical analyzer.

2.3 Results and Discussion

2.3.1. Analysis of mechanical and cell adhesion properties of hydrogels

After polymerization, all hydrogels were transparent and colorless in appearance and had a uniform and smooth surface. When in equilibrium with PBS buffer, the equilibrium water content of polyCBMA and polyHEMA (w/w) was measured to be 91.0 ± 0.4% and 40 ± 0.2%, respectively. The volume fraction was 0.019 ± 0.010 and 0.5 ± 0.02, respectively. Previous studies have indicated that the zwitterionic carboxybetaine groups are much more hydrophilic than the hydroxyethyl groups. As a consequence, the zwitterionic hydrogels can hold more water than polyHEMA hydrogels[62].

Cellular interactions with synthetic surfaces are directed by proteins adsorbed from the cell-culture medium. On materials that absorb cell adhesive proteins, cell attachment and growth is promoted. Surfaces with very low total protein adsorption usually exhibit less cell adhesion[76, 77]. The difference in cell binding on the surface of polyHEMA and polyCBMA hydrogels is shown quantitatively in **Figure 2.1**. After contacting COS-7 cells for 72 hours, a relatively large number of cells adhered to the surface of the polyHEMA hydrogels (**Figure 2.1a**). By contrast, polyCBMA hydrogels are highly resistant to cell attachment: there was an extremely low amount of cell adhesion to the

surface (**Figure 2.1b**). In fact, polyCBMA hydrogels reduced cell adhesion by 90% relative to polyHEMA hydrogels. This indicates the polyCBMA hydrogels experience lower nonspecific protein adsorption than do polyHEMA hydrogels. Thus, we expect that the polyCBMA will have better performance in complex media than polyHEMA hydrogels. These results, in conjunction with previous work[78, 79], suggest that the polyCBMA hydrogels exhibited a high degree of compatibility to blood samples.

2.3.2 Bare sensors without hydrogel coating

Bare sensors without any hydrogel coating were first tested with a glucose solution in PBS and in 10% blood serum solutions. **Figure 2.2a** compares the amperometric response of the Pt/GOx sensors to successive 4 mM incremental increases in the glucose concentration, in the presence and absence of 10% blood serum (diluted with PBS solution). The Pt/GOx sensors display very high sensitivity to glucose in PBS, consistent with previous results[43]. The narrower linearity of the bare sensor in PBS was observed, which is likely be due to the loss of immobilized enzymes. Furthermore, when the bare sensor is exposed to 10% blood serum, the amperometric response decreases dramatically, as expected from the previous studies[43, 49].

2.3.3 *In vitro* performance of Pt/GOx/hydrogel sensors via physical adsorption

1.2 μL of hydrogel solution was then physically adsorbed to the enzyme layer of Pt/GOx sensors via physical adsorption. In this case, the hydrogel layer served as the diffusion-limiting membrane as well as a biocompatible outermost coating. The response current of glucose sensors coated with polyHEMA hydrogel is shown in **Figure 2.2b**. The polyHEMA hydrogel-coated sensors displayed a fast response before exposure to 10% blood serum. However, compared to the Pt/GOx sensors, the hydrogel layer was

deleterious to the sensor linearity. Additionally, the sensitivity was significantly reduced relative to the response for the same concentration of glucose in PBS. Moreover, the exposure to the 10% blood serum resulted in a substantial (> 50%) suppression of the response of the Pt/GOx/HEMA sensor. This result was obtained following the procedure described before[43]. In that work, in addition to multi-component polyHEMA, a diffusion-limiting membrane such as epoxy-polyurethane was added to improve the linearity of measurements.

In contrast, as shown in **Figure 2.2c**, the polyCBMA hydrogel layer actually improved the sensor response linearity and did not significantly reduce sensitivity relative to the same concentration of glucose in PBS. Furthermore, only a negligible change of the response is observed at the polyCBMA hydrogel surface in the presence and absence of 10% blood serum. However, despite the excellent linearity and high sensitivity in the complex media, polyCBMA hydrogel-coated sensors failed when exposed to 50% human blood serum. The amperometric response did not change upon increasing the glucose concentration to 4 mM. Moreover, as compared with polyHEMA used in previous studies[43], the single-component polyCBMA hydrogel coating has excellent linearity without an epoxy-polyurethane membrane.

2.3.4 *In vitro* performance of Pt/GOx/CBMA sensors via chemical attachment

Although Pt/GOx/CBMA sensors prepared via physical adsorption exhibited significantly increased sensitivity compared to the published data[43], they still have insufficient accuracy and precision required for *in vivo* measurements due to the poor sensitivity when exposed to 50% blood serum. A few reports have sought to improve measurement reliability by adding an additional diffusion-limiting membrane such as low

permeability epoxy-polyurethane between the hydrogel layer and the enzyme layer membrane[16, 43]. In our experiments, (trimethoxysilyl)propyl methacrylate was used to modify the Pt surface via methoxysilyl group to improve the adhesion of the hydrogels. The response current from glucose sensors chemically coated with polyCBMA hydrogel is shown in **Figure 2.3**. Previous studies[43] with a polyHEMA coating showed that the sensor response was dramatically delayed for thicker coating. For these polyCBMA hydrogel-coated sensors, their response did not delay with excellent linearity over the 4-20 mM range. Compared to the Pt/GOx/CBMA physically coated sensors, the chemically coated sensors retained excellent linearity and high sensitivity in 10%, 50%, and even 100% human blood serum.

2.3.5 Long-term stability of Pt/GOx/CBMA chemically coated sensors

To examine the long-term stability of Pt/GOx/CBMA sensors in complex media, chemically coated sensor were placed in small tubes containing 0.5 mL 100% blood serum. The greatly enhanced biocompatibility imparted onto the polyCBMA hydrogel-coated surface was assessed by monitoring changes in the amperometric response following exposure to blood samples on consecutive days. As shown in **Figure 2.4**, the sensors did not show a decline in either sensitivity or linearity after exposure to blood samples over 12 days. However, after the sensors had been immersed in 100% blood serum for 21 days, a large decrease in sensor response was observed. There are such possibilities of the loss of the immobilized GOx on the sensors and/or the non-specific adsorption from the blood serum. The coatings exhibit a long-term stability, sensitivity, and linearity, and do not peel off from the electrode surface over the time the sensors were stored. After 30 days in 100% blood serum, all the sensors still displayed a response

to glucose in 100% blood serum, albeit with decreased sensitivity. In addition, it was found that hydrogels remained firmly attached to the sensor surfaces for over 30 days. This suggests that the addition of the chemically-attached polyCBMA hydrogel coating apparently improves the long-term performance of the implanted glucose sensors. For these reasons, it is most likely that the decrease in sensitivity and linearity is due to loss of the immobilized GOx. Furthermore, the hydrogel coating might enrich oxygen for an improved enzymatic reaction cycle due to its high water content.

2.4 Conclusions

In this work, glucose sensor coating based on zwitterionic poly(carboxybetaine) hydrogels is demonstrated to effectively minimize blood-materials interactions and related adverse effects for long-term applications in complex biological media such as undiluted blood serum. Pt/GOx electrochemical biosensors chemically coated with polyCBMA hydrogels possess very high sensitivity and good linearity to glucose for over 12 days in PBS, 10%, 50%, and 100% blood serum. With a single polyCBMA hydrogels coating, which could serve as both diffusion-limiting layer and biocompatible outermost coatings, significant improvements of the *in vivo* performance of implanted glucose sensors are anticipated.

2.5 Chapter Figures

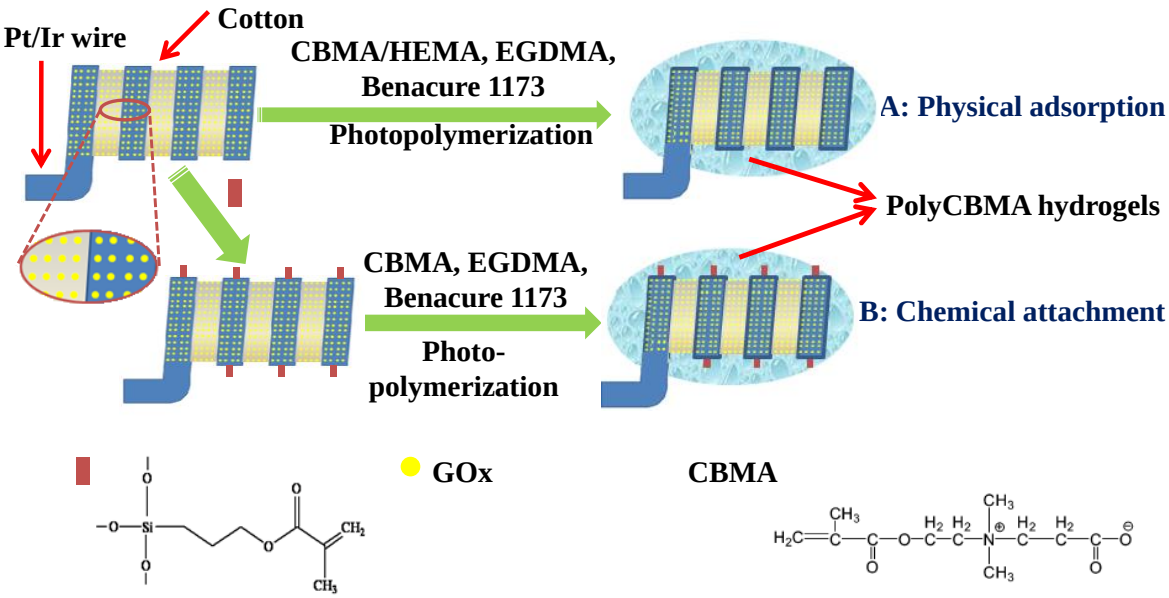

Scheme 2.1 Scheme of hydrogel-coated glucose sensors coated via physical adsorption (a) and chemical attachment (b).

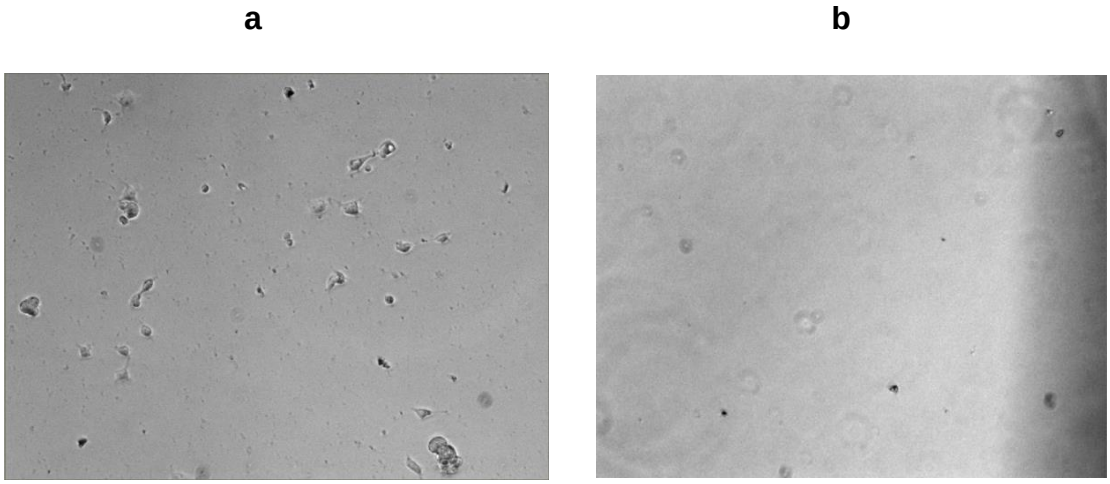

Figure 2.1 COS-7 cells on hydrogels, polyHEMA (a) and polyCBMA hydrogels (b) after a 3-day culture.

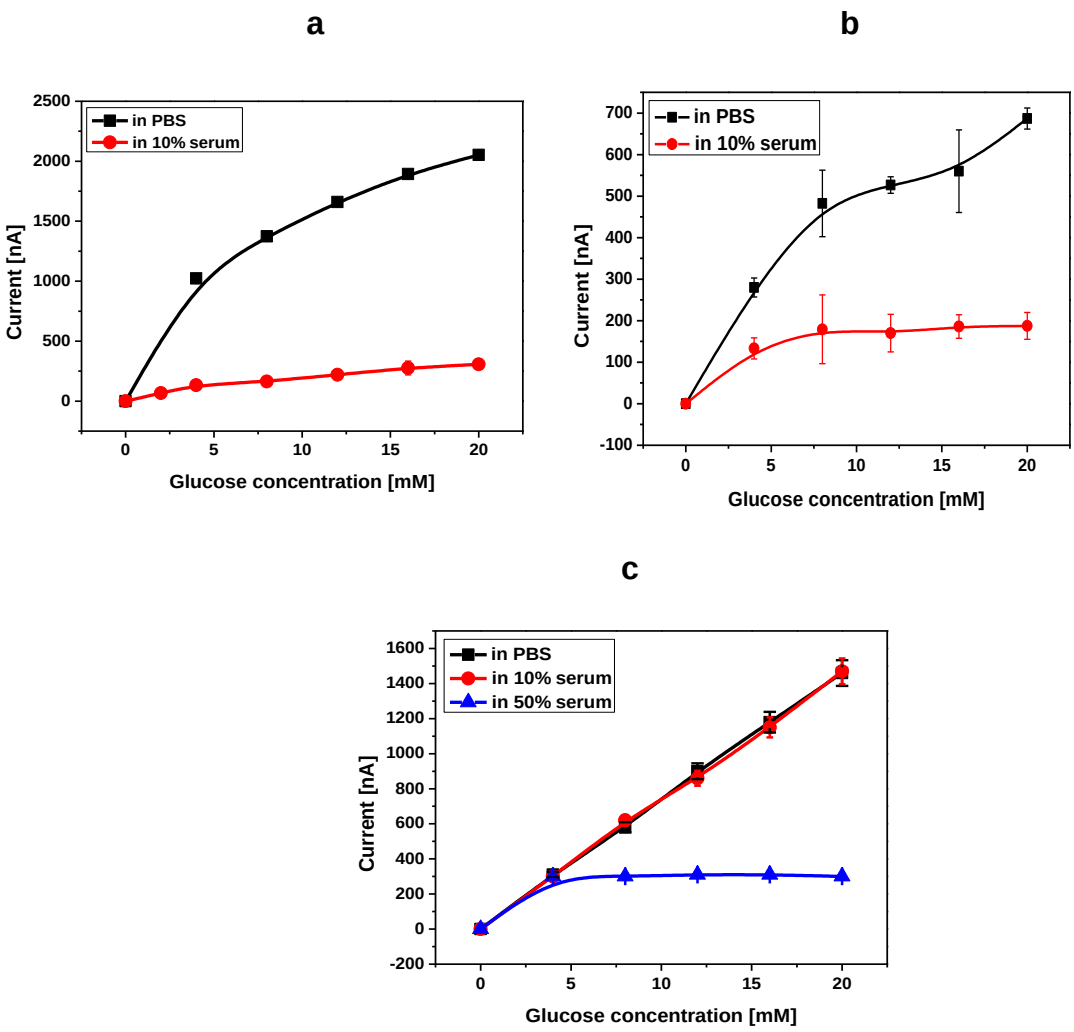

Figure 2.2. Current response of glucose sensors as a function of glucose concentration in different media: Pt/GOx without hydrogel coatings in PBS and 10% blood serum (a), Pt/GOx/HEMA in PBS and 10% blood serum (b), and Pt/GOx/CBMA in PBS, 10% and 50% blood serum (c). Operating potential: +0.75 V vs. Ag/AgCl reference electrode.

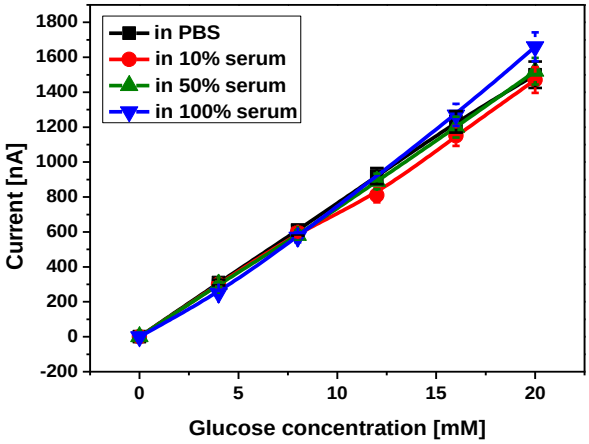

Figure 2.3 Current response of glucose sensors chemically coated with polyCBMA hydrogels as a function of glucose concentration in PBS, 10%, 50%, and 100% blood serum. Operating potential: +0.75V vs. Ag/AgCl reference electrode.

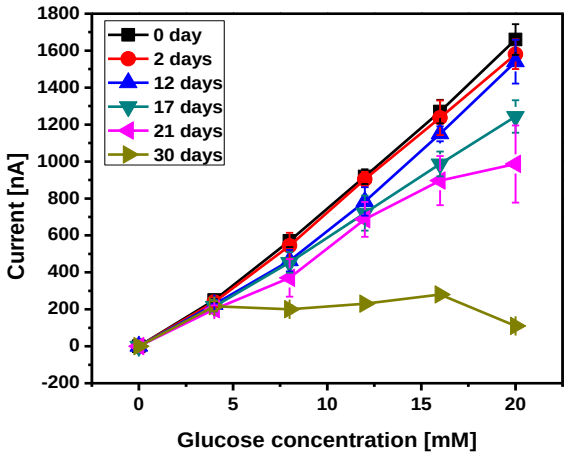

Figure 2.4 Current response of glucose sensors chemically coated with polyCBMA hydrogels incubated in 100% blood serum at 0, 2, 12, 17, 21, and 30 days as a function of glucose concentration. Experiments were conducted in 100% blood serum. Operating potential: +0.75V vs. Ag/AgCl reference electrode.

Chapter 3 The Effect of Lightly Crosslinked Poly(carboxybetaine) Hydrogel Coating on the Performance of Sensors in Whole Blood

Surface coatings of high packing densities have been routinely used to prevent nonspecific biomolecular and microorganism attachment. Hydrogels are another class of low fouling materials used to create three-dimensional matrixes for the free diffusion of analytes or drugs and the high-loading of bio-recognition elements. However, biomolecules are subject to diffusion into hydrogel matrixes, making them questionable for use in whole blood. Here, we demonstrate the feasibility of a lightly crosslinked poly(carboxybetaine) hydrogel in whole blood, as opposite to the conventional wisdom of high-packing density in surface coatings. Proteins are able to diffuse in and out of the matrix freely without being altered from their native conformations. In order to demonstrate its long-term performance in whole blood with high sensitivity, this hydrogel was coated onto a glucose sensor. This work paves a new way for the development of surface coatings and sensors to achieve long-term stability and high performance in whole blood.

3.1 Introduction

To date, numerous materials and coatings such as poly(ethylene glycol) (PEG)[6, 80], phosphorylcholine polymer[81, 82], poly(sulfobetaine methacrylate)[8], and polyCBMA[37], have been developed to reduce biofouling for surface-based diagnostic devices. In order to achieve low fouling in complex medium, high packing density surface coatings are regarded as a prerequisite. Hydrogels derived from both synthetic and natural polymers

have been widely used as medical device coatings, tissue scaffolds and drug delivery carriers, through which analytes or drugs of interest need to diffuse or within which bio-recognition elements of interest need to be immobilized. Among these materials, polyHEMA[83] hydrogels have been widely used for applications such as contact lenses, artificial cornea, drug delivery vehicles, and surface coatings for glucose sensors[17] since they are considered to low fouling. However, due to their low-density nature, conventional hydrogels (**Figure 3.1a**) are unable to achieve required high-packing densities as surface coatings (**Figure 3.1b**) in order to effectively resist fouling in complex media. For example, glucose sensor coated with polyHEMA hydrogel with additional epoxypolyurethane were shown previously to perform linearly in buffer[43], but failed when exposed to just 10% blood serum[84]. In this work, we demonstrate the necessity of the complete elimination of protein adsorption in a hydrogel and the feasibility of a polyCBMA hydrogel with lightly crosslinking density to ensure the long-term performance of this hydrogel in whole blood (**Figure 3.1c**). Although hydrogels are generally considered as low fouling, we will show that low fouling hydrogels are insufficient to achieve this challenging goal. Through a systematic study, we reveal that hydrogels with a low degree of crosslinking, as opposite to the conventional wisdom of high-packing density which has no protein entrapment in surface coatings, also have excellent performance against nonspecific protein adsorption. These lightly crosslinked (0.1% crooslinker in this work) hydrogels may appear to be "fouled" severely since proteins are able to diffuse into hydrogel matrixes. However, due to very high water content, very large-pore size and ultra-low fouling CB moiety inside hydrogel matrixes, proteins do not have a place to bind and are able to diffuse in and out freely, leading to

the complete elimination of protein adsorption on hydrogel matrixes. It should be emphasized that polyCBMA hydrogels with only single CB moiety are prepared from a CBMA monomer and a CBMA crosslinker. No conventional PEG-based crosslinker is used, which is unable to achieve long-term stability. To prove this concept, a glucose sensor with this extremely low fouling hydrogel is used to demonstrate its extraordinary performance in whole blood for 42 days.

An amperometric enzyme glucose sensor based on GOx, will be used to demonstrate the extraordinary performance of this polyCBMA hydrogel. It is well known that uncontrolled interactions between the surface of a sensor probe and biological media have been shown to be the major barrier to the development of a reliable glucose sensor[16, 45]. To minimize adverse biofouling effects, numerous surface coatings have been investigated with limited success[43, 45, 64, 65, 70]. Due to high fouling in complex media, these approaches suffer various issues, including low response, narrow dynamic range and difficult calibration. At present, no coatings have achieved the detection of glucose in whole blood for a long period of time. For example, some previous studies tested glucose sensors coated with an anti-interference layer such as heparin[49] or Nafion[64] in whole blood. Due to significant nonspecific protein adsorption from blood, a decrease in electrode sensitivity was observed after short exposure time to whole blood (120 min). Instead, several commercially available subcutaneously implantable glucose sensors have been shown to have good performance in tissue for 3-7 days[85-87]. Transcutaneous amperometric sensor-based systems such as Medtronic Minimed Guardian REAL-Time systems are on the market for continuous glucose monitoring[45]. They have drawn great attention over recent decades because of their excellent capability to continuously

monitor blood glucose levels in tissue. Although this sensor was developed for tissue implantation, in this work, we use it for comparison and show that whole blood poses a unique challenge and a sensor which works well for tissue implantation may not work in whole blood.

Previously, we have showed that zwitterionic polymer brush surfaces with very high packing density can completely resist nonspecific protein adsorption from undiluted blood plasma and serum[38] (**Figure 3.1b**). PolyCBMA is also unique in that it is also functionalizable via conventional 1-ethyl-3-(3-dimethylaminopropyl)-carbodiimide and N-hydroxysuccinimide (NHS/EDC) chemistry[37, 88, 89] for the convenient immobilization of enzyme. However, due to high packing density, polyCBMA surface coating are not able to support the high immobilization of enzyme and the free transport of glucose for glucose sensors. Thus, hydrogel coatings are often used instead. However, hydrogel coatings are not able to achieve high surface packing densities. Our preliminary studies showed that glucose sensors using polyCBMA hydrogels with low PEG-based crosslinker were stable in blood serum for 12 days[84]. These results pose questions why low crosslinking hydrogels work, when they fail, and how to extend their life span in even more complex media such as whole blood. A fundamental study is performed in this work to address these issues.

3.2 Materials and Methods

3.2.1. Chemicals

Pooled human blood serum was purchased from BioChemed Services (Winchester, VA). Dulbecco's Modified Eagle Medium, fetal bovine serum, nonessential amino acids, and penicillinstreptomycin were purchased from Invitrogen Corp (Carlsbad, CA). COS-7

cells (African Green Monkey fibroblast cells) were purchased from the American Tissue Culture Collection (Manassas, VA). CBMA was synthesized as described in previous papers[37]. Carboxybetaine-based crosslinker was synthesized using a method published previously[90]. Dextrose (D-glucose), 2-hydroxy-2-methylpropiophenone (Benacure 1173), ethyleneglycol dimethacrylate (EGDMA), GOx (EC 1.1.3.4, type X-S, Aspergillus niger, 5,000 U/g), methacrylic acid, ion exchange resin (IRA 400 OH form), N-hydroxysulfosuccinimide sodium (sulfo-NHS), EDC, Alexa Fluor 488 tagged fibrinogen from bovine (FTIC-Fg), phosphate buffer saline (PBS) were purchased from Sigma-Aldrich (St. Louis, MO). Dichloromethane and acetonitrile were purchased from EMD Biosciences (Gibbstown, NJ). Hydroquinone, t-Butyl bromoacetate and 2-(Cyclohexylamino)ethanesulfonic acid (CHES) were purchased from TCI America (Portland, OR). Toluene was purchase from Mallinckrodt Baker, Inc. (Phillipsburg, NJ). 2-(N-Morpholino)ethanesulfonic acid (MES) was purchased from Fisher Scientific (Fair Lawn, NJ). N-Methyldiethanolamine, methanesulfonic acid, and trifluoroacetic acid were purchased from Acros Organics (Morris Plains, NJ). Ethanol was purchased from Decon Labs (King of Prussia, PA). Sodium hydroxide was purchased from J.T. Baker (Phillipsburg, NJ). Water used in experiments was purified using a Millipore water purification system with a minimum resistivity of 18.0 MΩ•cm.

Φ0.125 mm Teflon-covered platinumiridium (9:1 in weight) was obtained from World Precision Instruments, Inc. (Sarasota, FL). Platinum wire counter electrodes and Ag/AgCl reference electrodes were purchased from CH Instruments, Inc. (Austin, TX).

3.2.2. Preparation of polyCBMA and polyHEMA hydrogels for characterization

CBMA monomer was first mixed with water and the solution was sonicated for 1 min to dissolve the monomer. CBMAX was added to the above solution and the mixture was sonicated for 1 min to complete dissolution at 0 ℃. The molar ratio of CBMAX and CBMA was 1:1000 (0.1%), 1:100 (1%), or 1:5 (20%) and the final concentration of CBMA was 10 M. 1% (w/w). Photoinitiator was added and the solutions mixed at 0 ℃. The solutions were transferred into a pair of glass plates, separated with a 0.4 mm PTFE spacer. The photo-polymerization reaction was carried out at room temperature for 30 min under a 365 nm UV light to polymerize the hydrogels. Then, the hydrogels were removed from the plates and immersed in a large volume of PBS. The PBS was changed daily for 5 days to remove residual chemicals before further use. The polyHEMA hydrogel was prepared by adding 8 M HEMA, 0.008 M EGDMA, and 1% (w/w) photoinitiator in a mixed solvent comprised of 1 part ethanol, 1.5 parts ethylene glycol, and 1.5 parts water. This hydrogel was also formed as above. To evaluate nonspecific protein interactions, hydrogels were exposed to 0.1 mg/mL of FITC-Fg in PBS for overnight at 4 ℃ followed by washing with PBS for 2 h. Protein was detected using CLSM).

3.2.3. Preparation of polyCBMA hydrogel-coated glucose sensors

Glucose sensors used for this study were based on the coil-type sensors[43]. Briefly, the coil-type glucose sensors were prepared by winding the top 10 mm of a 40-50 mm long platinum wire around a 25-gauge needle to form a coil-like cylinder. To improve the adhesion of the polyCBMA hydrogels, the surface of the coils was activated using a solution of 10% (trimethoxysilyl)propyl methacrylate and 0.5% water in toluene at 80 ℃. The hydrogel coating on the glucose sensor tip was formed by pipetting 0.8 μL of the

mixed solution (CBMA, CBMAX, and Benacure 1173 photoinitiator in water) onto the sensor tip. The molar ratio of CBMAX to CBMA was 1:1000 (0.1%), 1:10 (10%), or 1:5 (20%) and the final total concentration was 10 M. The solution was allowed to spread evenly over the surface of the tip. After polymerization via exposure to 254 nm UV light for 30 min, the sensors were stored in PBS until further use.

3.2.4. Enzyme immobilization via sulfo-NHS/EDC chemistry

The carboxylate groups of the polyCBMA hydrogels were activated by immersion in a freshly prepared solution of sulfo-NHS (5 mM) and EDC (100 mM) in 10 mM MES buffer (pH 5.5, 100 mM NaCl) for 2 h at 25 ℃. Then, the sensors were removed and immersed in a large volume of MES buffer for 2 h to remove residual chemicals. The MES buffer was changed several times over the 2-hour period. The sensors were then immersed in a freshly prepared solution of GOx (10 mg/mL) in MES buffer for 4 h at 4 ℃. Before glucose testing, the sensors were immersed in a large volume of PBS to remove any residual unbound enzyme.

3.2.5 Sensor evaluation

The in vitro performance of the sensors was examined in PBS solution containing glucose to determine their sensitivity and linear range. The sensitivity of the polyCBMA hydrogel-treated sensors was first measured using PBS solution containing 4-20 mM glucose. The difference between the base current of PBS and the steady state current of glucose in the sample was used to obtain the function relating the signal response and the glucose concentration. Then, the sensors were tested with glucose dispersed in 100% human blood serum. For the long-term sensor evaluation, the sensors were stored between measurements in 100% human blood serum at 4 ℃. When quantifying glucose

in a serum sample, the base current was recorded in the serum and then the sensors were transferred into the sample to obtain a steady state current. All experiments were carried out at room temperature and all the solution was stirred during the measurement. To test the glucose level in blood, rat blood samples were collected according to a protocol approved by University of Washington. All tests were performed in a biosafety cabinet, and the blood and sensors were stored at 4 ℃ between measurements. Amperometric measurements were performed at room temperature at +0.75 V vs. Ag/AgCl along with a platinum wire counter electrode and Princeton Applied Research Model PG580 electrochemical analyzer.

3.3 Results and Discussion

Here, we systematically studied four hydrogels with different crosslinking densities (0.1%, 1%, 10%, and 20% CBMAX/CBMA) via photopolymerization. PolyHEMA hydrogel was used as a control. Note that these hydrogels contain only one ultra-low fouling CBMA moiety since they are prepared from a CBMA monomer and a CBMA-based crosslinker (CBMAX) (**Figure 3.1d**), replacing the conventional PEG-based crosslinker used previously[84].

3.3.1 Hydrogel characterization

First, we examined the hydration of different hydrogels. As expected, an increase in crosslinker content results in a decrease of hydration. The highest equilibrium water content ($94.19 \pm 0.26\%$) is obtained when the crosslinker content is 0.1% (**Figure 3.2a**). At 20% CBMAX, hydration has fallen to about 50% equilibrium water content, which is slightly higher than the polyHEMA hydrogel. Next, we investigated the interactions of hydrogels with proteins. From **Figure 3.2b**, an evident protein adsorption dependency of

hydrogels on crosslinker contents can be seen. It was observed that the minimum protein adsorption was exhibited at the extremely low crosslinker content. After contact with FITC-Fg for 24 hours and complete wash with buffer, there is no apparent protein adsorption on the surface of polyCBMA hydrogel with 0.1% crosslinker content (**Figure 3.2b-c**). When the integrated intensity is plotted as a function of the scan depth, it is clear that protein adsorption does not change as the depth into the hydrogel increases, indicating that the hydrogel does not have any further significant interactions with proteins, such as entrapment or sequestration. By contrast, polyHEMA exhibits significant high fluorescent intensity on the surface but that decreases quickly when scanned inside the hydrogel, suggesting that proteins adhered to, but could not enter, the hydrogel surface (**Figure 3.2b-c**). The hydrogels with 1%, 10% and 20% crosslinker contents generally have low protein adsorption, but not as low as that with 0.1% crosslinker content (**Figure 3.2b**). We further examined COS-7 cellular interactions with polyHEMA and 0.1% polyCBMA hydrogels (**Figure 3.2d**). Results show that after contacting COS-7 cells for 72 hours, 0.1% polyCBMA hydrogel is highly resistant to cell attachment, a 99% reduction in cell adhesion as compared to that of the polyHEMA hydrogel (**Figure 3.2d**) even though polyHEMA itself exhibits only a small percent of cell adhesion on tissue culture polystyrene (TCPS)[91]. From the observations described above, it is clear that all polyCBMA hydrogels have low protein adsorption cell adhesion while the hydrogel with 0.1% crosslinker content possesses the best performance.

3.3.2 Hydrogel performance as a sensor coating

Four polyCBMA hydrogels are tested for their performance when they are used as glucose sensor coatings. For most GOx based sensors, glucose enzymes are often

physically adsorbed onto the sensor surface or via a carrier such as fiber or cotton, resulting in high enzyme leaching and low enzyme bioactivity[43, 88]. In this work, GOx was covalently linked onto the hydrogel framework via NHS/EDC chemistry to reduce enzyme leaching (**Figure 3.3**). It was observed that all the polyCBMA hydrogel-coated sensors displayed a fast response and they did not show a decline in sensitivity over a period of 40 days in PBS solution containing 4-20 mM glucose with ~100-fold response increase compared to the previous work[43] (**Figure 3.4**). However, when exposed to 100% serum, there was a large decrease in sensor response for the sensors coated with 1%, 10%, and 20% crosslinked hydrogels after 5 days (**Figure 3.5b-d**) although they have very low protein adsorption and cell adhesion as shown previously in **Figure 3.2b**. Only the sensors coated with 0.1% CBMAX/CBMA hydrogel retained long-term stability upon prolonged storage (>20 days) (**Figure 3.5a**). Therefore, the single polyCBMA hydrogel with 0.1% crosslinker content has superior performance in 100% blood serum over those with low PEG-based crosslinker[84].

Furthermore, compared to the sensor with PEG-based crooslinked hydrogel, this with CBMAX crosslinked hydrogel displayed a ~5-fold sensitivity increase. It should be pointed out that conventional glucose sensors suffer one major issue of calibration[16], resulting in nonspecific binding. A few reports have sought to improve measurement reliability by adding an additional diffusion-limiting membrane, but at the expense of current response signal[43]. Due to suppression in nonspecific binding, this single polyCBMA hydrogel coating achieved a strict linearity without any signal decline up to 30 mM glucose when tested in undiluted glucose-containing serum (**Figure 3.6**), which is

the upper limit of blood glucose levels for diabetics. Thus, this additional calibration-free feature makes this hydrogel highly promising for glucose detection in complex media.

3.3.3 Glucose sensor test in whole blood

To examine the performance of this polyCBMA hydrogel in complex media, the long-term stability and sensitivity of a glucose sensor coated with 0.1% CBMAX/CBMA hydrogel was evaluated with whole blood taken directly from rats. For the side-by-side comparison of sensor stability test, the experimental sensor coated with 0.1% polyCBMA hydrogel and the Medtronic sensor were placed in a small tube containing 0.5 mL fresh whole blood at the same time. Meanwhile, the blood glucose level was analyzed with a Bayer Contour glucose test strip for the purpose of validation. The amperometric response of the experimental sensor was monitored following exposure to the whole blood sample on consecutive days and converted to blood glucose level according to the current response plot (**Figure 3.5a**). The Medtronic sensor is connected to a transmitter that transmits data over a maximal distance of 3 m to a pager-sized monitor and the monitor displays the recording of glucose concentration[85]. As indicated by the manufacturer, the Medtronic sensor has a maximum life of 72 hours when inserted in the subcutaneous tissue. In the presence of whole blood, it failed to display reliable glucose readings after the sensor had been immersed in whole blood for more than 33.3±4.1 hour (**Figure 3.7**). The continuous exposure to 100% blood resulted in a substantial suppression of the response of the sensor, and contamination was visible on the sensor surface. On the other hand, the experimental sensor coated with 0.1% crosslinked hydrogel retained responsiveness, stability, and sensitivity after continuous and prolonged contact with whole blood. The blood sample was collected every two or three

days and the glucose level was measured with a test strip (**Figure 3.7**). All of the 6 sensors tested were fully functioning for 33 days while 3 out of 6 sensors were tested for up to 42 days with excellent performance. On the 42nd day of incubation in whole blood, one immersed experimental sensor, one newly-prepared sensor and one test strip have similar responses to the whole blood, indicating the long-term resilience of the new polyCBMA-based glucose sensor. Thus, it is expected that the life of the experimental sensor in whole blood can be more than 42 days if hydrogel adhesion on a surface is further improved.

In addition to blood withdrawal every 2-3 days, one experiment was performed for the direct and continuous measurements of glucose from one single whole blood sample taken from a rat and blood is changed every few days using the same blood sample taken at the beginning of experiments. Results also show the excellent performance of the experimental sensor (**Figure 3.8**). The glucose level diminished with time due to metabolic consumption by the cells in blood. Importantly, sensor validation indicates that our results agree well with those measured with Bayer Contour glucose test strips, differing only by 0.1 ± 0.5 mM (~2%) (**Figure 3.9**). This also shows that the sensor coated with 0.1% polyCBMA hydrogel is able to detect the fluctuation of blood glucose level rapidly and reliably. Thus, this hydrogel coating is promising to detect the sudden rises and falls in blood glucose levels with high sensitivity. Finally, it should be pointed out that to confirm the accuracy and reliability of the glucose readings from the Medtronic sensor, calibration has to be performed by measuring blood glucose concentrations with Bayer Contour glucose test strips at least twice a day (once every 12 hours) while it is

unnecessary for the experimental sensors because of the excellent linearity in complex media (**Figure 3.2b**).

Next, it is essential to determine the sensitivity of the experimental sensor in the diabetically-appropriate blood glucose level in the range of 2–30 mM. **Figure 3.4b** shows the glucose level measured by both the Medtronic sensor and our experimental sensor. The detection limit of the experimental sensor was much lower than that of the Medtronic sensor. The glucose detection curve for the Medtronic sensor reaches its saturation (2.8 mM) while the experimental sensor can be adapted to detect glucose with a sensitivity as low as 0.1 mM due to excellent nonfouling properties (**Figure 3.7b**). The test results agree well with those theoretical values calculated by dividing the initial value by dilution factor. In addition, as discussed above, the upper limit of the experimental sensor can be extended to 30 mM while that of the Medtronic sensor is 22.2 mM[45]. The experimental sensor with a wide dynamic range (0.1 to 30 mM) can match the required sensitivity and lifetime of diabetic diagnostics.

Although the purpose of this study is to evaluate lightly crosslinked hydrogel in whole blood using a glucose sensor, it should be pointed out that all matrices with blood for glucose sensing are the ultimate goal[16]. However, due to great challenges for sensing in whole blood, the tissue became the standard for continuous monitoring although there is a great delay between the actual blood glucose concentration and the value reported by the subcutaneous sensor[92]. The stability of this lightly crosslinked hydrogel in whole blood for 42 days well exceeds any reported results and will open up many new applications.

3.3.4 Proposed mechanism

High water content and large pore size are responsible for the fact that 0.1% hydrogel works so well in complex media for 42 days. The high water content and large pore size of this hydrogel allows the free movement of proteins in and out of the hydrogel matrix without any entrapment and sequestration (**Figure 3.1c**). Results from scanning electron microscopy (SEM) confirm that the bulk hydrogel with 0.1% CBMAX/CBMA is highly porous with a mean diameter of ~17 μm and the intact microstructure was unaffected by serum incubation (**Figure 3.10**). Additionally, the mesh size of the 0.1% crosslinked hydrogel is calculated to be 28.2 nm[90], which means that GOx molecules ($7 \times 5.5 \times 8$ nm)[92] and glucose molecules have access to the porous structure of the hydrogel[93]. The ability for GOx transport through the highly swollen hydrogel significantly increases the amount of immobilized GOx during hydrogel functionalization. Enzyme bioactivity is better preserved in this large porous and flexible polymer network[94, 95].The hydrogel coating may further enrich oxygen for an improved enzymatic reaction cycle due to its high water content. These factors explain why the 0.1% crosslinker content hydrogel possesses superior performance in complex media and provides a new direction for the design of ultra-low fouling hydrogels in blood.

3.4 Conclusions

We demonstrate one lightly crosslinked hydrogel composed of only CBMA moiety for extraordinary performance in whole blood for 42 days. Glucose sensors coated with this hydrogel have faster response, higher sensitivity/specificity, lower detection limit (0.12 as compared with 2.22 mM for the commercial sensor), and longer-term stability (≥42 days as compared to 33 hours for the commercial sensor) than a commercial sensor. The sensor coated with this polyCBMA hydrogel also exhibits a wide range of linearity with

outstanding stability without need for calibration. All of these excellent properties largely result from the complete elimination of protein adsorption in the hydrogel. This work proposes two unconventional points of view in materials and surface chemistry. It is generally believed that surface coatings with very high packing densities are the prerequisite against biofouling in complex media. However, results show that a lightly crosslinked hydrogel, the extreme opposite of high packing density surface coatings, also can work so well. It is generally believed that hydrogels have low fouling. However, it is shown in this work that low fouling is not sufficient and extreme low fouling is necessary for long-term applications in very complex media such as whole blood. This work provides a new concept of surface chemistry that is easily adaptable for other medical devices beyond glucose sensors in order to realize long-term stability and high performance in whole blood.

3.5 Chapter Figures

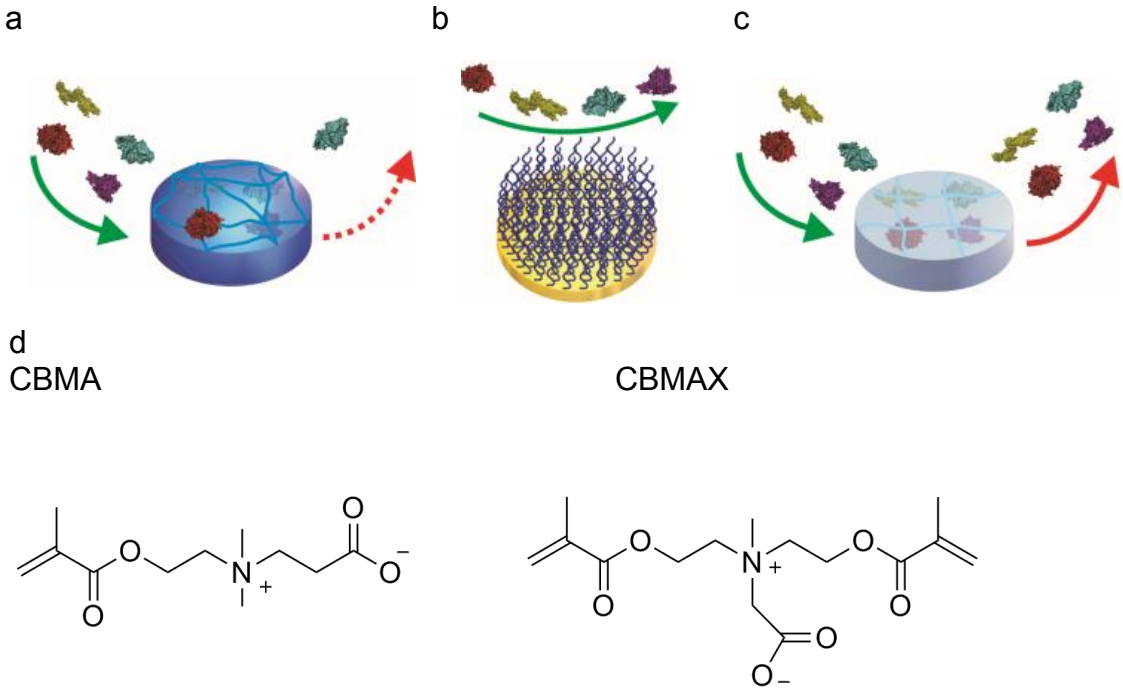

Figure 3.1 Schematic illustrations of (a) a low fouling conventional hydrogel, within which some proteins are entrapped and on which some proteins are adhered; (b) a polymer brush surface, which highly resists nonspecific protein adsorption; (c) an extremely low fouling hydrogel with low crosslinker density, which allows the free movement of proteins in and out of the hydrogel matrix without any nonspecific protein adsorption; and (d) chemical structures of carboxybetaine monomer (CBMA) and crosslinker (CBMAX).

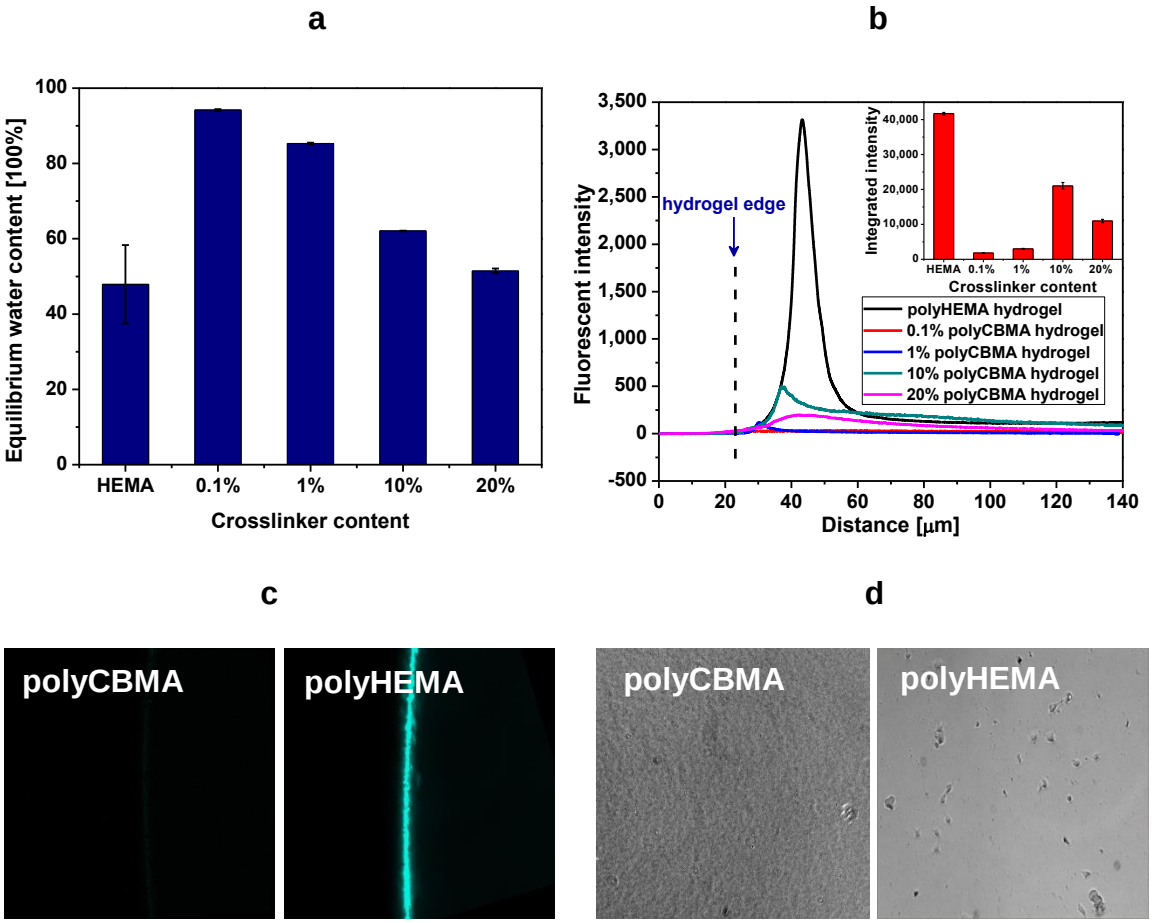

Figure 3.2 Characterization of hydrogels. (a) Water content of polyCBMA hydrogels with different crosslinker contents and polyHEMA hydrogel; (b) Fluorescent intensity as a function of the scan depth and integrated intensity of polyCBMA hydrogels with 0.1%, 1%, 10%, and 20% crosslinker contents and polyHEMA hydrogel after incubated in FITC-Fg for 24 h; (c) FITC-Fg adsorption on polyCBMA hydrogel with 0.1% crosslinker content and polyHEMA hydrogel. Scale bar is 100 μm; (d) COS-7 cell attachment on polyCBMA hydrogel with 0.1% crosslinker conten and polyHEMA hydrogel.

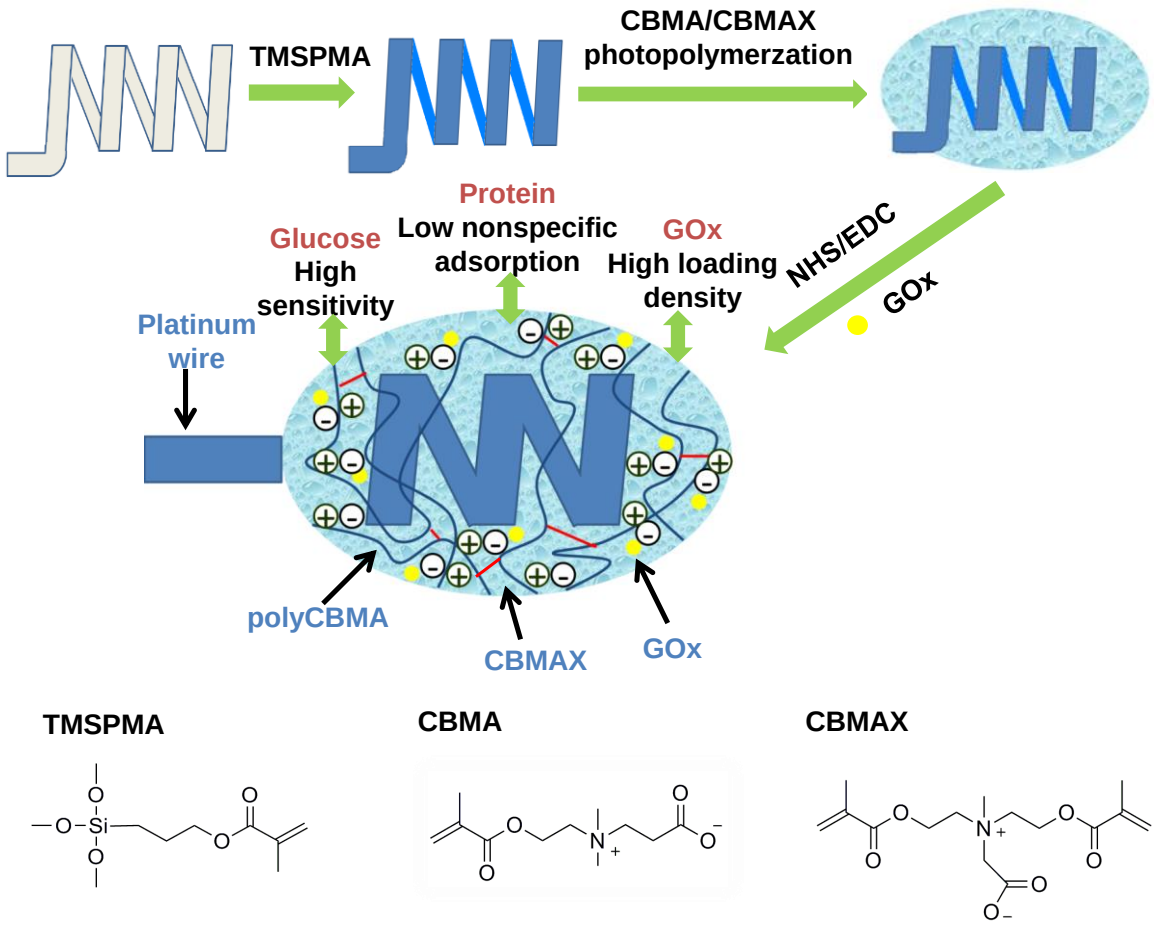

Figure 3.3 Schematic illustration of the preparation process of a glucose sensor coated with a polyCBMA hydrogel lightly crosslinked with a CBMAX crosslinker and loaded with covalently immobilized GOx, leading to high GOx loading density, high glucose detection sensitivity, and very low nonspecific protein adsorption.

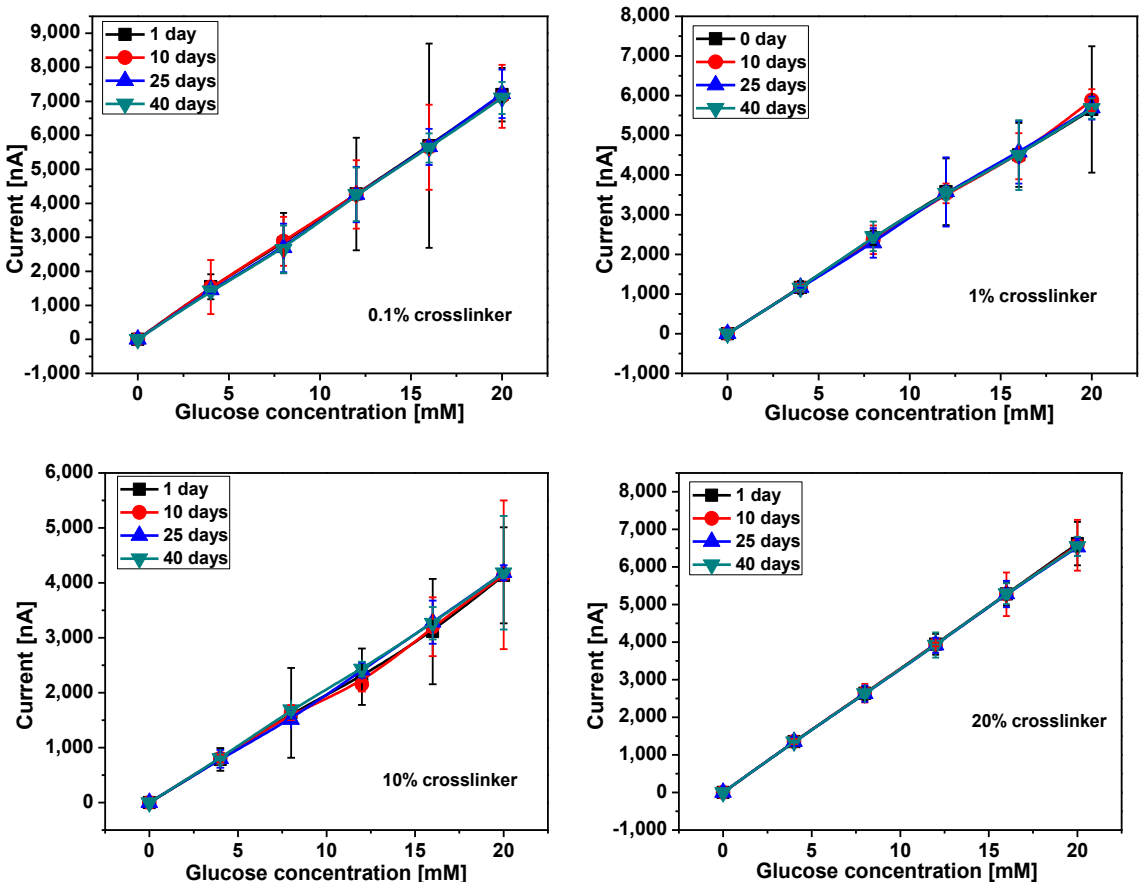

Figure 3.4 Current response of glucose sensors coated with polyCBMA hydrogels of 0.1%, 1%, and 20% crosslinker content different crosslinker contents as a function of glucose concentration in PBS. Operating potential: +0.75 V vs. Ag/AgCl reference electrode.

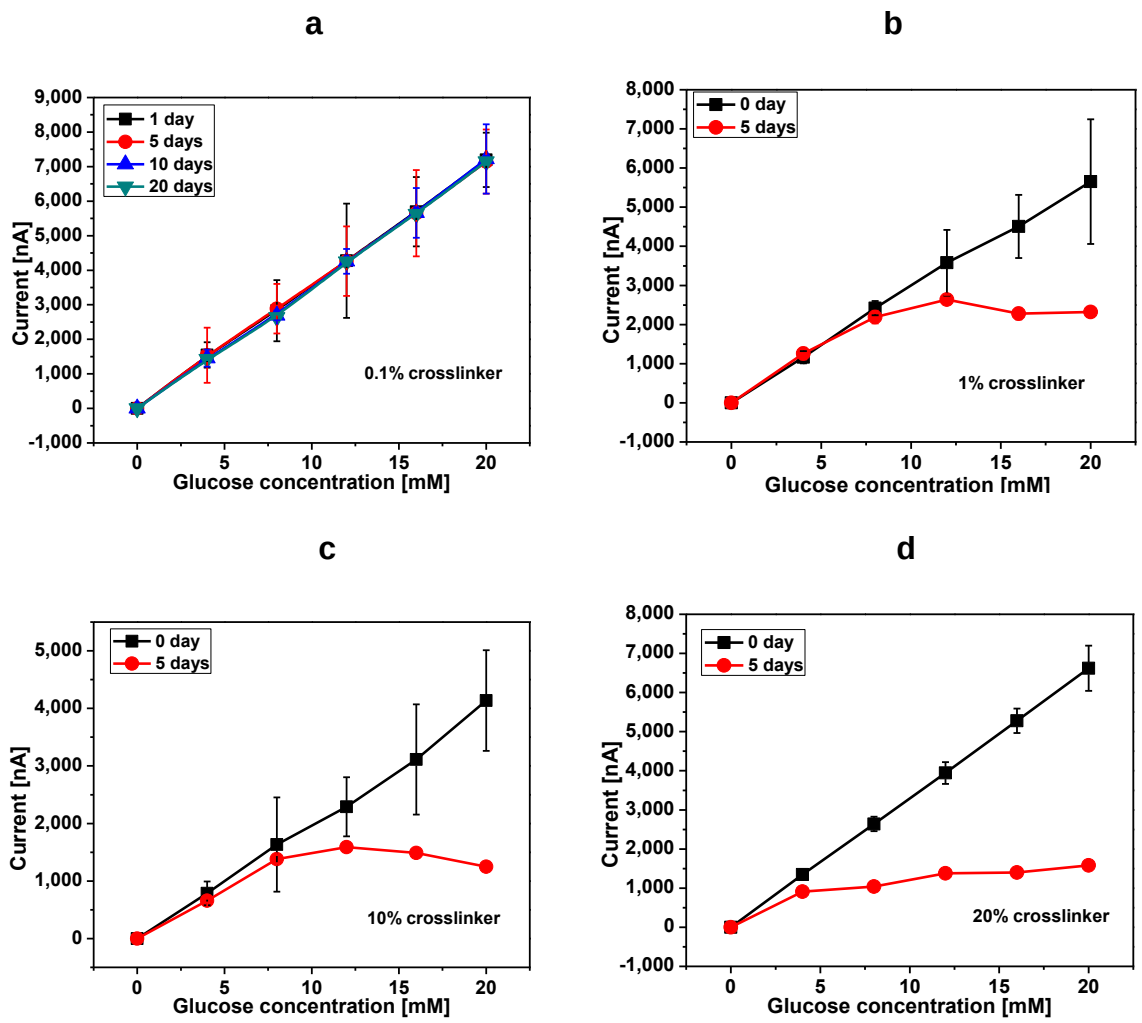

Figure 3.5 Performance of hydrogels as sensor coatings in 100% serum. (a), (b), (c), and (d) represent the current response of glucose sensors coated with polyCBMA hydrogels as a function of glucose concentration in undiluted blood serum with a crosslinking density of 0.1%, 1%, 10%, and 20%, respectively. Operating potential: +0.75 V vs. Ag/AgCl reference electrode.

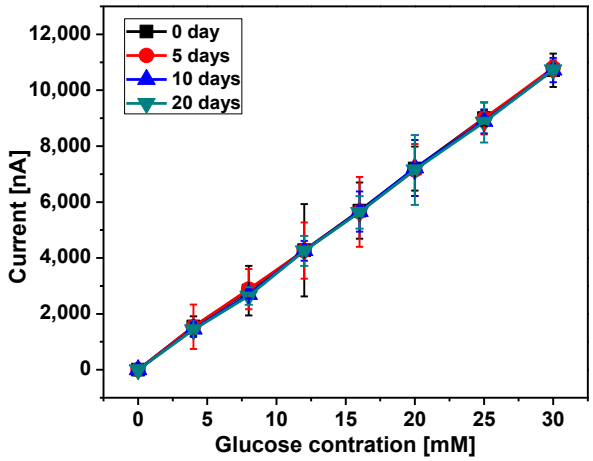

Figure 3.6 Upper limit of glucose sensor coated with polyCBMA hydrogels with 0.1% crosslinker content in PBS containing glucose (0-30 mM). Operating potential: +0.75 V vs. Ag/AgCl reference electrode.

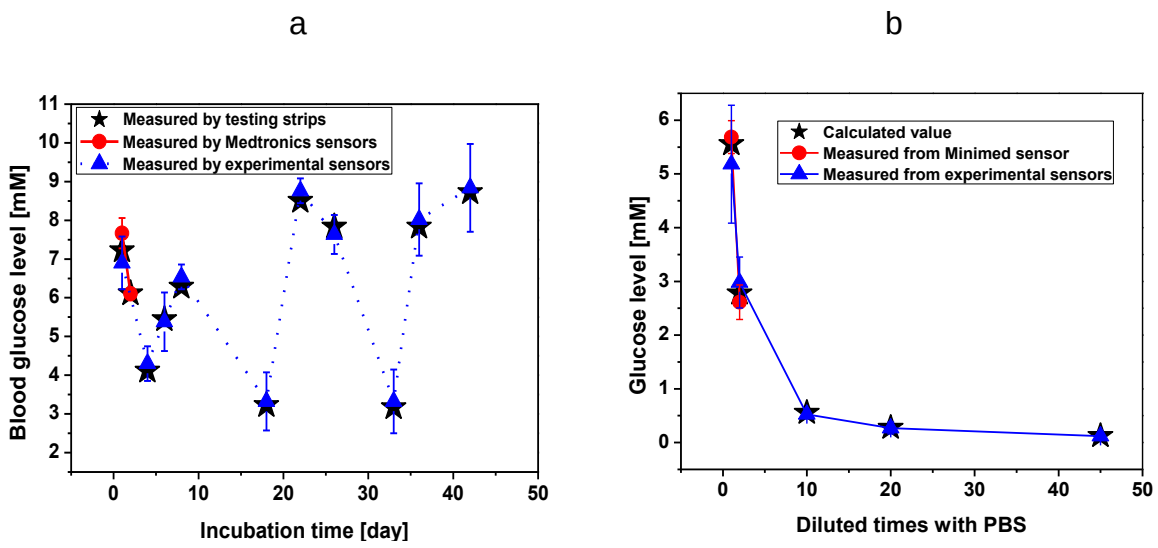

Figure 3.7 Comparison of the experimental glucose sensor coated with 0.1% polyCBMA hydrogel with the Medtronic sensor in whole blood taken from rat. (a) Comparison of sensor stability: Real-time blood glucose level is plotted as a function of time. Bayer Contour glucose test strips were used as reference for both sensors and also as calibration for the Medtronic sensor; (b) Comparison of sensor sensitivity: Blood glucose level is plotted as a function of PBS dilution. The blood glucose of the whole blood at the initial point was tested with the Bayer Contour glucose meter. The glucose content of the experimental sensor was achieved from the current response plot of the glucose sensor in **Figure 3.5**. The calculated value was obtained by dividing the initial value by dilution factor. There are 6 and 3 replicates for the experimental and commercial sensors, respectively.

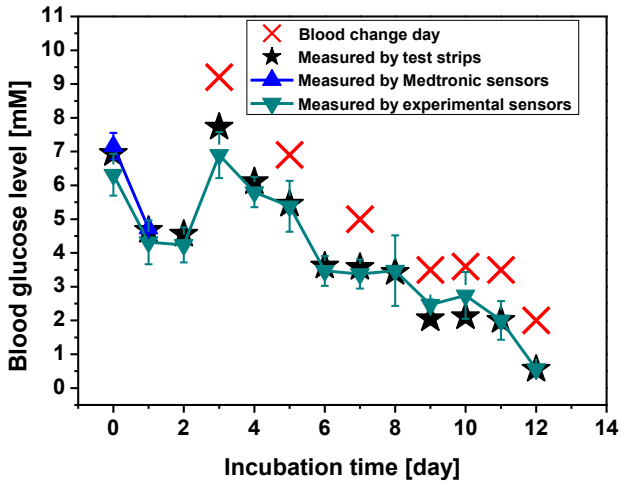

Figure 3.8 Blood glucose concentration obtained from glucose sensors coated with 0.1% polyCBMA hydrogel and Medtronic sensors as a function of incubation time in whole blood of rat. Bayer Contour glucose test strips were used as both reference and calibration for Medtronic sensors. Blood change is marked with cross.

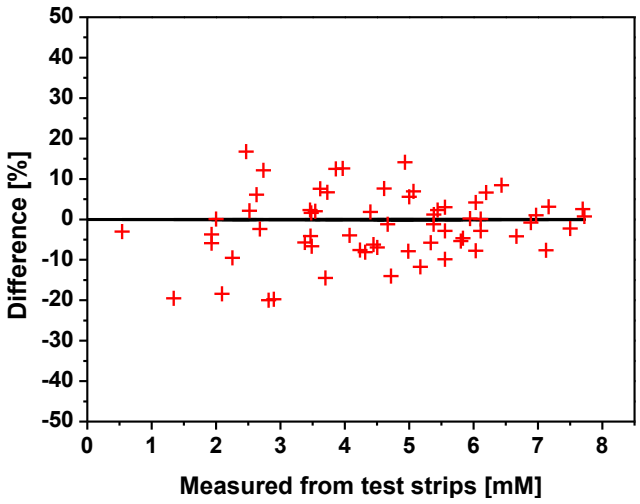

Figure 3.9 Sensor validation with Medtronic sensors. Scatter plots of the differences in blood glucose concentrations obtained from the experimental sensors and the reference Bayer Contour glucose test strips in the whole blood of rats.

a

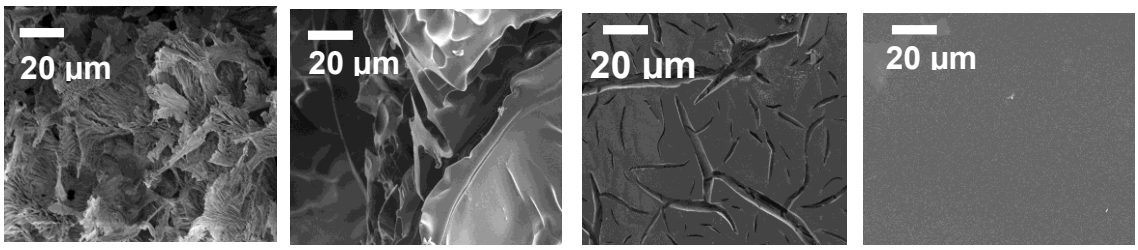

b

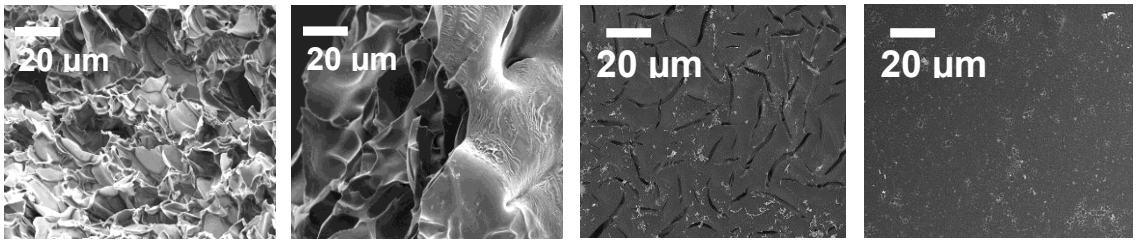

Figure 3.10 SEM images of hydrogels with different crosslinker contents. (a), PolyCBMA hydrogels with 0.1%, 1%, 10%, and 20% crosslinker content, respectively; (b), PolyCBMA hydrogels treated in undiluted blood serum for 5 days with 0.1%, 1%, 10% and 20% crosslinker content, respectively.

Chapter 4 Poly(carboxybetaine) Nanomaterials Enable Long Circulation and Prevent Polymer-specific Antibody Production

Poly(ethylene glycol) (PEG) has been incorporated into nanoparticles (NPs) to improve circulation time from systemic circulation for decades with limited success. Recent studies have shown that PEG indues the production of PEG-specific antibodies after repeated injections. Here, we demonstrate zwitterionic poly(carboxybetaine) (PCB)-based nanomaterials with no production of polymer-specific antibodies, while PEG-coated NPs generated PEG-specific antibodies. Furthermore, PCB-coated NPs exhibited prolonged circulation time and showed little change between the first and second doses ($t_{1/2}$ = 55.8 and 55.6 h), with no accelerated blood clearance suffered by PEG NPs ($t_{1/2}$ drops from 8.7 to 5.2 h). These findings are significant advances toward solving the long-standing clinical challenge of developing nanomaterials that are able to resist both immune response and immediate bodily clearance.

4.1 Introduction

To date, numerous nanoparticle-based technologies quickly surged to the forefront of drug delivery, diagnostics, and many other areas[4]. However, the body has evolved finely tuned processes involving the innate and adaptive immune systems to remove non-self materials from the body. This makes engineering clinically relevant therapeutic nanoparticles an extreme challenge[18, 24].When nanoparticles (NPs) enter the bloodstream, they immediately encounter a complex environment of plasma proteins and leukocytes[18]. NP uptake by phagocytes may occur through various pathways[24, 96] and can be facilitated

by the adsorption of plasma proteins (opsonins) to the particle surface[18]. The ideal NP platform is one whose integrity is undisturbed, providing extended systemic circulation to maximize delivery to the target site. Additionally, it should be nontoxic and invisible to the immune system. Various strategies have been studied for immunosuppression, including manipulating NP physical properties (e.g., size/architecture) or surface chemistry (e.g., PEGylation)[3, 18, 19, 27]. Although the modification with PEG can reduce nonspecific protein adsorption, preventing flocculation, opsonization, and subsequent complement activation[20], it was already shown in a toxicological study of PEG in 1950 that PEG has the propensity to induce blood clotting and clumping of cells, leading to embolism formation[5]. More recently, discovery of a PEG-specific immune response has triggered further investigation[5, 21, 22, 97]. It was suggested that PEGylated NPs also induce production of anti-PEG immunoglobulin M (IgM) antibodies. IgM antibodies stimulate the complement system and lead to the clearance of the NPs[5, 21, 97] (**Figure 4.1a**). Additionally, previous reports have shown a markedly higher occurrence (22%–25%) of anti-PEG antibodies in the healthy blood donor population[98]. Thus, it is important to keep in mind that the generation of PEG-specific antibodies will affect the efficacy of PEG-based therapeutics.

Various attributes of NPs need to be tailored for effective drug delivery applications, including circulation time, targeting, cellular internalization, and selective drug release[23, 99]. Among these, the ability of NPs to remain in circulation is one of the most important determinants of therapeutic effect[23]. Longer circulating NPs are more likely to reach their target, allowing high therapeutic efficacy and/or imaging sensitivity, as well as reduced accumulation in normal tissues and avoiding side effects[24]. However, most NPs are

susceptible to opsonization, resulting in the accelerated recognition and subsequent clearance by the mononuclear phagocyte system (MPS)[100]. Although numerous strategies involving PEG coatings have been applied to improve the circulation length of NPs, success has been limited to circulation times of 8 to 10 hours[23]. Previously, zwitterionic materials have been shown to have high resistance to nonspecific protein adsorption even in undiluted blood plasma and serum[101, 102]. These zwitterionic materials bind to water stronger than PEG via electrostatically induced hydration, where PEG interacts with water via hydrogen-binding[10]. It has been shown that superhydrophilic poly(carboxybetaine) (PCB) is superior to PEG at maintaining protein stability and bioactivity[11, 101]. Thus, it is conceivable that zwitterionic materials can shield NPs from nonspecific binding and thus prevent the production of antibody more effectively, thereby improving their circulation time. In this work, we hypothesize that NPs protected by ultra-low fouling and superhydrophilic zwitterionic PCB materials will have excellent stealth properties, thereby preventing bodily clearance (**Figure 4.1b**). To test this, gold nanoparticles (GNPs) were used as a model system, which also act as a label for detection. In order to investigate only the effect of the polymer coatings, the particle size and surface charge of the NPs are kept the same.

4.2 Materials and Methods

4.2.1 Chemicals

Pooled human blood plasma was purchased from BioChemed Services (Winchester, VA). 11-mercaptoundecyl 2-bromoisobutyrate ($Br(CH_3)_2COO(CH_2)_{11}SH$), was synthesized through the reaction of bromoisobutyryl bromide and 11-mercapto-1-undecanol using a previously published method[103]. PEG_{5000}-thiol was purchased from

Nektar (Huntsville, AL). Tetraoctylammonium bromide (TOAB) was purchased from Alfa Acesar (Ward Hill, MA). Phosphate buffer saline (PBS, 0.01M phosphate, 0.138 M sodium chloride, 0.0027 M potassium chloride, pH 7.4) was purchased from Sigma-Aldrich (St. Louis, MO). Toluene was purchase from Mallinckrodt Baker, Inc. (Phillipsburg, NJ). Copper(I) bromide (Cu(I)Br), sodium borohydride, chloroauric acid, *N*,*N*-dimethylformamide (DMF), 1,1,4,7,10,10-hexamethyltriethylenetetramine (HMTETA), were purchased from Sigma-Aldrich (Milwaukee, WI). Ethyl ether was purchased from J.T. Baker (Phillipsburg, NJ). Ethanol was purchased from Decon Labs (King of Prussia, PA). Water used in experiments was purified using a Millipore water purification system with a minimum resistivity of 18.0 MΩ• cm.

4.2.2 Synthesis of carboxybetaine-1-methacrylate tert-butyl ester (CBMA-1-tBu)

As shown in **Figure 4.2**, 2-(Dimethylamino)ethyl methacrylate (25.1 g, 160 mmol), *tert*-butyl-bromoacetate (35.4 mL, 239 mmol) and hydroquinone (150 mg, 1.36 mmol) were dissolved in anhydrous acetonitrile (150 mL) at room temperature. The solution was stirred at 60 ℃ for 12 hours and then cooled to room temperature. Ether (150 mL) was added to the stirring solution, resulting in the formation of a white precipitate after 30 min. The suspension was stirred for an additional 30 min and the solid was filtered out on a Buchner funnel. After washing with ether (3 x 50 mL), the obtained white powder was dried under high vacuum to afford the desired product without further purification: (48.7 g, 138 mmol). Yield: 87%. ^{1}H NMR (300 MHz, $CDCl_3$) δ: 6.10 (s, 1H), 5.74 (s, 1H), 4.60 (t, 2H, J = 4.0 Hz), 4.32 (s, 6H), 4.00 (t, 2H, J = 4.0 Hz), 3.34 (s, 3H), 1.87 (s, 3H), 1.44 (s, 9H). ^{13}C NMR (75 MHz, $CDCl_3$) δ: 168.2, 164.0, 135.1, 128.2, 86.7, 62.9, 62.7, 58.6, 53.0, 27.4, 17.6.

4.2.3 Synthesis of initiator-coated GNPs

TOAB-coated gold nanoparticles (diameter, 5 nm) in toluene were synthesized as previously reported[104]. A thiol-capped polymerization initiator, 11-mercaptoundecyl 2-bromoisobutyrate ($Br(CH_3)_2COO(CH_2)_{11}SH$), was synthesized through the reaction of bromoisobutyryl bromide and 11-mercapto-1-undecanol using a previously published method[103]. The initiator-coated GNPs, was synthesized according to literatures[105, 106]. Before mixed with polymerization initiator, TOAB-coated GNPs was purged with dry N_2 for 30 min under constant magnetic stirring. Then, initiator dissolved in 1 mL toluene was added to the solution in a dropwise fashion within 15 min. The reaction was allowed to proceed for overnight under nitrogen atmosphere, producing a dark-red solution of initiator-coated GNPs. Large volume of ethanol was added to the system to precipitate the GNPs. The turbid solution was allowed to stand on a bench overnight. The solution was subjected to solvent removal in a rotary evaporator (at 40 ℃) followed by multiple cleanings using ethanol. The precipitate was collected and re-dispersed in dimethylformamide (DMF).

4.2.4 Preparation of PCB-GNPs via surface initiated atom transfer radical polymerization (SI-ATRP)

In a typical reaction, 74 mg Cu(I)Br and 1.8 g carboxybetaine-1-methacrylate tert-butyl ester (CBMA-1-tBu) monomer were placed into a Schlenk tube and subjected to three vacuum-nitrogen cycles. Then, 7 mL of degassed dimethylformamide (DMF) was added and the content was purged with N_2 before 148.6 mg 1,1,4,7,10,10-hexamethyltriethylenetetramine was added to the flask via syringe. The reaction mixture was thoroughly purged with N_2 for an additional 15 min to yield solution A. Similarly,

initiator (11-mercaptoundecyl 2-bromoisobutyrate, $Br(CH_3)_2COO(CH_2)_{11}SH$) coated GNPs in DMF were deoxygenated by bubbling N_2 for 15 min to yield solution B. Polymerization was started by transferring solution A into solution B under N_2. After reaction was stirred at 750 rpm and 50 ºC for 24 h, the PCB-GNPs were precipitated in ethyl ether and collected by centrifugation. Hydrolysis was carried out by dissolving in acidic water (pH 3.0) overnight. Then the product was dispersed in deionized water, and other impurities including residual monomers, initiators, and catalysts were removed by using a 100 kDa molecular weight cutoff Amicon Ultra centrifugal filter. The polymer-modified GNPs were collected by centrifugation and redispersed in PBS before further use, yielding a dark red solution. See SI methods.

4.2.5 Animal studies

The *in vivo* antibody production, circulation time, and biodistribution of GNPs were studied using Spraque Dawley rats (body weight ~150 g) as the animal model. Each GNP sample was studies in six duplicates to generate statistical significance. All animal experiments adhered to federal guidelines and were approved by the University of Washington Animal Care and Use Committee. Two groups of rats were formed. For Group 1 rats, which received one injection, the GNPs (PEG-GNPs or PCB-GNPs) were administered via the tail vein at a dose of 1 mg/kg body weight under anesthesia and sterile treatment. Control animals received PBS instead of GNPs. To study the *in vivo* circulation time, at 5 min, 4 h, 8 h, 24 h, and 48h after the injection, a 50 μL blood sample was collected, digested, and analyzed by the elementary analysis method, inductively coupled plasma mass spectroscopy (ICP-MS). On the fifth day after the injection, 5 mL of blood were drawn from the aorta and serum was prepared for IgM measurement.

Biodistribution was assessed after the animals were euthanized by CO_2 inhalation, where organs (heart, liver, spleen, lung, and kidneys) were collected, digested in aqua regia, and analyzed by ICP-MS.

For Group 2 rats, which received two injections, PEG-GNPs or PCB-GNPs were administered intravenously at a dose of 1mg kg^{-1} body weight 7 days apart. Control animals received PBS instead of GNPs for both injections. On the fifth day after the second injection, 5 mL of blood were drawn from the aorta for IgG measurement. The *in vivo* circulation time and biodistribution tests were performed the same as in Group 1.

4.2.6 Determination of IgM and IgG levels with enzyme-linked immunosorbent assay (ELISA)

Using the 5 mL blood samples drawn as described in the previous section, serum samples were obtained by incubation for 30 min at room temperature followed by centrifugation at 3,000 rpm at 4 °C for 15 min. Quantification of IgM and IgG levels were performed using the Rat IgM ELISA Quantitation Kit and the Rat IgG ELISA Quantitation Kit from BETHYL Laboratories, TX, USA. Briefly, 100 µL of 1:100 diluted primary antibody (Goat anti-Rat IgM or anti-Rat IgG antibody) in coating buffer (50 mM carbonate-bicarbonate, pH 9.6) was added to each well of a 96-well plate and then incubated at room temperature for 1 h. The wells were then washed five times with wash solution (50 mM Tris, 0.14 M NaCl, 0.05% Tween 20, pH 8.0). Then, 200 µL of blocking solution (50 mM Tris, 0.14 M NaCl, 1% BSA, pH 8.0) was added to each well and incubated 30 min at room temperature. After incubation, the blocking solution was aspirated and the wells were washed five times with wash solution and 100 µL of 1:100 standard or sample in the sample diluent (50 mM Tris, 0.14 M NaCl, 1% BSA, 0.05%

Tween 20, pH 8.0) was added to the wells. After incubation for 1 h at room temperature, the blocking solution was removed and the wells were washed five times with the wash solution. 100 μL of secondary antibody conjugated to horseradish peroxidase (HRP) for detection (Goat anti-Rat IgM-HRP or Goat anti-Rat IgG-HRP conjugate) in the conjugate diluent (50 mM Tris, 0.14 M NaCl, 1% BSA, 0.05% Tween 20, pH8.0) was transferred to each well. After incubation for 1 h at room temperature, the detection antibody was removed and the wells were washed five times with the wash solution. The enzyme assay was initiated by adding 3,3',5,5'-Tetramethylbenzidine substrate solution. After a 15 min incubation, the reaction was stopped by adding 100 μL of 0.18 M H_2SO_4 and the absorbance was measured at 450 nm using a microplate reader.

4.2.7 Determination of IgM levels in serum incubated with GNPs

125 μL PEG-GNPs or PCB-GNPs (1 mg mL-1) was incubated in 500 μL of serum derived from rats administered with PEG-GNPs at 37°C for 15min. GNPs was separated out of serum by centrifugation (13,200 rpm for 30 min). The IgM level of the supernatant was directly measured by ELISA as described above. The centrifuged aliquot was re-dispersed in PBS and centrifuged for two more times to remove unbound IgM. The final centrifuged pellet was dispersed in diluent solution (50 mM Tris, 0.14 M NaCl, 1% BSA, 0.05% Tween 20, pH 8.0) and the IgM level was measured by ELISA.

4.3 Results and Discussion

4.3.1 GNPs characterization

Size is an important parameter in the design of long-circulating NPs. The size should be large enough to avoid renal clearance[107], but not too large as to induce opsonization and MPS clearance[108]. Thus, comparisons are only useful between NP formulations of

similar sizes. PCB-GNPs were made by performing SI-ATRP off the GNPs. Since the ATRP initiator is hydrophobic while the CB monomer is hydrophilic, the hydrophobic CBMA-1-tBu monomer was chosen to graft well-controlled polymer brushes with high packing densities on GNPs in an organic solvent. Upon subsequent acid hydrolysis of the protected monomer, densely coated PCB-GNPs were achieved (Fig. 1b). The average hydrodynamic diameter was 40.2 nm, measured by dynamic light scattering based on intensity (DLS). Similar to the size of PCB-GNPs, the average hydrodynamic diameter of the corresponding PEG-GNPs is 39.8 nm.

It has been shown previously that the particles bearing a cationic or anionic surface charge can attract more phagocytes than neutral particles of the same size[96]. Thus, neutral PCB-GNPs and PEG-GNPs are preferable. To demonstrate this, PCB-GNPs and PEG-GNPs were suspended in phosphate-buffered saline (PBS) at a concentration of 1 mg/mL and monitored by DLS for surface zeta potential at different pH values. Zeta potential was found to be neutral for both PCB-GNPs (-0.09 mV) and PEG-GNPs (-0.08 mV) at pH 7.4 (**Figure 4.3a**). Moreover, GNPs coated with PEG and PCB were further studied in undiluted human plasma at 37 ℃. This was done by measuring the change in particle size over time using DLS. For PEG-GNPs, the diameter increased to 300 nm after the incubation period, indicating instability through protein adsorption and particulate aggregation (**Figure 4.3b**). The adsorption of proteins can increase the effective size of NPs, change their effective surface charges, and increase phagocyte uptake[18]. Meanwhile, the PCB-GNPs remained the same size over the incubation period, showing protection against aggregation afforded by the PCB coating. Since the opsonization of NPs leads to

their accelerated recognition, phagocytosis, and elimination, PCB-GNPs with no plasma opsonin adsorption will evade immune detection[23, 27].

4.3.2 *In vivo* circulation evaluation

We then investigated the *in vivo* circulation half-life of the PEG-GNPs and PCB-GNPs after repeated injections. In a clinical setting, repeated injections are often necessary, such as in the case of multiple courses of chemotherapy[21]. However, PEG suffers from the accelerated blood clearance (ABC) phenomenon. Dams et al. first reported that for multiple administrations of PEG liposomes in rats, the second dose showed a drastically reduced blood liposome content when compared to that of the first dose, from 52.6±3.7 to 0.6±0.1%[109]. This was evidence of the ABC phenomenon for PEG. There has been growing evidence showing that the ABC phenomenon not only affects the bioavailability of drugs, but targeting is also decreased[21].

From the pharmacokinetics analysis of PEG-GNPs and PCB-GNPs after repeated injections (**Figure 4.4 and Table 4.1**), PEG-GNPs were seen to stimulate the ABC phenomenon: the first dose of PEG-GNPs ($t_{1/2}$ = 8.7 hours) accelerated the clearance of the second dose ($t_{1/2}$ = 5.2 hours) given one week later. In contrast, the one-compartment circulation time of PCB-GNPs showed little change from $t_{1/2}$ = 55.8 hours to $t_{1/2}$ = 55.6 h (**Figure 4.4a and 4.4b**). A same trend was observed when the two-compartment model was applied (**Figure 4.4c and 4.4d**). These results show how PCB coatings are able to provide long circulation times to NPs and also prevent induction of the ABC phenomenon (**Figure 4.1**). We believe the stealth characteristics of PCB come from mimicking the ionic natural chemistry found on the surface of proteins[11]. Previous studies have also shown that by using mechanobiological mimicry of red blood cells (RBCs),

elimination half-life was improved[110]. In another study, RBC membrane-camouflaged polymeric NPs were used to extend circulating time[22].

4.3.3 Quantification of antibody production

Since it was suggested that the production of anti-PEG antibodies is responsible for the ABC phenomenon[21], we measured IgM and immunoglobulin G (IgG) levels after the first and second injections, respectively. Previous research studied IgM production as a function of time after injection and found that the IgM level reached peaked after 5 days[111]. Another study also showed that the IgG level continues to increase with additional injections[112]. IgG production, which is dependent on IgM stimulation, is a secondary and more effective immune response to foreign materials in the body. Based on these studies, we tested IgM levels 5 days after a single injection (Group 1), and IgG levels 12 days after two injections (Group 2), with a second injection administered 7 days after the first injection. These results are summarized in **Figure 4.5**. Blood sampling from control groups were used to establish baseline antibody levels. IgM levels in rats that received PEG-GNPs were 13.9 times higher than baseline levels. The same trend was seen for IgG, which was 3.8-fold higher than the baseline. In contrast, the effect of administering PCB-GNPs showed no noticeable increase in either IgM or IgG. As shown in the insets of Fig. 3, the changes in level of IgM and IgG from PCB-GNPs were almost zero after subtracting baseline levels. These results show how PCB coatings, through their stealth properties, can avoid stimulation of the adaptive immune system, observed by the lack of IgM and IgG antibody productions.

4.3.4 Biodistribution of GNPs

To further investigate how the GNPs were cleared from circulation, biodistribution studies were performed. **Figure 4.6** shows the GNPs accumulation in each organ as a percent of the total administered dose 5 days after a single injection (Group 1). It can be observed that the majority the NPs were either found in the blood or the liver. The majority of the PEG-GNPs were found in the liver, as is often observed with NPs. While some PCB-GNPs were also found in the liver, a large portion was still found in the blood. Group 2, after euthanasia, was also evaluated for biodistribution, but this involved two injections over a 12-day period. This data can be seen in **Figure 4.6** as a percent of the sum of both doses. Similar to Group 1, there was a significant amount of PCB-GNPs still in the blood, but this time no detectable PEG-GNPs. The ABC phenomenon was observed by the absence of PEG-GNPs in the blood after the second injection. This is the most compelling evidence showing the clinical potential of PCB coatings for injectable, long circulating NPs.

4.3.5 Determination of serum proteins associated with GNPs

Finally, to determine whether IgM generated in rats administered with PEG-GNPs specifically binds to PEG, PEG-GNPs and PCB-GNPs were incubated separately in serum derived from these rats and levels of IgM bound to each of GNPs were measured (**Figure 4.7**). When serum incubated with PEG-GNPs was centrifuged to pellet the GNPs, some IgM is present in the supernatant, representing the nonspecific IgM not bound to PEG-GNPs and a larger amount is present in the pellet due to binding with PEG-GNPs prior to centrifugation. On the other hand, when serum incubated with PCB-GNPs was centrifuged, the majority of IgM antibody remains in the supernatants with some present in the pellet but not at a significant level. What appears to be missing

between the total antibody concentration between the no-GNP control and the PEG-GNP and PCB-GNP tests would be loss due to repeated centrifugation steps not done in the control. This supports the idea that the elevated IgM present in test rats subjected to PEG-GNPs was induced by PEG-GNPs and selectively binds to PEG.

4.4 Conclusions

In summary, we demonstrated that zwitterionic nanomaterials can prevent the production of polymer-specific antibodies while maintaining long circulation, even after repeated injections. Our findings emphasize the importance of extremely low fouling[3], stealth PCB coatings with high packing densities for avoiding the ABC phenomenon. It should be noted that avoiding this mechanism of adaptive clearance is a major hurdle for practical use of nanomedicine in a clinical setting. The majority of reported injectable NPs rarely address this issue due to its difficulty. This PCB surface material exhibits superior *in vivo* performance over its PEG counterpart, including extremely low antibody response, along with prolonged residence time in blood, thus demonstrating its great potential as a robust coating for drug delivery and diagnostic platforms.

4.5 Chapter Figures

Table 4.1 Pharmacokinetics analysis of PEG-GNPs and PCB-GNPs after repeated injections

Injections	Samples	One-compartment model (h)	Two-compartment model (h)	
			Distribution half-life	Elimination half-life
First dose	PCB-GNPs	55.78	5.40	243.89
	PEG-GNPs	8.65	3.53	10.69
Second dose	PCB-GNPs	55.57	4.59	268.04
	PEG-GNPs	5.21	2.10	8.21

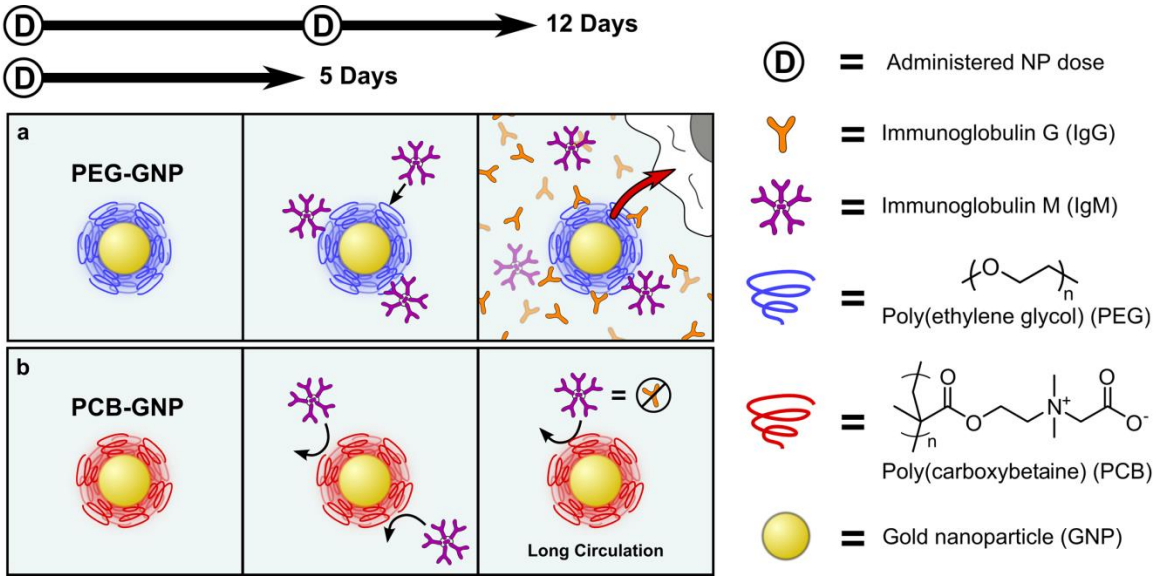

Figure 4.1 Schematic illustrations of the sequence of events after PEG-GNPs and PCB-GNPs enter the blood stream. a, PEG-GNPs, anti-PEG IgM, produced from spleen in response to an injected dose of PEG-GNPs, selectively binds to the PEG on a second dose of these GNPs, injected several days later, and subsequently activates the complement system; b, PCB-GNPs, extreme low fouling stealth PCB coating effectively shield NPs from nonspecific opsonins adsorption and immune response, leading to long-circulating NPs with zero immune response.

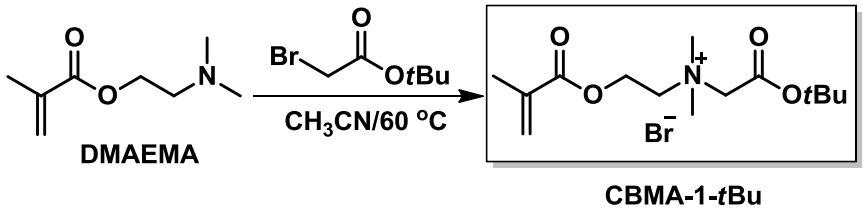

Figure 4.2 Synthesis route of carboxybetaine-1-methacrylate tert-butyl ester (CBMA-1-tBu).

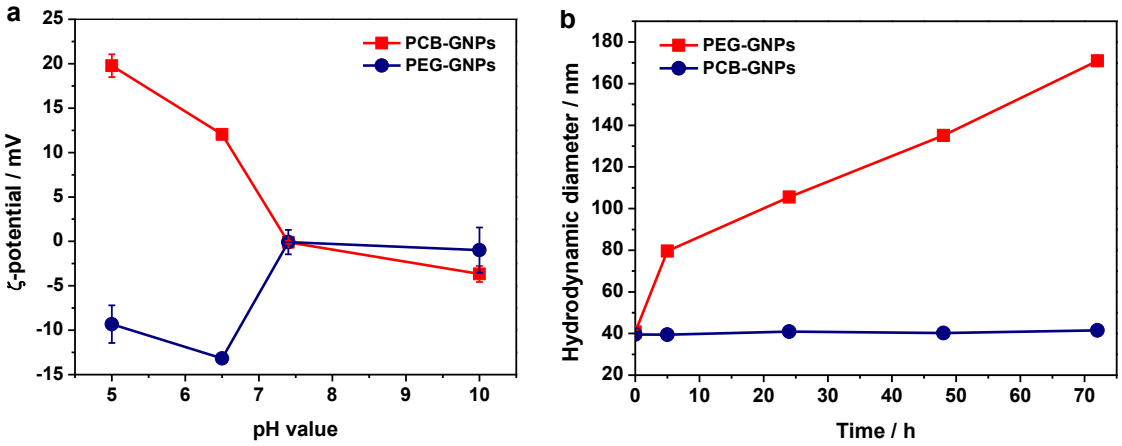

Figure 4.3 Structural characterization and stability of PCB-GNPs and PEG-GNPs. (a), DLS measurements of surface zeta potential of the nanoparticles over in different pH range; **(**b), Hydrodynamic size change of PCB-GNPs and PEG-GNPs incubated in 100% human blood plasma at 37 ℃ for 72 h.

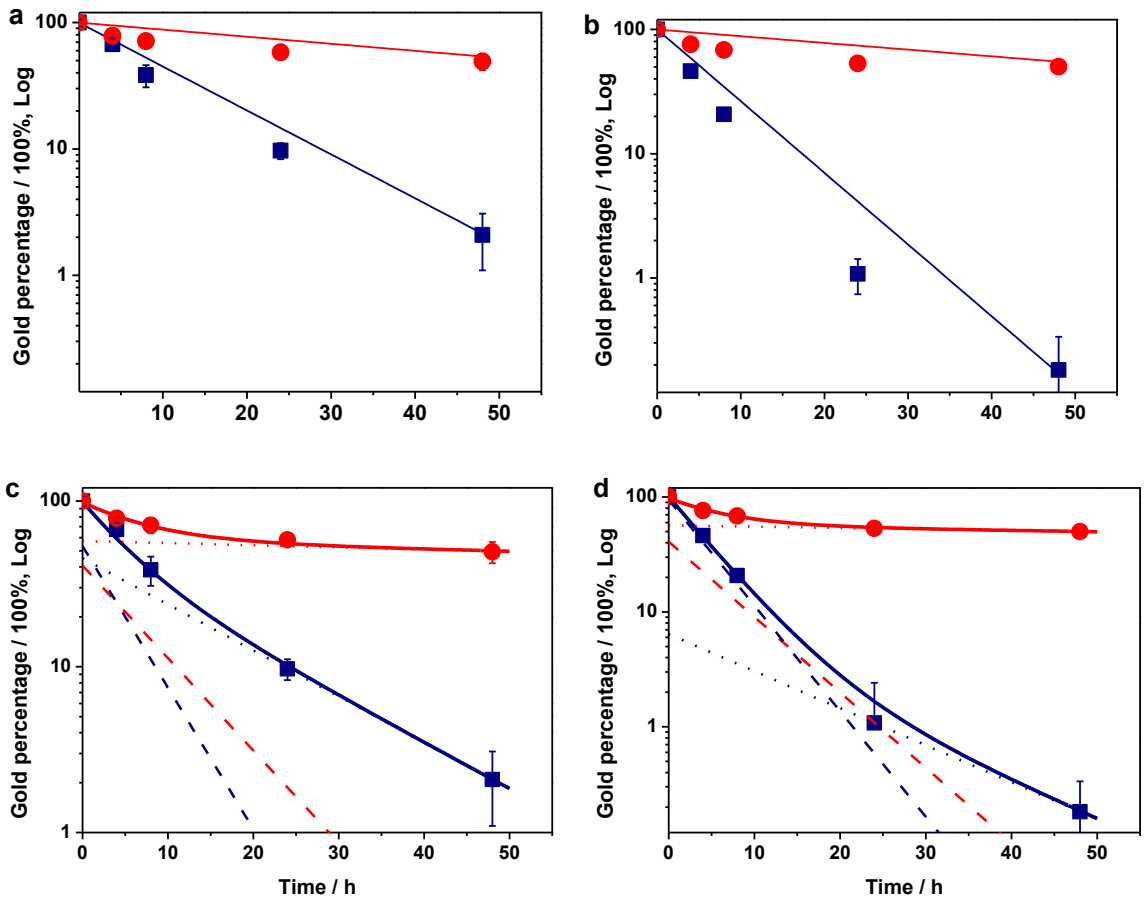

Figure 4.4 *In vivo* circulation time of the GNPs after the first and second administrations based on one-compartment model and two-compartment model. (a), (b), Blood clearance profile of the first and second dose of PCB-coated GNPs (red circle) and PEG-coated GNPs (blue square) based on one-compartment model, respectively. (c), (d), Blood clearance profile of the first and second dose of PCB-coated GNPs (red circle) and PEG-coated GNPs (blue square) based on two-compartment model, respectively. The solid lines are curves fitted to a two-compartment model. Dash lines and dot lines present the distribution phase and elimination phase, respectively.

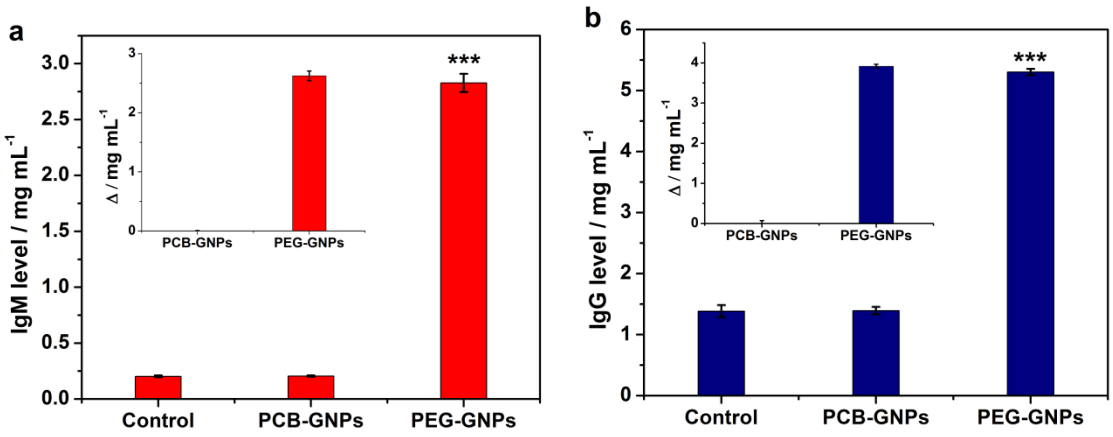

Figure 4.5 IgM and IgG levels following one and two intravenous injections of PBS or GNPs in rats. (a), IgM levels after the first injection; (b), IgG levels after the second injection. The insets are plots when the antibody level of control group with PBS is subtracted.100 μL of each GNP sample was administered into the rat via tail vein injection. Control animals received PBS instead of GNPs. Blood was taken on the fifth day after the first and second injections for IgM and IgG measurements, respectively. Blood sampling from control group was used to establish baseline antibody level for each rat. IgM (red bar) and IgG (blue bar) were detected using ELISA. Each value represents the mean ± S.D. of six animals from each sample. P values apply to differences against the control with $P<0.05$ being considered as statistically significant. *$P<0.05$, **$P<0.01$, ***$P<0.001$, two-tailed unpaired Student t test.

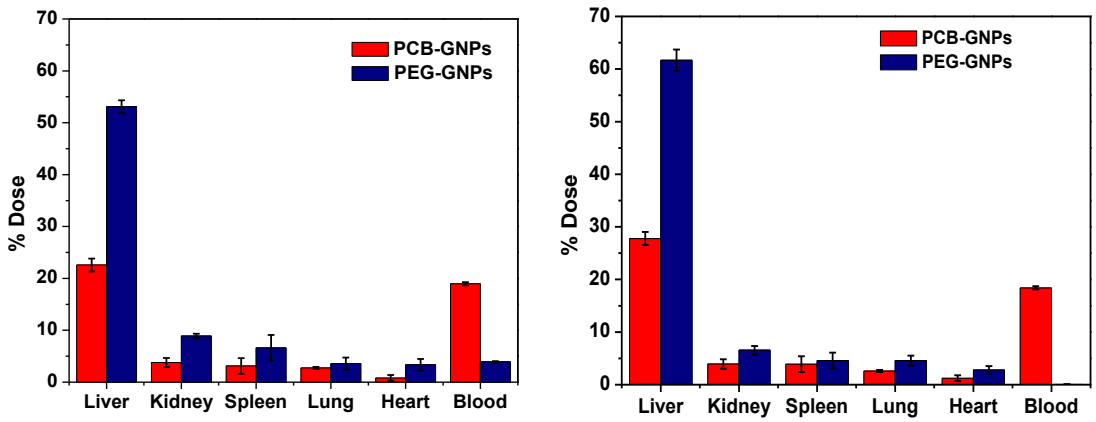

Figure 4.6 Biodistribution of the PEG-GNPs and PCB-GNPs after the first injection. GNPs were injected intravenously into the rats. On the fifth day after the first and second injection, the organs from all groups of rats were collected, digested in aqua regia, and analyzed by ICP-MS. GNP accumulation in each organ is normalized to the total dose after the first injections. Each value is averaged from 6 rats. Standard deviations are shown as error bars.

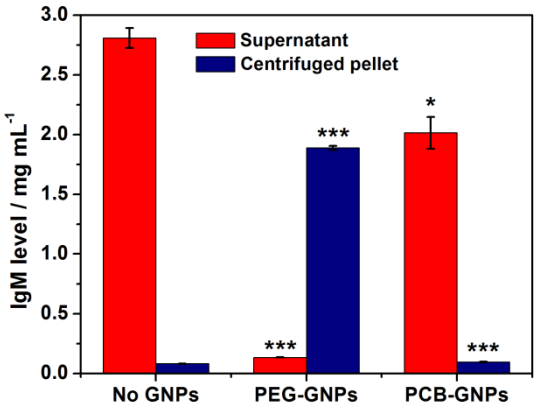

Figure 4.7 IgM levels in serum incubated with GNPs. PEG-GNPs or PCB-GNPs were incubated in serum collected from rats administered with PEG-GNPs to allow IgM association and binding. They were separated from serum by centrifugation and IgM levels in the supernatant or the pellets containing GNPs were determined by ELISA. Each value represents the mean ± S.D. of three separate samples. P values apply to differences from serum with no GNP incubation with $P<0.05$ being considered as statistically significant. *$P<0.05$, **$P<0.01$, ***$P<0.001$, two-tailed unpaired Student t test.

Chapter 5 Zwitterionic Polymer Surface Evades the Immune System and Enables Long Circulation

Avoiding blood clearance is a major hurdle faced by everyone working on the practical use of nanomaterials for drug delivery and diagnostics in a clinical setting. An even greater challenge is to avoid the eventual development of antibodies by the adaptive immune system. Here, we prepared PCB and PEGMA coated GNPs with same packing density and compared the *in vivo* performance. Results show that the PCB coating can achieve a consistent prolonged *in vivo* circulation half-life of ~58 hours after three repeated injections without any antibody production. These findings are significant advances toward solving the long-standing clinical challenge of developing nanomaterials that are able to resist both immune response and immediate bodily clearance.

5.1 Introduction

Immunogenicity, antigenicity, toxicity, and rapid renal clearance of exogenous therapeutic agents are critical concerns for the pharmaceutical industry[98]. With the recent advancements in nanotechnology, numerous strategies have been implemented to enable nanoparticle immune evasion[113]. PEG functionalization is the most widely adopted immune evasion strategy. These polymers hide the nanoparticles behind a hydration layer and reduce their immune clearance[113, 114]. However, the circulation half-life times of PEG are limited to 8 to 10 hours. To make things worse, recent observation of anti-PEG immunological response has triggered the interest of further investigation on its

biological relevance[22]. Clinical study has shown that the body will clear out PEGylated enzymes at a very fast rate in individuals with anti-PEG antibodies[98]. Recently, a new strategy for synthesizing biomimetic nanoparticles has been inspired by the body's own long-circulating entities, red blood cells (RBCs). The non-immunogenic nature of RBC membranes allow the immune system to selectively process the toxin cargoes while ignoring the rest of the nanoparticle carrier[115].

Previously, we have shown that PCB-based nanomaterials do not induce polymer-specific antibodies production, while PEG-coated NPs generated PEG-specific antibodies [116]. In order to compare with the literature, PEG_{5000}-GNPs were used as a positive control since PEG-GNPs have been studied extensively and results are all consistent in two aspects: (a) circulation half-life times are around 8 to 10 hours and (b) all lead to significant antibody production. Thus, we decided to focus on gold nanoparticles for these proof-of-concept experiments. The PEG-GNP results we got are consistent to those reported in many publications before[21, 117]. Previous studies have provided evidence for the induction of anti-PEG antibodies in rabbits exposed to methoxyPEG (mPEG) conjugates of proteins[118] and for the presence of anti-PEG antibodies in the sera of a small percentage of healthy blood donors[119, 120]. Recent study has shown that antibodies with high affinity for methoxy groups contribute to the loss of efficacy of mPEG conjugates, especially if multiply-PEGylated[116]. Thus, using monofunctionally activated PEG with hydroxyl group instead of mPEG in preparing conjugates for clinical use is recommended to decrease the undesirable effect raised by immunogenicity[119]. Based on these findings, poly(ethylene glycol) monomethacrylate (PEGMA) with hydroxyl groups

with same density will be used a control to decorate the surfaces of GNPs via ATRP method.

Another improvement is the extended time frame in this work. In the previous work, the circulation half-time, immune response test, and biodistribution studies for PCB- and PEG-GNPs with repeated injections for a maximum of two times has been tested. Since these particles have such extended circulation times relative to PEG particles, any immune response that occurs may be similarly delayed relative to the PEG particles. Thus, in order to confirm that PCB-coated NPs are able to completely abrogate the immunogenicity, the number of repeated injections is extended from 2 to 5 weeks. We hypothesize that NPs protected by PCB materials will possess superior performance over PEGMA with hydroxyl group after extended injection time.

5.2 Materials and Methods

5.2.1 Materials

Poly(ethylene glycol) monomethacrylate macromonomer (PEGMA, n=6, Mn ~360 g/mol) and 2,2 ´-bipyridine (BPY) were purchased from Sigma-Aldrich (St. Louis, MO). Diamedix EZ Complement CH50 test was purchased from Diamedix Corporation. Osmium tetroxide solution (OsO_4, 4%), uranyl acetate (1%), lead citrate, and Embed 812 embedding kit were purchase from VWR (Visalta, CA). Glutaraldehyde solution (50%) was purchased from Electron Microscopy Sciences (Hatfield, PA). Neutral buffered formalin (10%) was purchase from Fisher Scientific (Fair Lawn, NJ),

5.2.2 Preparation of PEGMA-GNPs via ATRP.

The synthesis of PEGMA coated GNPs is shown in **Scheme 5.1**. In a typical reaction, 2.2 mg Cu(I)Br and 4.5 mg BPY were placed into a Schlenk tube and subjected to three

vacuum-nitrogen cycles. Then, 1.7 mL of degassed DMF and 0.8 mL of degased methanol was added and the content was purged with N_2 before 0.5 mL of PEGMA was added to the flask via syringe. The reaction mixture was thoroughly purged with N_2 for an additional 15 min. In another und bottom reactor, 1 mL of initiator ($Br(CH_3)_2COO(CH_2)_{11}SH$) coated GNPs in DMF were deoxygenated by bubbling N_2 for 15 min. The ATRP reaction was then initiated by introducing the degassed catalyst solution under N_2. After reaction was stirred at 750 rpm and 50 ℃ for 24 h, the PCB-GNPs were precipitated in ethyl ether and collected by centrifugation. Then the product was dispersed in deionized water, and other impurities including residual monomers, initiators, and catalysts were removed by using a 100 kDa molecular weight cutoff Amicon Ultra centrifugal filter. The polymer-modified GNPs were collected by centrifugation and redispersed in PBS before further use, yielding a dark red solution.

5.2.3 Animal studies.

The *in vivo* antibody production, circulation time, and biodistribution of GNPs were studied using Spraque Dawley rats (body weight ~150 g) as the animal model. Each GNP sample was studies in six duplicates to generate statistical significance. All animal experiments adhered to federal guidelines and were approved by the University of Washington Animal Care and Use Committee. Two groups of rats were formed. For Group 1 rats, which received one injection, the GNPs (PEGMA-GNPs or PCB-GNPs) were administered via the tail vein at a dose of 1 mg/kg body weight under anesthesia and sterile treatment. Control animals received PBS instead of GNPs. To study the *in vivo* circulation time, at 5 min, 4 h, 8 h, 24 h, and 48h after the injection, a 50 μL blood sample was collected, digested, and analyzed by ICP-MS. At Day 5, 5 mL of blood were

drawn by heart punch and serum was prepared for IgM and IgG measurement. Biodistribution was assessed after the animals were euthanized by CO_2 inhalation, where organs (heart, liver, spleen, lung, and kidneys) were collected, digested in aqua regia, and analyzed by ICP-MS.

For Group 2 rats, which received two injections, PEG-GNPs or PCB-GNPs were administered intravenously at a dose of 1mg/kg body weight 7 days apart (Day 1 and Day 8). Control animals received PBS instead of GNPs for both injections. On the twelfth day after the second injection (Day 19), 5 mL of blood were drawn for IgM and IgG measurement. The *in vivo* circulation time and biodistribution tests were performed the same as in Group 1.

For Group 3, which received three injections, the first and second dose was injected in a same way as Group 2 and the third injection of PEG-GNPs or PCB-GNPs were administered intravenously at a dose of 1mg/kg body weight two weeks after the second one (Day 22). On the twelfth day after the third injection (Day 33), 5 mL of blood were drawn for IgM and IgG measurement. The *in vivo* circulation time and biodistribution tests were performed the same as in Group 1.

5.2.4 Determination of IgM and IgG levels with ELISA.

Using the 5 mL blood samples drawn as described in the previous section, serum samples were obtained by incubation for 30 min at room temperature followed by centrifugation at 3,000 rpm at 4 ℃ for 15 min. Relative quantification of IgM and IgG levels were performed using the Rat IgM ELISA Quantitation Kit and the Rat IgG ELISA Quantitation Kit.

5.2.5 TEM observation of liver tissue

The TEM observation of liver tissue was performed according to previous study[121]. One rat of each group (PEGMA-GNPs or PCB-GNPs administered along with control) was anaesthetised with Isoflurane. After the anaesthesia, random section of liver was cut and quickly fixed within 1% v/v glutaraldehyde in 0.1 M cacodylate buffer (pH 7.2) overnight, washed by the same buffer and subsequently post-fixed in 1% w/v OsO_4 for 30 min. After being washed with water, the samples were dehydrated in graded series of ethanol, transferred to propylene oxide and embedded in Epon-812. Ultrathin sections (70 to 80 nm) were cut, stained with uranyl acetate and lead citrate, and collected on copper meshwork. The sections were examined with a Transmission electron microscopy (TEM) (J.E.O.L. 1320).

5.2.6 Histological observation of liver

Histological observation of liver tissue was carried out following previous method[121]. After the scarification of rats at Day 5 (Group 1), Day 19 (Group 2) and Day 33 (Group 3), livers were collected and fixed in 10% neutral buffered formalin. After routine processing, samples were embedded into paraffin, sectioned into 4 μm, and stained with haematoxylin and eosin (H&E). The sections were examined using a microscopy (Olympus IX71).

5.2.7 Complement activation test

A slight modification of the Diamedix EZ Complement CH50 TEST (Diamedix Corporation) was used to test the complement activation[122]. Briefly, antibody-sensitized sheep erythrocytes were incubated (60 min, 37℃) with rat serum in gelatin Veronal buffer. Cells were centrifuged and hemoglobin release was measured (λ=415 nm).

Background was measured in the absence of sheep erythrocytes or in the absence of serum and subtracted from all samples.

5.3 Results and Discussion

5.3.1 Characterization

Size is an important parameter in the design of long-circulating NPs. Different reaction conditions such as catalyst ratio, reaction time, reaction temperature, and solvents were performed to prepare PEGMA-coated GNPs with similar size as PCB-GNPs (around 40 nm. Both PCB-GNPs were made by performing ATRP off the GNPs. Resulting NPs were suspended in PBS at a concentration of 1 mg/mL and then monitored by DLS for particle size and the polydispersity index. The average hydrodynamic diameter of the corresponding PEGMA and PCB-GNPs is 40.2 nm, and 39.6 nm, respectively. Over a span of one month the particle size did not change and the PDI remained relatively the same at 0.194, indicating that the GNPs after PEGMA or PCB coating is pretty stable over time.

5.3.2 *In vivo* circulation

We then tested the *in vivo* circulation half-life of the PEGMA-GNPs and PCB-GNPs after repeated injections. As shown in **Figure 5.1,** the PCB-coated GNPs had superior blood retention compared to the PEGMA-coated GNPs after each injection. At 48 hours after the first dose, PCB-GNPs exhibited 53% overall retention, as compared to 26% exhibited by the PEGMA-GNPs. Using a one-compartment model, the blood half-lives of PCB-GNPs and PEGMA-GNPs were 61.4 and 28.3 hours after the first dose. This is comparable to previous results of PEGMA-coated silicone dioxide NPs via SI-ATRP method[123]. Furthermore, the PEGMA-coated GNPs still suffer from the ABC

phenomenon. The blood half-life keeps on decreasing with repeated doses. The one compartment circulation time of PEGMA-GNPs is 28.3 h, 17.5 h, and 8.3 h after the first, second, and third injections, respectively. In contrast, that of PCB-GNPs showed little change from $t_{1/2}$ = 61.4 hours to $t_{1/2}$ = 56.0 hours. The ABC phenomenon was observed by the absence of PEG NPs in the blood after the second injection[21, 109]. Thus, the consistent circulation time after three doses is the most compelling evidence showing that the PCB coatings are able to provide long circulation times to NPs and also prevent induction of the ABC phenomenon. Previous studies have shown that T cell-independent B cell response is responsible for ABC phenomenon induced by repeated injection of PEGylated NPs[124]. Thus, we believe that PEGMA will still induce antibody production while the stealth characteristics of PCB will not.

5.3.3 Immune response measurement

Previous studies have shown that the production of anti-PEG antibodies is responsible for the ABC phenomenon[21], so we further tested the IgM and IgG levels 5 days after the first injection (Group 1), 12 days after the second injections (Group 2), and 12 days after the third injection. These results are summarized in **Figure 5.2**. Blood sampling from control groups were used to establish baseline antibody levels. Both IgM and IgG level of the control samples increase with injections. After the first injection, the IgM levels in rats that received PEG-GNPs were 11.5 times higher than baseline levels. There is no significant change of the IgM level after the second and third injections, indication that IgM level has reached the peak after the first injection. This result is consistent with previous studies that IgM level reached the maximum after 5 days[111]. Similar trend was observed for IgG, which was 2.2-fold higher than the baseline after the first injection.

However, the IgG level keeps increasing with repeated injections. There is 2.5 times of increase compared to the one after the first injections. Previous research also showed that the IgG level continues to increase with additional injections[112]. In contrast, the effect of administering PCB-GNPs showed no noticeable increase in either IgM or IgG after each injection. Again, the lack of IgM and IgG antibody productions indicates that the PCB coatings can avoid stimulation of the adaptive immune system.

5.3.4 Biodistribution evaluation

Biodistribution studies were performed to further investigate how the GNPs were cleared from circulation. The major organs responsible for removing nanoparticles including liver, spleen, lung, heart, kidney, and blood were collected. **Figure 5.3** shows the GNPs accumulation in each organ as a percent of the total administered dose. It is clear that non-targeted organs such as the kidneys, lung, and heart possess relatively low elimination of the GNPs whereas the accumulation of GNPs in liver and spleen is high for both PEGMA-GNPs and PCB-GNPs. The percentages of retained nanoparticles in the liver and spleen at 5 days post-treatment of the first injection ranged from 43.1% to 21.3% and from 10.0% to 6.1% for PEGMA-GNPs and PCB-GNPs, respectively. Similarly, the majority of the PEGMA-GNPs were found in the liver, as is often observed with NPs[125]. On the contrast, a large portion was still found in the blood even though there is some PCB-GNPs in the liver. Laverman et al. have proposed that it is hepatosplenic macrophages that are responsible for the production of opsonin(s) in response to the uptake of the first dose[125, 126]. We also tested the biodistribution of Group 2 and Group 3 after euthanasia. Both of them involved two or three injections. This data can be seen in **Figure 5.3b** and **Figure 5.3c** as a percent of the sum of two or three doses. Similar to

Group 1, there was a significant amount of PCB-GNPs still in blood, 15% and 12% for Group 2 and Group 3, respectively. However, the percentage of PEGMA-GNPs in blood was pretty low and there was no detectable PEGMA-GNPs in blood 12 days after the third dose. We noticed that the calculated recovery of GNPs is less than 100% for both PEGMA-GNPs and PCB-GNPs. The missing percentage of dose is accounted for by the carcass, skin, limbs, urine, etc as shown in the previous studies[127]. The organs measured in this work account for enough of the injected GNPs to support the conclusions.

5.3.5 Histological observation of liver

Intracellular localization of PCB- or PEGMA-GNPs *in vivo* can be clearly observed from the ultrathin TEM section images of livers. As shown in **Figure 5.4**, due to strong phagocytosis process, the GNPs accumulating in liver mainly located in phagolysosomes. Many NPs were also located in lysosomes, which indicated the pinocytosis of GNPs by the Kupffer cells also existed[128]. GNPs in cytosol were found, indicating that the polymer coating is able to help the GNPs to escape from lysosomes and accomplish cytosol delivery[128]. Additionally, there was no uptake in the nuclei, mitochondria, or the Golgi complex structures. The number of both PCB- and PEGMA-coated GNPs in the cells increased in a time dependent manner after treatment. However, the aggregate number of PCB-GNPs is significantly less than that of PEGMA-GNPs after each injection.

5.3.6 *In vivo* toxicity studies of GNPs

We then tested the H&E staining of the liver tissue sample. As shown in **Figure 5.6**, the apoptotic necrosis and acute inflammation in the liver occurs after the first injection of PEGMA-GNPs and they increased after the second and third injection of PEGMA-GNPs. At 12 days after the third injection, inflammation was significantly increased in

animals injected with PEGMA-GNPs. Previous study has shown that there are two phases of toxicity regarding inflammation in the liver[129]. One that is seen immediately after administration of nanoparticles and the second phase at 7 days when the particles disappeared from the circulation and localized in the tissues, primarily in the liver and spleen[129]. We did not find notable histological toxicity on the liver after the first and second intravenous injections of PCB-GNPs. But after the third injection, apoptotic necrosis of hepatocytes was present in all animals.

5.3.7 Complement activation

Finally, it is important to test the complement activation which may be activated without the presence of IgG or IgM (non-classical pathways). We investigated the effect of PEGMA- or PCB-GNPs treated serum on the classical pathways to further elucidate if the repeated injections of PEGMA- or PCB-GNPs will induce the complement activation. As can be seen in **Figure 5.7**, compared to PEGMA-GNPs treated serum, the PCB-treated serum did not induce lysis of antibody coated sensitized sheep erythrocytes in a CH50 hemolytic assay, indicating that the classical complement pathway was not induced by PCB-GNPs. This is in line with recent evidence showing that PEGylated liposomes are prone to opsonization by various serum proteins such as components of the complement system[125, 130].

5.4 Conclusions

In this work, we compared the *in vivo* performance of PCB-GNPs to PEGMA-GNPs via ATRP method. PCB-GNPs possess consistent blood half-life after three injections while PEGMA-GNPs still suffer from ABC phenomenon. Non-classic and classic pathway of immune response test indicates that PCB surface can highly resist

immunogenicity. Further biodistribution and hislogical test confirm that PEGMA-GNPs induced significant hepatic accumulation. These results strongly suggest that the PCB surface modification can serve as an effective strategy to form an ultrastable nanolayer on materials and improve their biocompatibility for *in vivo* application.

5.5 Chapter Figures

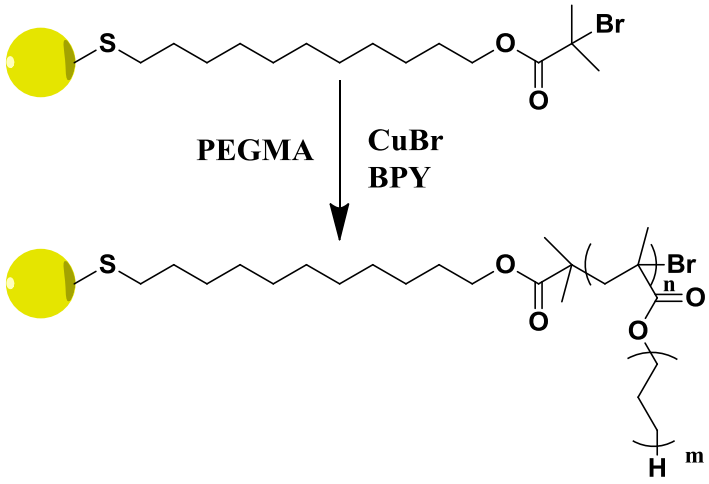

Scheme 5.1 Synthesis scheme of PEGMA-GNPs.

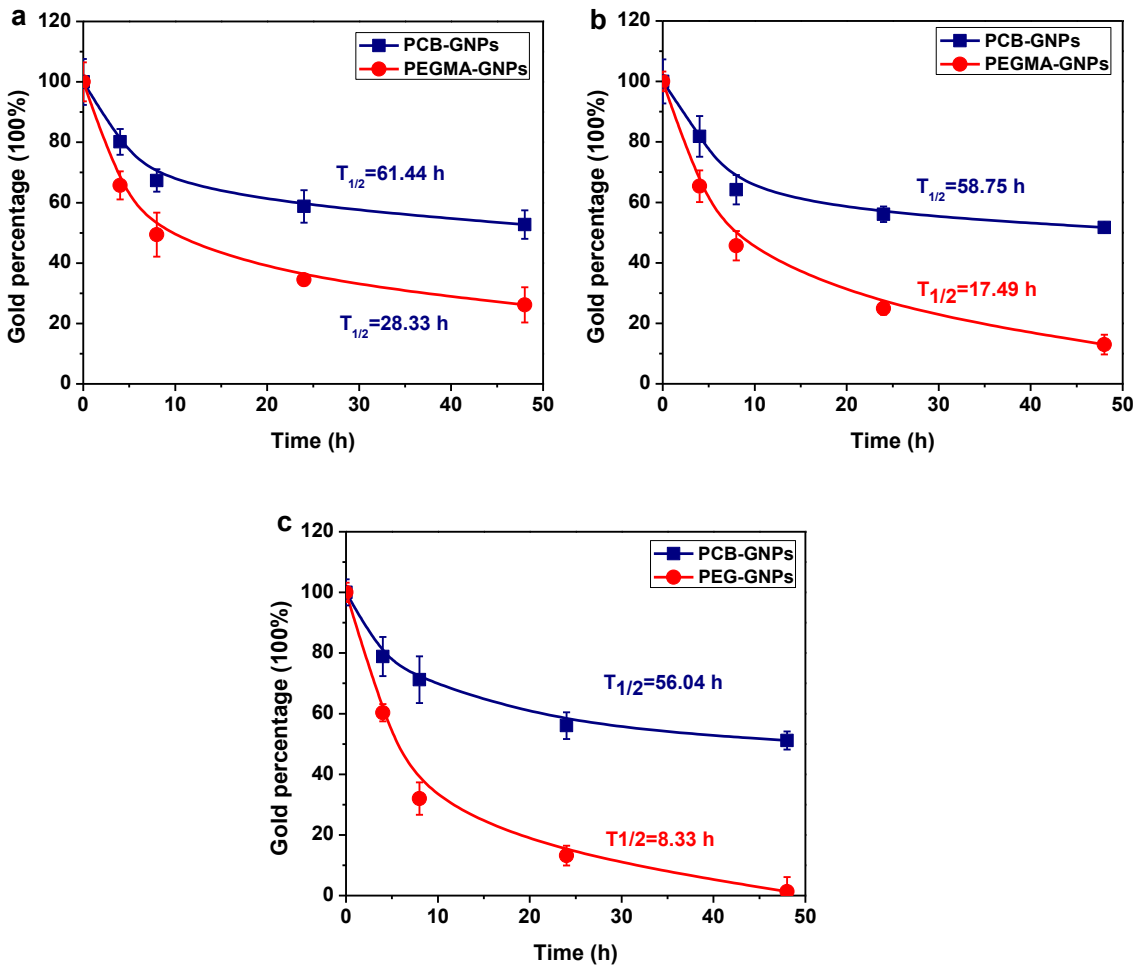

Figure 5.1 *In vivo* circulation time of the GNPs after the first, second, and third dose administration. (a), (b), (c), Blood clearance of first, second, and third dose of PEG-coated GNPs (red dot) and PCB-coated GNPs (blue square), respectively. The GNPs, at a dose of 1mg/kg body weight, are injected intravenously through the tail vein of rats. At various time points blood samples are taken from tail nick or lateral tail vein and measured for gold concentration with ICP-MS to evaluate the systemic circulation lifetime of the nanoparticles. Each value is averaged from 6 rats. Standard deviations are shown as error bars.

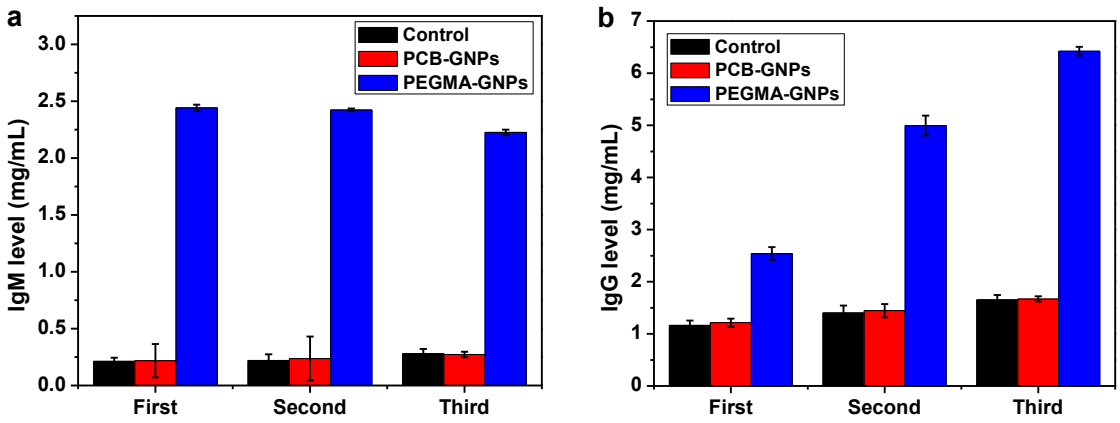

Figure 5.2 IgM and IgG levels following one and two intravenous injections of PBS or GNPs in rats. (a) and (b), IgM and IgG levels after each injection. 100 μL of each GNP sample was administered into the rat via tail vein injection. Control animals received PBS instead of GNPs. Blood was taken on the fifth day after the first and second injections for IgM and IgG measurements, respectively. Blood sampling from control group was used to establish baseline antibody level for each rat. IgM (red bar) and IgG (blue bar) were detected using ELISA. Each value represents the mean ± S.D. of six animals from each sample.

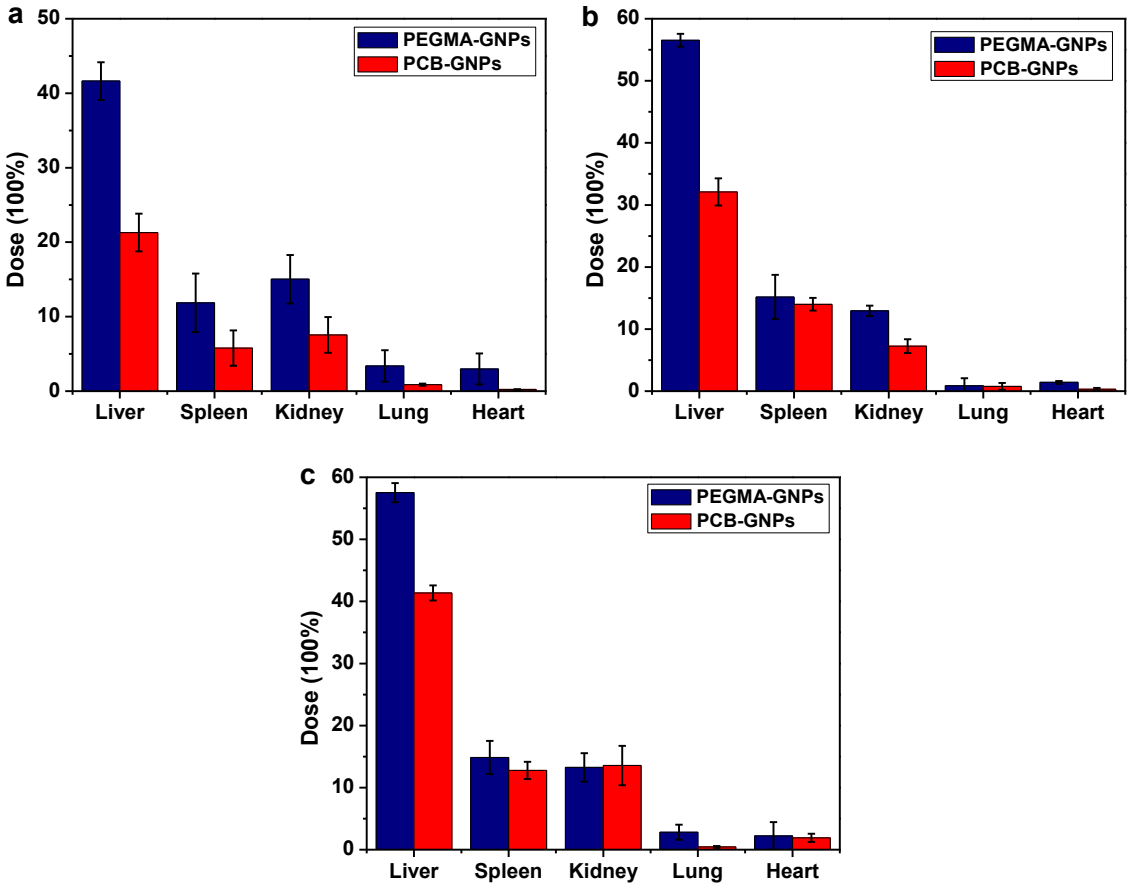

Figure 5.3 Biodistribution of the PEG-GNPs and PCB-GNPs after each injection. GNPs were injected intravenously into the rats. On the fifth day after the first injection and on the twelfth day after the second and third injection, the organs from all groups of rats were collected, lysed in aqua regia, and analyzed by ICP-MS.

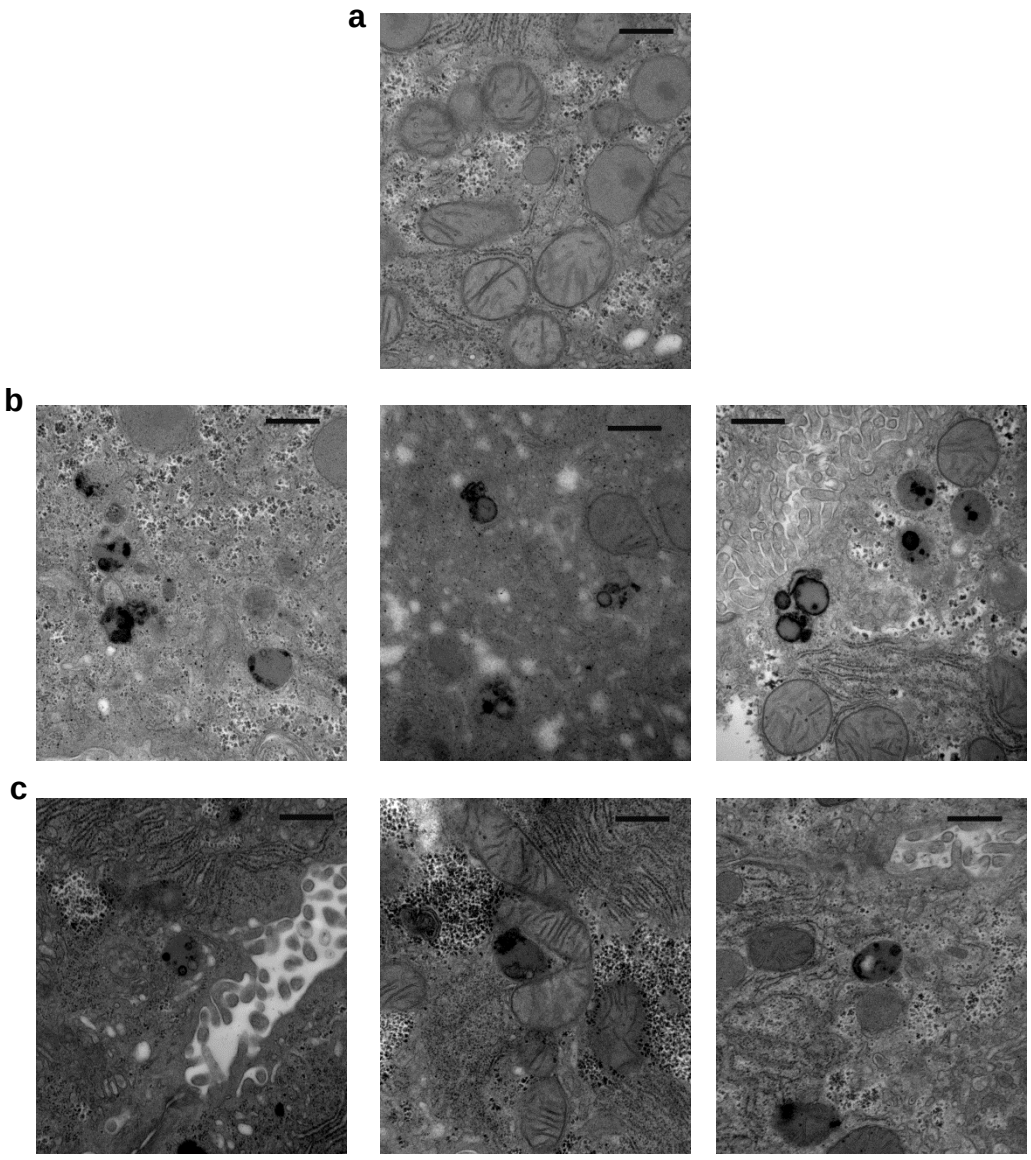

Figure 5.4 TEM images of rat liver tissues after intravenous injection of PCB- or PEGMA-GNPs. The micrographs show entrapped GNPs, and their clustering and localization in intracellular organelles (a), Liver tissue images of rat injected with PBS. (b) and (c), Liver tissue images of rat injected with PEGMA-GNPs or PCB-GNPs after the first (left), second (middle), and third doses (right), respectively. Magnification: 50000 ×, Scale bar is 500 nm.

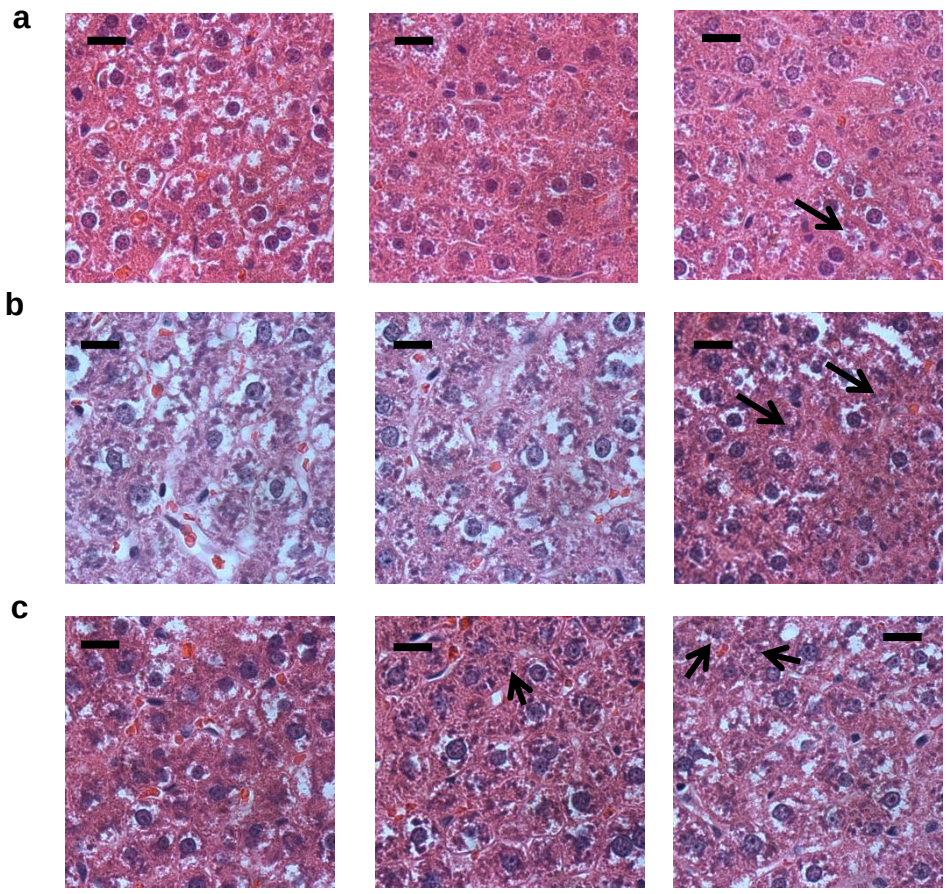

Figure 5.5 Histopathology images of rat livers following an intravenous injection of PBS, PEGMA-GNPs or PCB-GNPs via a tail vein. Representative liver sections of control rats (left), PCB-treated rats (middle) or PEGMA-treated rats (right) receiving one injection (a), two injections (b) and three injections (c), respectively. Hematoxylin and eosin stain. Arrows show the apoptotic necrosis of hepatocytes. (Magnification: 100 ×, Scale bar: 50 μm.)

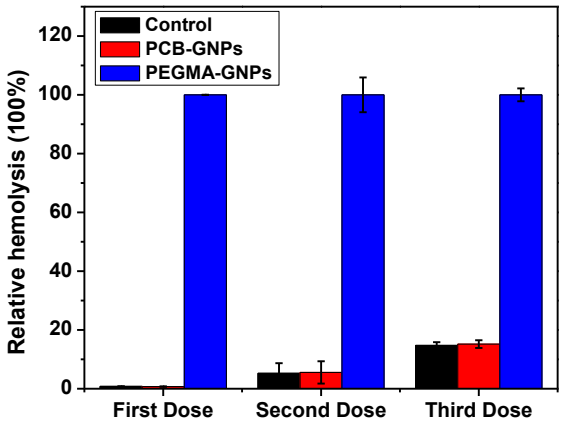

Figure 5.6 Complement activation induced by GNPs normalized by the absorbance of serum treated with PEGMA-GNPs after each injection. The values represent the mean ± S.D. of six independent experiments.

Chapter 6 Crosslinked Carboxybetaine SAMs Enable Nanoparticles with Remarkable Stability in Complex Media

A photo-crosslinkable carboxybetaine (CB)-terminated thiol with only one CB head group was introduced to modify gold nanoparticles (GNPs) via self-assembled monolayers (SAMs). This CB-terminated thiol consists of three moieties – (a) an anchoring thiol group, which binds directly to the GNP surface, (b) a CB terminal group, which is highly resistant to protein adsorption, and (c) a diacetylene group in the middle, which is converted to a poly(enyne) structure during UV-irradiation via 1,4-topochemical polymerization. Results show that after crosslinking, CB-modified GNPs are highly resistant to protein adsorption from undiluted human blood serum and cell uptake, and are stable at low pH and high temperature. This crosslinkable CB thiol holds tremendous potentials for biomedical applications where stable and thin coatings are needed.

6.1 Introduction

In the past two decades, nanoparticle-based biotechnology has been introduced for the treatment of cancer, pain and infectious diseases[131]. For practical applications, one of the largest obstacles is nonspecific protein adsorption from complex media, which can result in cellular uptake, nanoparticle aggregation, immune response and other disastrous problems. There is a significant lack of versatile and effective nonfouling materials and coatings for many nanoparticle-based applications[4, 29, 30]. Polyethylene glycol (PEG) has been the most widely studied polymer so far to create a steric barrier around nanoparticles to prevent nonspecific adsorption from complex media[23, 131]. However,

PEG is subject to oxidation in the presence of oxygen and transition metal ions[6, 33]. We have shown that zwitterionic materials such as sulfobetaine, carboxybetaine (CB), and mixed charge materials are highly resistant to nonspecific protein adsorption[101]. Previously, we have applied poly(carboxybetaine) polymers to coat iron oxide[132] or gold nanoparticles[73] (GNPs) via a "graft-to" or "graft-from" method, showing their excellent stability in complex media in both cases. We have also shown that superhydrophilic poly(carboxybetaine) is superior to amphiphilic PEG to protect nanoparticles or proteins in undiluted blood plasma and serum[133]. However, it is still very challenging to create thin coatings, for example with only one CB group, stable in complex media.

Since the first report of diacetylene polymerization in the solid state, diacetylene derivatives have attracted much attention owing to their physical, chemical and materials properties[134, 135] The enormous interest in diacetylene derivatives arises from the highly conjugated eneyne backbone and tailored side chains that lead to intriguing optical and electronic properties. It is promising in many potential applications[134] such as nonlinear optical materials[136], ultrathin photoresists[137], semiconductors and photoconductors[138] and biomimetic liposome for drug delivery[139]. Diacetylene derivatives can be obtained by the topochemical polymerization of monomeric diacetylenes in different forms[140] including self-assembled monolayers (SAMs) in order to achieve stable diacetylene thin films[134, 141, 142]. Incorporation of conjugated diacetylene groups within thiol or disulfide compounds has led to the formation of the conjugated polydiacetylene backbone structure, which can be initiated by photoirradiation or thermal treatment[143]. Recently, diacetylene derivatives have also been used to cap nanoparticles[135, 140, 144, 145]. Previous studies have shown that a crosslinked shell protected the GNPs from aggregation at high temperatures[105]. However,

most of these studies focus on polymerization conditions or structure changes; only a few are studies of nanoparticle (NP) stability. Moreover, NPs are commonly tested for their stability in saline solutions rather than undiluted human blood serum[145]. Previous studies show that undiluted human blood serum are far more challenging than single protein solutions or diluted blood serum for surface coatings[146]. Thus, in this work, undiluted human serum is utilized to challenge the nanoparticles.

The use of GNPs for biological applications such as *in vivo* diagnosis[147], drug delivery[148], and bio-sensing[149] is a growing field[150]. For practical applications, it is important to modify the surface of GNPs to improve their biocompatibility and colloidal stability in complex media[151]. Our previous studies show the excellent stability of GNPs grafted with PCB polymers via "graft-to" or "graft-from" methods. The objective of this work is to examine if a crosslinkable CB thiol with only one CB head group is sufficient to create a stable thin coating, which is desirable for such applications as quantum dots, but poses great challenges for its stability in complex media. Herein, a photo-crosslinkable CB-terminated thiol will be used to modify GNPs via SAMs. CB-terminated thiol consists of three moieties – (a) an anchoring thiol group, which binds directly to the GNP surface, (b) a CB terminal group, which is highly resistant to nonspecific protein adsorption, and (c) a diacetylene group in the middle, which is converted to a poly(enyne) structure during UV irradiation via 1,4-topochemical polymerization. This surface will create a stable thin coating in complex media.

6.2 Materials and Methods

6.2.1 Chemicals.

Pooled human blood serum was purchased from BioChemed Services (Winchester, VA). Dulbecco's modified Eagle's medium (DMEM), fetal bovine serum (FBS), and penicillin–streptomycin were purchased from Invitrogen Corp (Carlsbad, CA). Ethyl acetate and hydrochloric acid were purchased from Mallinckrodt Baker Inc (Phillipsburg, NJ). Docosa-10,12-diynedioic acid, sulfuric acid, tetrahydrofuran, methanol, lithium hydroxide, sodium sulfate, sodium citrate, N,N-dimethyl-ethylenediamine, dichloromethane, $HAuCl_4$, N,N-dimethylformamide, N-ethyl-N'-(3-diethylaminopropyl) carbodiimide hydrochloride (EDC), N,N-diisopropylethylamine (DIPEA), acetone, β-propiolactone, were purchased from Sigma–Aldrich (Milwaukee, WI). Hexane, sodium bicarbonate, sodium phosphate monobasic, sodium phosphate dibasic, sodium hydroxide, and diethyl ether were purchase from J. T. Baker (Center Valley, PA). 1-Hydroxybenzotriazole (HOBt) hydrate was purchased from Oakwood Products Inc (West Columbia, SC). Phosphate-buffered saline (PBS, 0.01 M phosphate, 0.138 M sodium chloride, 0.0027 M potassium chloride, pH 7.4) was purchased from Sigma Chemical Co. Ethanol (absolute 200 proof) was purchased from AAPER Alcohol and Chemical Co. Water used in these experiments was purified using a Milliporewater purification system with a minimum resistivity of 18.0 MΩ cm.

6.2.2 Dimethyl-docosa-10,12-diynedioate (2).

Docosa-10,12-diynedioic acid (14.9 g, 41.1 mmol) and concentrated sulfuric acid (25.0 mL, 450 mmol) were dissolved in anhydrous methanol (250 mL). The solution was refluxed at 70 ℃ for 72 h after which the solvent was removed on the rotovap. The residue was dissolved in ethyl acetate (250 mL) and the organic phase was washed with H_2O (4 x 50 mL) and saturated sodium bicarbonate (2 x 50 mL). The organic phase was

dried over sodium sulfate, filtered and concentrated. The product was dried further under high vacuum to afford a light blue solid (15.8 g, 40.5 mmol). Yield: 99%. ^{1}H NMR (300 MHz, $CDCl_3$) δ (ppm): 3.66 (s, 6H), 2.29 (t, 4H, J = 7.6 Hz), 2.23 (t, 4H, J = 6.9 Hz), 1.61 (m, 4H), 1.50 (m, 4H), 1.29 (m, 16H). ^{13}C NMR (75 MHz, $CDCl_3$) δ (ppm): 174.2 (C=O, 2 carbons), 77.3 (2 carbons, CH_2-C≡C), 65.2 (2 carbons, -C≡C-C≡C-), 51.3 (2 carbons, $COOCH_3$), 33.9 (2 carbons, CH_2-$COOCH_3$), 29.0 (2 carbons, CH_2-$(CH_2)_3$-C=O), 28.9 (2 carbons, CH_2-$(CH_2)_2$-C=O), 28.8 (2 carbons, CH_2-$(CH_2)_4$-C=O), 28.6 (2 carbons, CH_2-CH_2-CH_2-C≡C), 28.2 (2 carbons, CH_2-CH_2-C≡C), 24.8 (2 carbons, CH_2-CH_2-C=O), 19.1 (2 carbons, CH_2-C≡C).

6.2.3 22-Methoxy-22-oxodocosa-10,12-diynoic Acid (3).

Dimethyl-docosa-10,12-diynedioate (15.8 g, 40.5 mmol) was dissolved in a 3:1:1 mixture of tetrahydrofuran (90 mL), methanol (30 mL) and water (30 mL). Lithium hydroxide (1.69 g, 40.3 mmol) was added to the solution, which was stirred at room temperature for 12 h. Methanol and tetrahydrofuran were evaporated on the rotovap and the remaining aqueous solution was washed twice with hexane. The aqueous solution was acidified to pH 1 with 6 N hydrochloric acid and the product was extracted with ethyl acetate (5 x 50 mL). The organic solution was dried over sodium sulfate, filtered and concentrated. The obtained residue was further concentrated under high vacuum to afford the pure product as a blue solid (7.61 g, 20.2 mmol). Yield: 50%. ^{1}H NMR (300 MHz, $CDCl_3$) δ (ppm): 3.63 (s, 3H), 2.31 (t, 2H, J = 7.5 Hz), 2.27 (t, 2H, J = 7.5 Hz), 2.20 (t, 4H, J = 6.9 Hz), 1.58 (m, 4H), 1.47 (m, 4H), 1.26 (m, 16H). ^{13}C NMR (75 MHz, $CDCl_3$) δ (ppm): 179.9 (COOH), 174.3 (COOMe), 77.3 (2 carbons, CH_2-C≡C), 65.2 (2 carbons, -C≡C-C≡C-), 51.4 ($COOCH_3$), 34.0 (CH_2-COOH), 33.9 (CH_2-COOMe), 29.0 (2

carbons, $\underline{C}H_2$-$(CH_2)_3$-C=O), 28.9 (2 carbons, $\underline{C}H_2$-$(CH_2)_2$-COOH), 28.8 ($\underline{C}H_2$-$(CH_2)_2$-COOMe), 28.7 (2 carbons, $\underline{C}H_2$-$(CH_2)_4$-C=O), 28.5 (2 carbons, $\underline{C}H_2$-CH_2-CH_2-C≡C), 28.1 (2 carbons, $\underline{C}H_2$-CH_2-C≡C), 24.7 ($\underline{C}H_2$-CH_2-COOH), 24.5 ($\underline{C}H_2$-CH_2-COOMe), 19.0 (2 carbons, $\underline{C}H_2$-C≡C).

6.2.4 Methyl 22-((2-(dimethylamino)ethyl)amino)-22-oxodocosa-10,12-diynoate (4).

22-Methoxy-22-oxodocosa-10,12-diynoic acid (5.99 g, 15.9 mmol) and *N*,*N*-dimethyl-ethylenediamine (1.82 mL, 16.7 mmol) were dissolved in a mixture of dichloromethane (50 mL) and *N*,*N*-dimethylformamide (5 mL) and the solution was cooled to 0 ℃. HOBt hydrate (3.65 g, 23.8 mmol), EDC hydrochloride (4.57 g, 23.8 mmol) and DIPEA (16.6 mL) were added successively and the solution was allowed to warm up to room temperature while stirring for 48 h. The solution was diluted with dichloromethane (50 mL) and methanol (5 mL) and the combined organic phases were washed with water (3 x 10 mL). The organic phase was dried over sodium sulfate, filtered and concentrated on the rotovap. The crude residue was purified by silica gel chromatography using a gradient of dichloromethane and methanol (9:1 to 4:1). The pure product was isolated as a blue solid (6.39 g, 14.3 mmol). Yield: 90%. ^{1}H NMR (300 MHz, $CDCl_3$) δ (ppm): 6.07 (bs, 1H), 3.60 (s, 3H), 3.26 (td, 2H, J = 11.3, 5.9 Hz), 2.34 (t, 2H, J = 5.9 Hz), 2.24 (t, 4H, J = 7.5 Hz), 2.19 (t, 2H, J = 6.9 Hz), 2.17 (s, 6H), 2.11 (t, 2H, J = 7.7 Hz), 1.55 (m, 4H), 1.44 (m, 4H), 1.24 (m, 16H). ^{13}C NMR (75 MHz, $CDCl_3$) δ (ppm): 174.1 ($\underline{C}$=ONH$(CH_2)_2NMe_2$), 173.5 ($\underline{C}$OOMe), 77.2 (2 carbons, CH_2-$\underline{C}$≡C), 65.1 (2 carbons, -C≡$\underline{C}$-$\underline{C}$≡C-), 57.8 ($\underline{C}H_2$-NMe_2), 51.2 (COO$\underline{C}H_3$), 44.8 (CH_2-N($\underline{C}H_3)_2$), 38.1 ($\underline{C}H_2$-CH_2-NMe_2), 36.4 ($\underline{C}H_2$-C=ONH$(CH_2)_2NMe_2$), 33.8 ($\underline{C}H_2$-COOMe), 28.9 ($\underline{C}H_2$-$(CH_2)_3$-COOMe), 28.8 ($\underline{C}H_2$-$(CH_2)_2$-COOMe), 28.7 ($\underline{C}H_2$-$(CH_2)_3$-C=ONH$(CH_2)_2NMe_2$), 28.6 (2

carbons, $\underline{C}H_2$-$(CH_2)_3$-C≡C), 28.5 ($\underline{C}H_2$-$(CH_2)_2$-C=ONH$(CH_2)_2NMe_2$), 28.4 (2 carbons, $\underline{C}H_2$-CH_2-CH_2-C ≡ C), 28.0 (2 carbons, $\underline{C}H_2$-CH_2-C ≡ C), 25.4 ($\underline{C}H_2$-CH_2-C=ONH$(CH_2)_2NMe_2$), 24.6 ($\underline{C}H_2$-CH_2-COOMe), 18.9 (2 carbons, $\underline{C}H_2$-C≡C).

6.2.5 22-((2-(Dimethylamino)ethyl)amino)-22-oxodocosa-10,12-diynoic Acid (5).

Methyl 22-((2-(dimethylamino)ethyl)amino)-22-oxodocosa-10,12-diynoate (6.31 g, 14.1 mmol) was dissolved in a 3:1:1 mixture of tetrahydrofuran (60 mL), methanol (20 mL) and water (20 mL). Lithium hydroxide (1.78 g, 42.4 mmol) was added to the solution, which was stirred at room temperature for 12 h. Methanol and tetrahydrofuran were evaporated on the rotovap and the remaining aqueous solution was washed twice with hexane. The aqueous phase was acidified to pH 1 using 6 N hydrochloric acid and the product was extracted with ethyl acetate (4 x 50 mL). The organic solution was dried over sodium sulfate, filtered and concentrated. The obtained residue was further concentrated under high vacuum to afford the pure product as a blue solid (5.48 g, 12.7 mmol). Yield: 90%. ^{1}H NMR (300 MHz, $CDCl_3$) δ (ppm): 7.94 (bs, 1H), 3.50 (td, 2H, J = 10.9, 5.7 Hz), 3.19 (t, 2H, J = 5.7 Hz), 2.80 (s, 6H), 2.13 (m, 8H), 1.46 (m, 4H), 1.37 (m, 4H), 1.16 (m, 16H). ^{13}C NMR (75 MHz, $CDCl_3$) δ (ppm): 175.5 ($\underline{C}$OOH), 175.2 ($\underline{C}$=ONH$(CH_2)_2NMe_2$), 77.1 (2 carbons, CH_2-$\underline{C}$≡C), 64.9 (2 carbons, -C≡$\underline{C}$-$\underline{C}$≡C-), 56.9 ($\underline{C}H_2$-NMe_2), 43.0 (CH_2-N($\underline{C}H_3)_2$), 38.3 ($\underline{C}H_2$-CH_2-NMe_2), 35.7 ($\underline{C}H_2$-C=ONH$(CH_2)_2NMe_2$), 34.2 ($\underline{C}H_2$-COOH), 29.1 ($\underline{C}H_2$-$(CH_2)_3$-COOH), 28.9 ($\underline{C}H_2$-$(CH_2)_2$-COOH), 28.8 ($\underline{C}H_2$-$(CH_2)_3$-C=ONH$(CH_2)_2NMe_2$), 28.7 (2 carbons, $\underline{C}H_2$-$(CH_2)_3$-C≡C), 28.6 ($\underline{C}H_2$-$(CH_2)_2$-C=ONH$(CH_2)NMe_2$), 28.3 (2 carbons, $\underline{C}H_2$-CH_2-CH_2-C≡C), 27.9 (2 carbons, $\underline{C}H_2$-CH_2-C ≡ C), 25.0 ($\underline{C}H_2$-CH_2-C=ONH$(CH_2)_2NMe_2$), 24.5 ($\underline{C}H_2$-CH_2-COOH), 18.7 (2 carbons, $\underline{C}H_2$-C≡C).

6.2.61-N-(2-(dimethylamino)ethyl)-22-N-(2-mercaptoethyl)docosa-10,12-diynediamide (6).

22-((2-(Dimethylamino)ethyl)amino)-22-oxodocosa-10,12-diynoic acid (4.95 g, 11.4 mmol) and 2-aminoethanethiol (0.883 g, 11.4 mmol) were dissolved in dichloromethane (50 mL) and *N*,*N*-dimethylformamide (10 mL) and the solution was cooled to 0 ℃. HOBt hydrate (2.63 g, 17.1 mmol), EDC hydrochloride (3.29 g, 17.2 mmol) and DIPEA (6.00 mL) were added successively and the solution was allowed to warm up to room temperature while stirring for 60 h. The solution was diluted with dichloromethane (50 mL) and methanol (5 mL) and the combined organic phases were washed with water (3 x 10 mL). The organic phase was dried over sodium sulfate, filtered and concentrated on the rotovap. The crude residue was purified by silica gel chromatography using a gradient of dichloromethane and methanol (9:1 to 4:1). The pure product was isolated after drying under high vacuum as a blue solid (3.67 g, 7.46 mmol). Yield: 65%. ^{1}H NMR (300 MHz, $CDCl_3$) δ (ppm): 6.21 (bs, 1H), 6.16 (bs, 1H), 3.39 (td, 2H, J = 12.6, 6.4 Hz), 3.29 (td, 2H, J = 11.4 Hz, 5.6 Hz), 2.64 (t, 2H, J = 6.4 Hz), 2.39 (t, 2H, J = 5.9 Hz), 2.21 (s, 6H), 2.20 (m, 2H), 2.18 (t, 2H, J = 6.9 Hz), 2.16 (t, 2H, J = 7.9 Hz), 2.13 (t, 2H, J = 7.9 Hz), 1.58 (m, 4H), 1.47 (m, 4H), 1.26 (m, 16H). ^{13}C NMR (75 MHz, $CDCl_3$) δ (ppm): 173.3 ($\underline{C}$=ONH$(CH_2)_2NMe_2$), 173.2 ($\underline{C}$=ONH$(CH_2)_2$SH), 77.3 (2 carbons, CH_2-$\underline{C}$≡C), 65.1 (2 carbons, -C≡$\underline{C}$-$\underline{C}$≡C-), 57.7 ($\underline{C}H_2$-NMe_2), 44.9 (CH_2-N($\underline{C}H_3)_2$), 42.2 ($\underline{C}H_2$-CH_2-SH), 38.8 ($\underline{C}H_2$-CH_2-NMe_2), 36.5 ($\underline{C}H_2$-C=ONH$(CH_2)_2NMe_2$), 36.4 ($\underline{C}H_2$-C=ONH$(CH_2)_2$SH), 29.0 (2 carbons, CH_2-$(CH_2)_4$-C≡C), 28.9 (2 carbons, CH_2-$(CH_2)_3$-C≡C), 28.7 ($\underline{C}H_2$-$(CH_2)_2$-C=ONH$(CH_2)_2NMe_2$), 28.6 ($\underline{C}H_2$-$(CH_2)_2$-C=ONH$(CH_2)_2$SH), 28.5 (2 carbons, CH_2-$(CH_2)_2$-C≡C), 28.1 (2 carbons, $\underline{C}H_2$-CH_2-C≡C), 25.5 (CH_2-$\underline{C}H_2$-SH), 25.1 ($\underline{C}H_2$-

CH_2-C=ONH$(CH_2)_2NMe_2$), 24.4 ($\underline{C}H_2$-CH_2-C=ONH$(CH_2)_2$SH), 18.9 (2 carbons, $\underline{C}H_2$-C≡C).

6.2.7 Carboxybetaine thiol crosslinker (CBSH-X) (7).

1-*N*-(2-(dimethylamino)ethyl)-22-*N*-(2-mercaptoethyl)docosa-10,12-diynediamide (1.00 g, 2.03 mmol) was dissolved in anhydrous acetone (10.0 mL) . The solution was cooled to 0 ºC and β-propiolactone (0.129 mL, 2.05 mmol) was added dropwise. The mixture was stirred and allowed to warm up to room temperature for 12 h. A precipitate forms in the solution, which was diluted with diethyl ether (20 mL), resulting in an increase of the precipitation. The solid was filtered on a Buchner funnel and washed with diethyl ether (3 x 10 mL). The resulting off-white solid was dried under vacuum to afford the pure product without further purification (0.688 g, 1.22 mmol). Yield: 60%. ^{1}H NMR (300 MHz, MeOD) δ (ppm): 6.21 (bs, 1H), 6.16 (bs, 1H), 3.67 (m, 4H), 3.64 (t, 2H, J = 7.6 Hz), 3.43 (t, 2H, J = 6.7 Hz), 3.15 (s, 6H), 2.63 (t, 2H, J = 7.5 Hz), 2.34 (t, 2H, J = 7.5 Hz), 2.27 (m, 8H), 1.63 (m, 4H), 1.53 (m, 4H), 1.36 (m, 16H). ^{13}C NMR (75 MHz, MeOD) δ (ppm): 177.5 ($\underline{C}OO^-$), 173.3 ($\underline{C}$=ONH$(CH_2)_2NMe_2$), 173.2 ($\underline{C}$=ONH$(CH_2)_2$SH), 77.3 (2 carbons, CH_2-$\underline{C}$≡C), 65.1 (2 carbons, -C≡$\underline{C}$-$\underline{C}$≡C-), 62.8 ($\underline{C}H_2$-$N^{(+)}Me_2$), 58.0 ($\underline{C}H_2$-CH_2-COO^-), 52.0 (CH_2-$N^{(+)}(\underline{C}H_3)_2$), 42.2 ($\underline{C}H_2$-$CH_2$-SH), 36.5 ($\underline{C}H_2$-C=ONH$(CH_2)_2N^{(+)}Me_2$), 36.4 ($\underline{C}H_2$-C=ONH$(CH_2)_2$SH), 34.0 ($\underline{C}H_2$-$CH_2$-$N^{(+)}$Me2), 29.1 ($\underline{C}H_2$-$COO^-$), 29.0 (2 carbons, CH_2-$(CH_2)_4$-C≡C), 28.9 (2 carbons, CH_2-$(CH_2)_3$-C≡C), 28.7 ($\underline{C}H_2$-$(CH_2)_2$-C=ONH$(CH_2)_2N^{(+)}Me_2$), 28.6 ($\underline{C}H_2$-$(CH_2)_2$-C=ONH$(CH_2)_2$SH), 28.5 (2 carbons, CH_2-$(CH_2)_2$-C≡C), 28.1 (2 carbons, $\underline{C}H_2$-CH_2-C≡C), 26.3 (CH_2-$\underline{C}H_2$-SH), 25.6 ($\underline{C}H_2$-CH_2-C=ONH$(CH_2)_2N^{(+)}Me_2$), 25.0 ($\underline{C}H_2$-CH_2-C=ONH$(CH_2)_2$SH), 18.9 (2 carbons, $\underline{C}H_2$-C≡C).

6.2.8 Synthesis of CBSH-X coated GNPs.

GNPs were prepared as described in previous papers[152]. A typical solution of 15.5 nm diameter gold particles exhibited a characteristic surface plasmon band centered at 523.2 nm. The surface of the gold nanoparticles was capped with the CBSH-X monomers via thiol covalent bonding according to previous literature[145]. Freshly prepared CBSH-X solution in methanol (5 mg/mL, 100 μL) was added to an aqueous solution of GNPs (5mL, 10 nM) while stirring in the dark. After 10min of stirring at room temperature, 0.2 M phosphate buffer solution (5 mL, 0.3 M NaCl, pH 8.0) was introduced. The reaction mixture was kept overnight at 4 ℃ in dark to accomplish complete coating of CBSH-X molecules. GNPs were purified by 3 cycles of centrifugation (13,200 rpm, 15 min). Particles were suspended in pH 8.0 0.1 M phosphate buffer and photo-polymerization was carried on by 254 nm UV light for 15 min (10 cm from the UV lamp).

6.2.9 Preparation of CBSH-X SAMs on flat gold chips.

The gold-coated sensor chip was cleaned in UV ozone cleaner for 20 minutes. Then, the chip was rinsed with MilliQ water and ethanol and dried with filtered air. Then, the surface was functionalized with CBSH-X SAMs by incubating the cleaned substrate in methanol and water (1:50) with a final concentration of 1 mg/mL. Same volume of 0.2 M phosphate buffer solution (0.3 M NaCl, pH 8.0) was introduced after 20 min. After the formation of the SAMs, the chip was removed from the solution, rinsed with water, dried with filtered air and soaked in 0.1 M phosphate buffer (pH 8.0). Photopolymerization was initiated by using 254 nm UV-light for 15 min as described above. The chip was then immediately mounted to the prism on the Surface Plasmon Resonance (SPR) sensor. Nonspecific protein adsorption was measured by SPR according to previous procedure[38].

6.2.10 Cell uptake tests.

Mouse macrophage cell line (RAW264.7 cells), HeLa cells, and bovine aortic endothelial cells (BAEC) were cultured in DMEM medium with 10% FBS and 1% penicillin/streptomycin in a 6-well plate. Prior to the test, cells were washed with PBS three times, then gold nanoparticles with or without crosslinking at gold concentration of 10 ppm in fresh culture media were added. After 4 h incubation at 37 ℃, 5% CO_2, cells were washed three times with PBS and lysed with 1 mL of 50 mM NaOH solution. Intracellular gold concentration was determined by the inductively coupled plasma atomic emission spectroscopy (ICP-AES, Elan DRC-e, PerkinElmer).

6.2.11 Stability tests.

Stability of nanoparticles with and without crosslinking in different pH value (pH 1.0-9.0) was monitored. The stability of CBSH-X coated GNPs with and without crosslinking was also tested at elevated temperatures. Nanoparticles were heated and incubated at 80 ℃ for 3 h. The UV-spectra of GNPs was monitored to determine the degree of dispersion. Then, the stability of GNPs coated with CBSH-X with and without crosslinking in complex media (100% human blood serum) at 37 ℃ was tested. Due to high protein concentrations, these nanoparticles were separated from human blood plasma proteins by centrifugation and re-dispersed in PBS buffer. The average diameter of the nanoparticles was then evaluated by dynamic light scattering (DLS) (Nano ZS, Zetasizer Nano, Malvern).

6.2.12 Characterization.

UV-visible spectra of colloidal GNPs were collected using a Cary 300 Bio UV-vis spectrophotometer over the range from 350 to 800 nm. Surface enhanced Raman

spectroscopy (SERs) samples of CBSH-X coated GNPs with or without crosslinking were prepared using lyophilization. A fresh gold-coated chip was rinsed with deionized (DI) water and cleaned in a UV ozone cleaner for 20 min. GNPs samples or CBSH-X solid was added on the gold chip surface and compacted with a thin glass slide. The SERS measurements were conducted using a Renishaw InVia Raman spectrometer connected to a Leica DMLM upright optical microscope. A 785 nm diode laser was used to excite the Raman scattering and the laser power after a 10× objective was measured using a handheld power meter (Edmund Optics). The SERS spectra in different polarization directions were acquired by mounting the chip on a small rotation stage.

6.3 Results and Discussion

6.3.1 Synthesis of carboxybetaine thiol crosslinker (CBSH-X).

As shown in **Scheme 6.1**, zwitterionic carboxybetaine crosslinker (CBSH-X, **7)** was synthesized in six steps starting with docosa-10,12-diynedioic acid **1**. Dimethyl diester **2** was obtained quantitatively by refluxing **1** in methanol in the presence of 10% of sulfuric acid as catalyst. Mono-hydrolysis of **2** was achieved by using slightly less than the stoichiometric amount of lithium hydroxide in a mixture of tetrahydrofuran, methanol and water and stirring for 12 h. The resulting mono-acid **3** was then coupled to *N*,*N*-dimethyl-ethylenediamine to afford amino ester **4** in very good yield. The ester moiety of **4** was hydrolyzed to produce amino acid **5** which was subsequently coupled with 2-amino-ethanethiol to give thiol intermediate **6**. Formation of the carboxybetaine-containing final product **7** was done by stirring **6** with β-propiolactone in acetone and recovering the product via filtration.

6.3.2 Crosslinked CBSH-X coated GNPs.

CBSH-X coated GNPs, as illustrated in **Scheme 6.1** were synthesized via photo-polymerization. The average diameter of GNPs cores was 15.5 nm. The hydrodynamic diameter of CBSH-X coated GNPs without crosslinking measured by DLS showed an average diameter of 40.4 nm, indicating that the CBSH-X coating thickness was around 12.5 nm. After polymerization, the hydrodynamic size did not show any significant change.

6.3.3 Characterization of crosslinked ligands on the surface of GNPs by SERs.

SERs was used to evaluate the photo-polymerization process of the monomers attached to the GNPs. Bands assigned to the unsaturated double and triple bond stretching vibrations in the polymerized assemblies are located at 1620 and 2260 cm^{-1}, respectively[143]. As indicated in **Figure 6.1**, the SERS spectra of the free CBSH-X and that of the CBSH-X coated GNPs without crosslinking clearly show the fingerprints of the free diacetylene group located at 2260 and 2252 cm^{-1}. This is consistent with the previous studies about the SERs spectra of free diacetylene group[143], indicating that CBSH-X monomer was successfully attached onto the GNPs surface and there was no crosslinking before UV-irradiation. After UV-irradiation, the diacetylene group undergoes 1,4-topochemical polymerization. A new peak was observed in the spectral region of 1554 cm^{-1} (**Figure 6.1b**), which is attributed to the double carbon-carbon bond vibrations[145, 153]. There is one smaller peak in the triple-bond vibrations region, which is probably due to a degree of ambiguous packing of the molecules on the surface of NPs or a possible partial polymerization of the monomers, as shown in previous work[143].

6.3.4 Nonspecific protein adsorption on gold surfaces measured by SPR.

Nonspecific protein adsorption on gold surfaces was further measured by SPR to quantify the protein adsorption of CBSH-X on flat surfaces at 25 ℃. Two common proteins (i.e., fibrinogen (340 kD, pI 5.5) and lysozyme (14 kD, pI 12))[37] were tested. Results show that the surfaces coated with CBSH-X have pretty high lysozyme and fibrinogen adsorption, which are 19.1 and 7.2 ng/cm^2, respectively (**Figure 6.2**). However, after crosslinking, all the surfaces showed less than 0.3 ng/cm^2 lysozyme and fibrinogen adsorption from their protein solution of 1mg/mL, which is the detection limit of our SPR sensor. It is clear that the crosslinked CBSH-X can protect the GNPs from aggregation at single protein solution.

6.3.5 Nonspecific adsorption of GNPs on cells.

Next, resistance to cell uptake is also important to evaluate of nanoparticles *in vitro.* Macrophage cells, HeLa cells, and BAEC were used in this work. Cell sampling without GNPs incubation was used to establish the baseline of cell uptake levels. As shown in **Figure 6.3**, uptake of GNPs without crosslinking by cells is much higher than the control baseline, indicating high nonspecific interactions for CBSH-X coated GNPs without crosslinking. In contrast, the uptake of crosslinked CBSH-X coated GNPs showed no noticeable increase as compared to the control when they were incubated with all kinds of cells, which is in agreement with previous SPR result. This test further shows the advantage of the crosslinking of CB coating.

6.3.6 Stability tests of CBSH-X coated GNPs in complex media.

Previous studies show that single protein solutions or diluted blood serum are not challenging enough for surface coatings[146]. Thus, protein adsorption onto GNPs with and without crosslinking in undiluted (100%) human blood serum was further studied. Due to

high protein concentrations, these nanoparticles were separated from human blood serum proteins by centrifugation and re-dispersed in PBS buffer. The average diameter of the nanoparticles was then evaluated by DLS. As shown in **Figure 6.4**, CBSH-X coated GNPs without crosslinking showed a size increase of ~56 nm in a half hour. At the end of 72 h, the diameter increased to ~150 nm, indicating significant protein adsorption and particulate aggregation. However, with the protection of CBSH-X crosslinked coating, the interactions between proteins and nanoparticles did not cause any agglomeration and the particle sizes after their separation from human blood serum proteins was almost the same as that without serum (40.4 nm), again indicating their excellent stability.

6.3.7 Stability tests of CBSH-X coated GNPs in different pH values.

To use colloidal nanoparticles in advanced biomedical applications, particles must be resistant to aggregation caused by pH variation[145]. The stability of polymeric CBSH-X coated GNPs over a wide range of pH values was tested. **Figure 6.5** shows a colorimetric test of CBSH-X coated GNPs with and without crosslinking and associated visible spectra. It is evident that for pH values lower than 3.0, the CBSH-X coated GNPs without crosslinking are not stable and the color of GNPs is purple, indicating that there were some aggregates. By contrast, those with crosslinking keep excellent stability in pH values ranging from 1.0 to 9.0. The hydrodynamic size measurement also indicated that the CBSH-X-coated GNPs with crosslinking are stable at various pH values whereas those without corsslinking are not. This notable stability results from enhanced surface coatings on GNPs.

6.3.8 Stability tests of CBSH-X coated GNPs at high temperature.

In this work, we further tested the stability of GNPs at high temperature. The solutions of CBSH-X coated GNPs with and without crosslinking were tested at 80 ℃. After 3 h at 80 ℃, almost all of the N-CBSH-X coated GNPs precipitated from solution and could not be re-dispersed into solution even with sonication and the hydrodynamic size increased to 220.6 nm. UV spectra confirmed that the formation of irreversible aggregation of the particles (**Figure 6.6a**). In striking contrast, C-CBSX GNPs were extraordinarily stable after 3 h at 80 ℃, as evidenced by the color and UV spectra (**Figure 6.6b**). DLS test confrimed the GNPs aggregate. After 3 h at 80 ℃, the hydrodynamic diameter is 41.4 ± 0.2 and 217.4 ± 1.3 nm for CBSH-X coated GNPs with and without polymerization, respectively. Previous study has shown that SAM-coated NPs are not stable over 70 ℃[154]. However, after crosslinking, CBSH-X modified GNPs are free from aggregation at high temperatures, resulting in stable GNPs for an extended period of time as also observed previously[105, 155.] As shown in previous studies, the marked enhancement of stability is attributable to the impeded surface diffusion of the thiol ligands on the nanoparticle surface[144]. Thus, the shell cross-linking of polymeric micelles surrounding the GNPs stabilizes GNPs modified with CB thiol.

6.4 Conclusions

In conclusion, a diacetylene-containing CB thiol was synthesized and used to cap nanoparticles via SAMs. It is showed that GNPs modified with CB thiol with only one CB group are stable in undiluted human blood serum and at low/high pH and high temperature upon UV-irradiation. In addition, it presents an abundance of functional groups to create multiple functional nanoparticles under mild conditions[88]. Thus, CBXH-

coated nanoparticles have great potentials for a broad range of biomedical applications for GNPs and other types of inorganic nanoparticles.

6.5 Chapter Figures

a

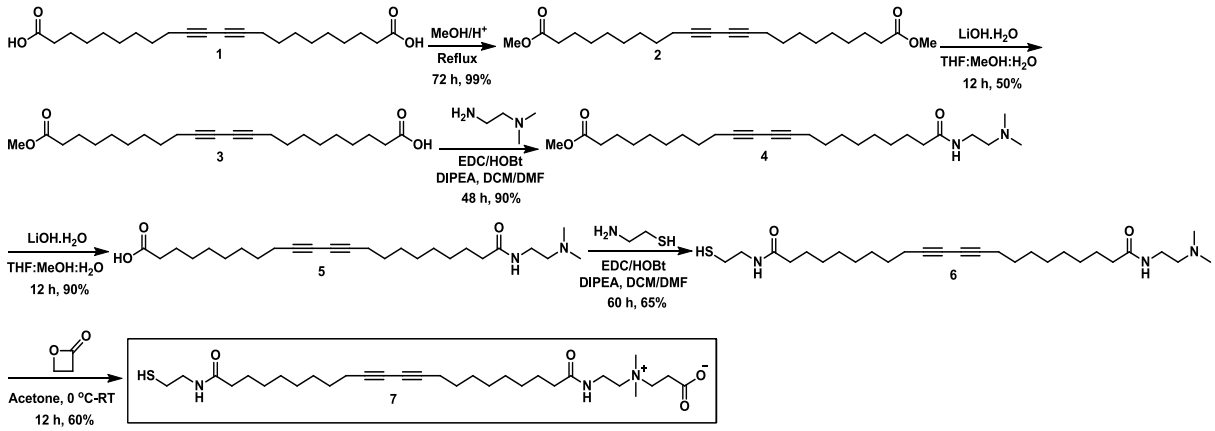

b

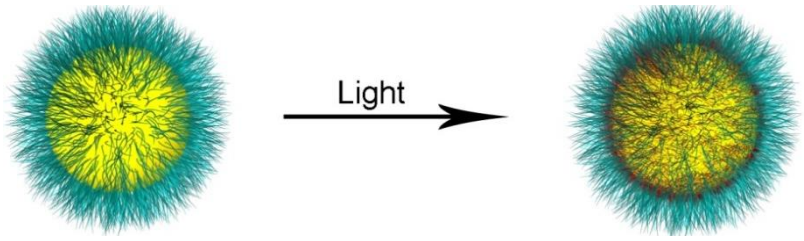

Scheme 6.1 (a) Synthetic route of CBSH-X and (b) schematic of crosslinked GNPs with CBSH-X Synthesis route of CB-thiol crosslinker (CBSH-X).

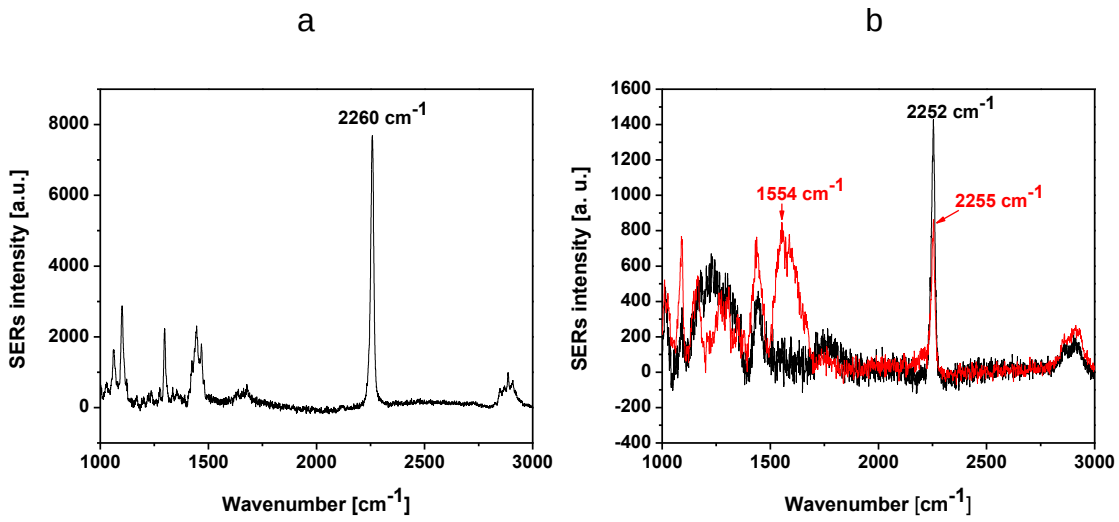

Figure 6.1 A schematic illustration of the photopolymerization of diacetylene groups. a, SERS spectra of CBSH-X monomer, where 2260 cm^{-1} is a feature band of the diacetylene group; b, CBXH-coated GNPs before (black line) and after photopolymerization (red line), where 2255 and 2252 cm^{-1} are the feature band of the diacetylene group and 1554 cm^{-1} is the stretching vibration of carbon-carbon double bond.

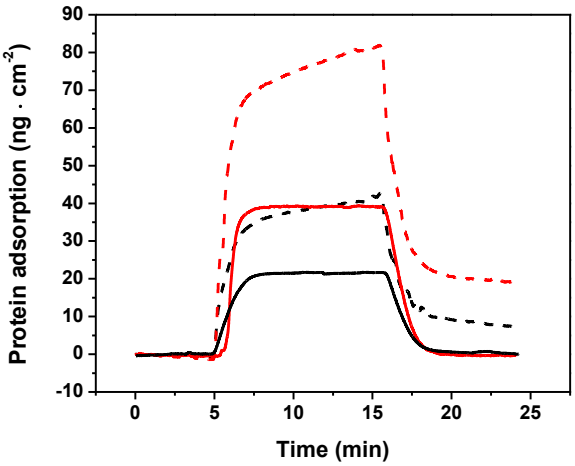

Figure 6.2 Typical SPR sensorgram of CBSH-X-coated surfaces with (dash line) and without (solid line) crosslinking when exposed to 1mg/mL lysome (black line) and fibrinogen (red line).

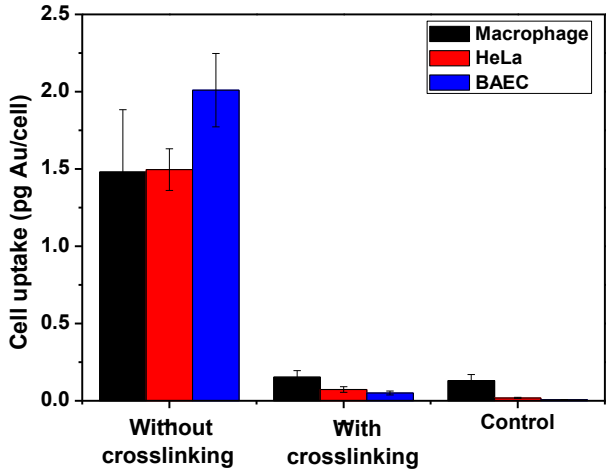

Figure 6.3 Cell uptake of CBSH-X-coated GNPs with and without crosslinking at the Au concentration of 10 μg/mL for macrophage, HeLa, and BAEC cells (n= 3).

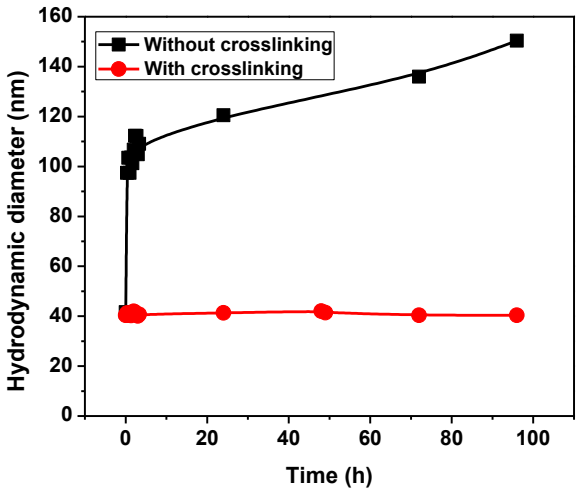

Figure 6.4 Hydrodynamic size of CBXH-X coated GNPs with or without crosslinking in 100% blood serum at 37 ℃. These GNPs were separated from serum and re-suspended in buffer before detection.

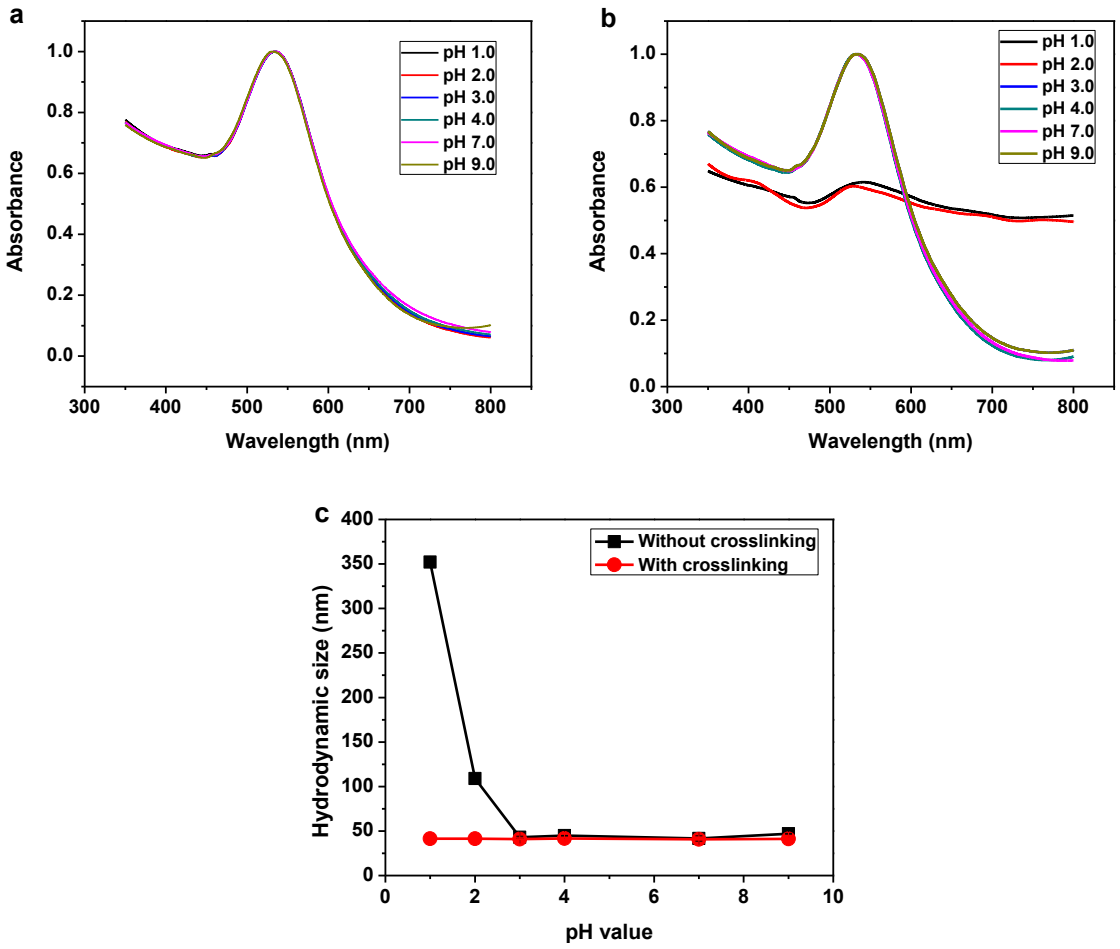

Figure 6.5 (a) and (b), UV-visible spectra of CBSH-X-coated GNPs with or without crosslinking at various pH values (1.0-9.0), respectively. (c)Hydrodynamic size of CBSH-X-coated GNPs without or with crosslinking at various pH values (1.0-9.0).

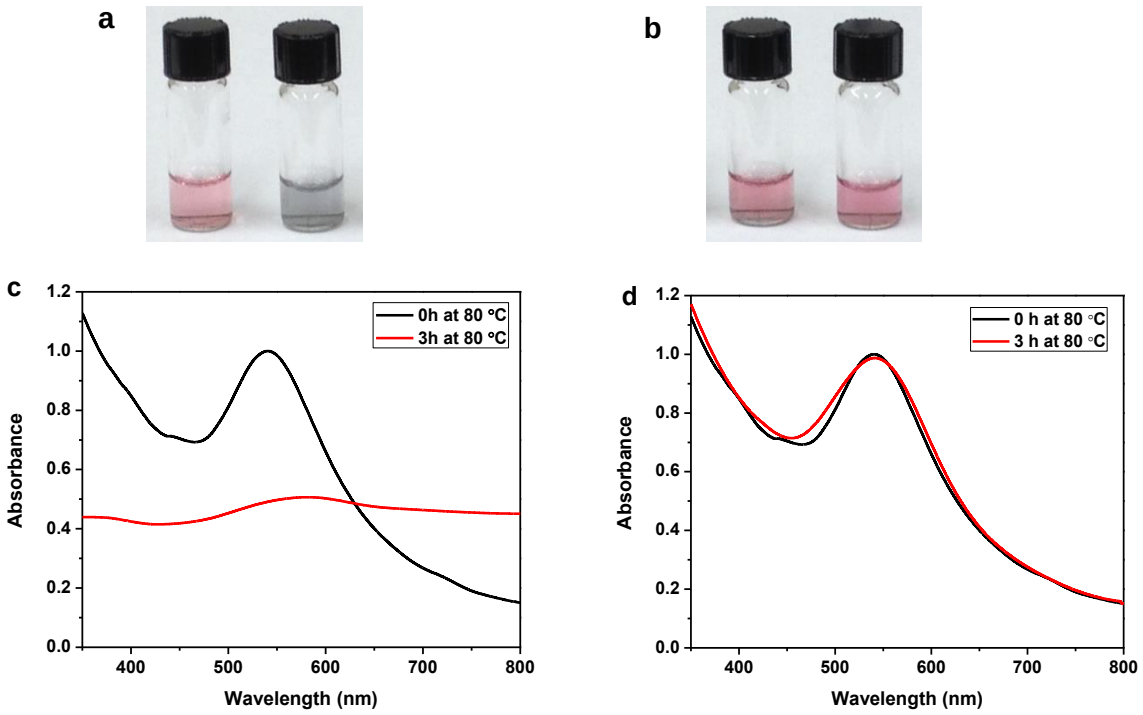

Figure 6.6 (a) and (c), Appearance and UV-visible spectra of CBSH-X-coated GNPs without crosslinking at 80 ℃ for 0 and 3 h. (b) and (d), Appearance and UV-visible spectra of CBSH-X-coated GNPs without crosslinking at 80 ℃ for 0 and 3 h.

Chapter 7 Stable Quantum Dots with Zwitterionic Carboxybetaine Modification

A new type of quantum dot ligand chemistry with zwitterionic carboxybetaine end groups (CBSS) is introduced to promote nonfouling properties and quantum dot (QD) functionalization. Results show that after coating, QD solutions are stable over a broad pH range. Surface binding assays and cellular internalization and imaging showed that QDs capped with CBSS possess extremely low nonspecific adsorption. Furthermore, the CBSS ligands can be used in conjunction with other functional groups, which allows simple conjugation for highly specific targeting while retaining the nonfouling background. This QD chemistry offers a different approach to covalent coupling techniques with extremely low nonspecific protein adsorption and holds significant potential for imaging applications in the future.

7.1 Introduction

Semiconductor nanocrystal quantum dots (QDs) can be powerful and photostable nano-emitters with uniquely narrow and tunable emissions ranging from the visible to infrared frequencies[156]. Luminescent QDs (such as those made of CdSe-ZnS core-shell nanocrystals), in particular, have generated an increasing interest for use in developing bio-oriented applications[157]. Ideally, the QDs should be easily derivatized such that various secondary reporters or biomolecules can be appended to the QD to allow for sensing and/or targeting of cellular receptors[158]. In doing so, the QDs must maintain their

properties of low nonspecific binding to cells, small size, high quantum yield, and good pH stability[158].

Dihydrolipoic acid (DHLA) has been widely used as a surface ligand for cap exchange to prepare water soluble QDs[159]. DHLA-QDs are negatively charged and exhibit strong nonspecific electrostatic interactions with their biological environment[159]. These interactions can be limited by coupling PEG strands to DHLA[157]. However, PEG QDs tend to aggregate in high salinity buffers, and the PEG polymer substantially increases the size of the QDs, which may restrict access to confined spaces and prevent renal elimination in *in vivo* applications[160]. Recently, zwitterionic materials terminated with sulfate groups were developed to reduce nonspecific interactions with cells[156, 161]. Previous studies have shown that cysteine[162], sulfobetaine[160] or phosphorylcholine[161] coated QDs exhibit much smaller diameters, weak nonspecific interactions with proteins, and good resistance to pH variations and salinity.

Most ligands including the current zwitterionic materials have not allowed easy implementation of common QD bioconjugation techniques, such as avidin-biotin binding and covalent conjugation chemistry via NHS/EDC coupling due to lack of accessible functionalities at their lateral end[157]. To introduce functional groups for subsequent coupling to target biomolecule conjugation, a series of DHLA-PEG ligands having a variety of functional end groups such as biotin, amino, and carboxyl groups have been developed and mixed with DHLA-PEG[157]. However, using NHS/EDC chemistry for QDs encapsulated with polymeric shells bearing carboxyl groups produces large conjugates with poor control over the number of biomolecules attached to a single nanocrystal[163].

Moreover, this chemistry is prone to cause crosslinking and aggregation of QDs[163]. Success in bioconjugation is intimately tied to development of new caps[163].

In this work, we designed a novel material with CB end groups (CBSS). This surface platform presents an abundance of functional groups to create multiple functional nanoparticles and an ultra-low fouling background to maintain the high stability and efficiency of QDs. Proteins can be conveniently and effectively immobilized on carboxybetaine groups via simple NHS/EDC chemistry under mild conditions.

7.2 Materials and Methods

7.2.1 Materials

Lipoic acid, *N*,*N*-dimethylethylenediamine, 1-Hydrobenzotriazole hydrate, 1-Ethyl-3-(3-dimethylaminopropyl)carbodiimide hydrochloride, n-hexane, β-Propiolactone, and diisopropylethylamine was purchased from TCI America (Portland, OR). Controlled pore glass beads were purchased from Millipore Corp (Billerica, MA). TOPO-QDs (Qdot® 605 Organic Quantum Dots, CdSe/ZnS QDs) was purchased from Life technologies (Carlsbad, CA). Biotin labeled silicon bead (10 mg/mL) was purchased from Chemicell GmbH (Berlin, Germany). Streptavidin from Streptomyces avidinii was purchased from Sigma (St. Louis, MO).

7.2.2 Synthesis of CBSS

***N*-(2-dimethylamino)ethyl)-5-(1,2-dithiolan-3-yl)pentanamide (1).** Lipoic acid (5.20 g, 25.2 mmol) and *N*,*N*-dimethylethylenediamine (3.03 mL, 27.7 mmol) were dissolved in dichloromethane (50.0 mL) and the solution was cooled to 0 ℃. After stirring for 5 min, 1-Hydrobenzotriazole hydrate (5.80 g, 37.9 mmol), 1-Ethyl-3-(3-dimethylaminopropyl)carbodiimide hydrochloride (7.25 g, 37.8 mmol) and

diisopropylethylamine (26.3 mL, 151 mmol) were successively added to the solution. The mixture was allowed to warm to room temperature overnight and stirred for 48 h. The solution was diluted with dichloromethane and extracted with water (3 x 20 mL) and brine (1 x 20 mL). The organic phase was dried over sodium sulfate and the solvent was removed on the rotovap. The crude residue (yellow oil) was clean enough to be used in the next step without further purification. ^{1}H NMR (300 MHz, $CDCl_3$) δ (ppm): 6.10 (bs, 1H), 3.54 (m, 1H), 3.28 (dt, 2H, J = 11.4 Hz, 5.5 Hz), 3.12 (m, 2H), 2.42 (m, 1H), 2.37 (t, 2H, J = 5.9 Hz), 2.19 (s, 6H), 2.16 (t, 2H, J = 7.5 Hz), 1.89 (m, 1H), 1.65 (m, 4H), 1.44 (m, 2H)

3-((2-(5-(1,2-dithiolan-3-yl)pentanamido)ethyldimethylammonio)propanoate (2) (CBSS). Compound 1 (6.97 g, 25.2 mmol) was dissolved in anhydrous tetrahydrofuran (50.0 mL) and the solution was cooled to 0 °C. β-Propiolactone (1.66 mL, 26.4 mmol) was added dropwise and the solution was stirred and warmed up to room temperature overnight. The mixture turns into a yellow suspension, and the yellow precipitate was filtered on a Buchner funnel, washed with acetone (3 x 50 mL) and dried under high vacuum. The pure product is obtained as a yellow powder (g, mmol). Yield: 42%. ^{1}H NMR (300 MHz, D_2O) δ (ppm): 3.60 (t, 2H, J = 6.7 Hz), 3.53 (t, 2H, J = 5.9 Hz), 3.47 (t, 2H, J = 7.9 Hz), 3.31 (t, 2H, J = 6.4 Hz), 2.99 (s, 6H), 2.78 (m, 1H), 2.55 (t, 2H, J = 7.6 Hz), 2.34 (m, 1H), 2.14 (t, 2H, J = 7.1 Hz), 1.48 (m, 4H), 1.28 (m, 2H)

7.2.3 Synthesis of CBSS-QDs

CBSS-QDs were synthesized as previously reported[156]. Briefly, 1 mL of 75/25 methanol/isopropanol mixture was added to the TOPO-QDs (250 pmol, 250 μL of 1 μM) to precipitate TOPO-QDs. They were mixed well and placed in a sealable centrifuge tube,

sealed and centrifuged for 3-5 minutes at 3000 rpm. The supernatant was discarded and the pellet was re-dispersed in chloroform (1 mL).

10^5 equivalent amounts of the oxidized form of ligands to QDs were dissolved in water (1 mL). Two equivalents of sodium borohydride to ligands were added to the solution and vigorously stirred for 20 min under N_2 gas flow at room temperature. The QD solution was added to the ligand solution and then intensely vortexed for 30 min at room temperature. The QDs were transferred from the organic layer to the aqueous layer. To remove excess free ligands, the QD solution was dialyzed using Amicon 50 kDa MW cutoff centrifugal filters.

7.2.4 Synthesis of LA-QDs

LA-QDs used for this study were prepared based on the procedure previously described[164]. After the Methanol/Isopropanol precipitation, the TOPO-QDs was re-dissolved in n-hexane (100 pmol). LA solution (800 nmol, 8 μL of 100 mM/EtOH), $NaBH_4$ (1 μL, 12 wt % in 14 N NaOH) and H_2O (31 μL) were added to the QDs solution. The mixture then intensely vortexed for 30 minutes at room temperature. The n-hexane layer containing TOPO were removed and the LA-QDs was collected with filter and re-dispersed in PBS.

7.2.5 Imaging of the intracellular localization of QDs on cells by TEM

TEM was applied to test the intracellular localization of QDs on cells[156]. COS-7 cells were incubated with the LC-QDs or CBSS-QDs for 24 h. To investigate the location of the QDs in the COS-7 cells, the cells were treated for TEM observation. The cells were fixed with 2.5% glutaraldehyde in 0.1 M, pH 7.2 cacodylate buffer for 24 h at 4 °C and rinsed with same buffer three times. The cells were then fixed with 1% OsO_4 for 1 h at 4 °

C and washed with water three times. The cells were dehydrated through a series of graded ethanol (50%, 60%, 70%, 80%, 90%, 95%, 98%, and 100%) and propylene oxide and finally embedded with epoxy resin (Epon 812). The samples were then polymerized at 60 °C for 24 h, cut into thin slices using an ultramicrotome and collected on 200-mesh copper grids. The thin sections were stained with uranyl acetate and lead citrate and observed with TEM (J.E.O.L., 1320).

7.2.6 Bead adsorption with QDs

Glass bead assay, as described previously[156], was used to observe the nonspecific adsorption with proteins. Glass bead (diameter: 100 μ m) were dispersed in PBS buffer. BSA was added to the solution (final concentration is 1mg/mL). The solution was stirred overnight and centrifuged twice to remove the excess BSA. The beads in the solution were mixed with CBSS-QDs or LA-QDs in PBS buffer for 2 h. The QDs to beads ratio was 10^7:1. The mixed solution was washed with PBS buffer and D.I. water three times each to remove the excess QDs.

7.2.7 Cytotoxicity assays of CBSS-QDs on cells

To determine the cytotoxicity of CBSS-QDs, HeLa cells and COS-7 cells were tested by MTT method using a Vybrant® MTT Cell Proliferation Assay Kit[28]. Cells were seeded in 96-well cell culture plates in 100 μL medium with 10% FBS serum under 5% CO_2 at 37 to allow 80-90% confluence. On the day of the test, cells were washed with PBS and incubated with 200 mL fresh medium containing CBSS-QDs at various concentrations (10, 50, and 100 nM). After 24 h, cells were washed with PBS and incubated with 100 mL medium and 50 mL of 12mM MTT stock solution for 4 h at 37 ℃. Then, the medium

was removed and 150 mL DMSO was added and incubated for 10 min. The absorbance at 570 nm was measured using a plate reader.

7.2.8 Biomolecule conjugation with QD conjugates

Finally, biomolecule conjugation with QD conjugates was performed according to previous method[160]. For the conjugation to streptavidin (SA), CBSS-QDs were first activated with 10^4 equivalents of NHS/EDC in water (100 mM, pH 5.5) for 30 min. Excess coupling reagent was removed twice by ultrafiltration through a 50 kDa cutoff filter. Activated QDs were then mixed with SA (50 equivalents) in sodium bicarbonate buffer (100 mM, pH 8.0) and incubated for 1 h. The SA-QDs were concentrated by ultrafiltration through a 50 kDa cutoff filter. The efficiency of the conjugation was checked by mixing 6 pmol of SA-QDs with silicon-biotin particles (diameter: 1 μm) for 15 min. The particles were washed three times in PBS by centrifugation.

7.3 Results and Discussion

7.3.1 Characterization

After the ligand exchange with LA or CBSS, the absorption and emission profiles of CdSe/ZnS QDs had a slight change (**Figure 7.1**). The emission centeres at 605 nm before and after the CBSS or LA ligand exchange. The hydrodynamic size of CBSS-QDs is around 13.5 nm and the original size of QDs is around 10 nm, so the CBSS surface coating is about 1.8 nm. We then test the particle stability in different pH value. **Figure 7.2** shows the hydrodynamic size of LA-QDs and CBSS-QDs at various pH value. It is evident that aggregate forms of LA-QDs due to poor QD stability in high basic/acidic buffers. By contrast, those with CBSS coating keep excellent stability in pH values ranging from 5.0 to 10.0.

7.3.2 Nonspecific adsorption bead

Nonspecific interactions of the QDs were investigated using bead adsorption assays (**Figure 7.3**). BSA and glass beads (diameter ~100 μm) were incubated with CBSS or LA-QDs. BSA was chosen since it is a common surface for ELISA or immunoblotting[156]. As shown in **Figure 7.3**, no detectable fluorescence signal was found for beads incubated with CBSS-QDs, indicating extremely low nonspecific protein adsorption. On the contrast, considerable numbers of LA-QDs were adsorbed on the BSA surfaces. Similar results were reported previously about the zwitterionic sulfobetaine coated QDs[156]. Our test along with the other previous studies indicates that the zwitterionic material can highly reduce the nonspecific protein adsorption.

7.3.3 Intracellular distributions of QDs

Intracellular distributions of QDs after 24 h of incubation with COS-7 cells were investigated by using TEM. As shown in **Figure 7.4**, most of the LA-QDs are located in the cytoplasm in COS-7 cells, which is indicative of lysosomal localization[156]. Some of the localized QDs can be also found in lysosomes. Individual QDs were also found in lysosome and cytoplasm although most QDs were found in aggregates. However, no uptake was observed in the nuclei, indicating that LA-QDs are not able to penetrate cell nuclei. Conversely, whereas both endosomes and lysosomes are observed in the TEM images, no CBSS-QDs are located within them. This indicates that the zwitterionic QD surface helps QD to escape from the cell uptake.

7.3.4 Cytotoxicity of CBSS-QDs

The cytotoxicity of CBSS-QDs was evaluated by an MTT assay. As shown **Figure 7.5**, no significant cell viability decrease can be observed when incubated with HeLa cells or

COS-7 cells at the tested concentration range. This test further shows the advantage of the CBSS coating.

7.3.5 Functionalization of CBSS-QDs

Besides the enhanced stability of CBSS-QDs in different environments, the CB end group also provided abundant functional groups for ligand immobilization. We next demonstrated the functionalization of CBSS-QDs with biomolecules and the absence of nonspecific adhesion *in vitro*. NHS/EDC standard bioconjugation chemistry was used for subsequent coupling to SA. This commonly used coupling technique allowed us to obtain stable bioconjugates that retained the high quantum yield and stability of the nanoparticles as well as the functionality of the conjugated SA protein[160]. **Figure 7.6** shows the high specificity of QDs-SA tested on biotinylated silicon particles. The subsequent efficient bioconjugation can be easily adjusted by controlling the ratios of functional ligands. We also noticed that the SA-QDs did not bind silicon streptavidin particles, indication low nonspecific protein adsorption after functionalization. Our previous study has shown that unreacted activated sites of PCB can be converted back to nonfouling carboxylate anions groups via hydrolysis, ensuring the ultra-low fouling properties of post-functionalized surfaces in undiluted blood plasma and serum[88].

7.4 Conclusions

In conclusion, a functionalizable and stable surface platform that preserves QD optical properties, endows excellent stability, and remains the small size of QDs has been demonstrated. The zwitterionic coating provides excellent nonfouling properties, as demonstrated by the absence of nonspecific adsorption by proteins and cells. Furthermore, bio-recognition elements such as SA can be easily conjugated to CBSS via the NHS/EDC

method and the subsequent efficient bioconjugation can be easily adjusted by controlling the ratios of functional ligands. The uniqueness of CBSS (i.e., ultra-low fouling and multiple functionalities) makes this zwitterionic polymer very attractive as a next-generation QD coating in biological imaging applications.

7.5 Chapter Figures

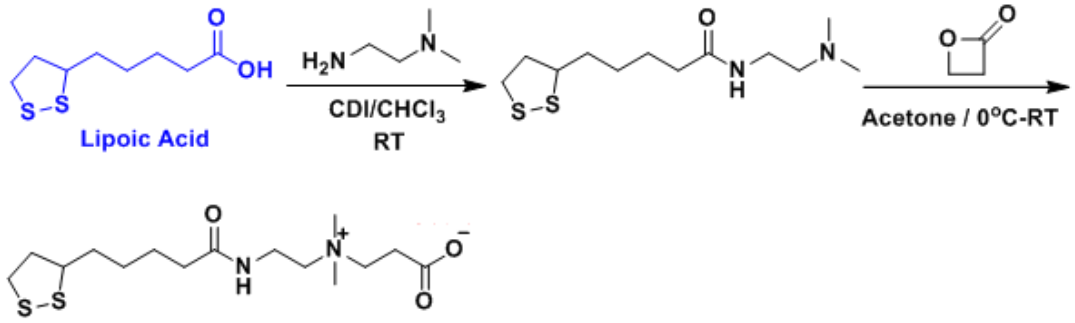

Scheme 7.1 Synthesis scheme of CBSS.

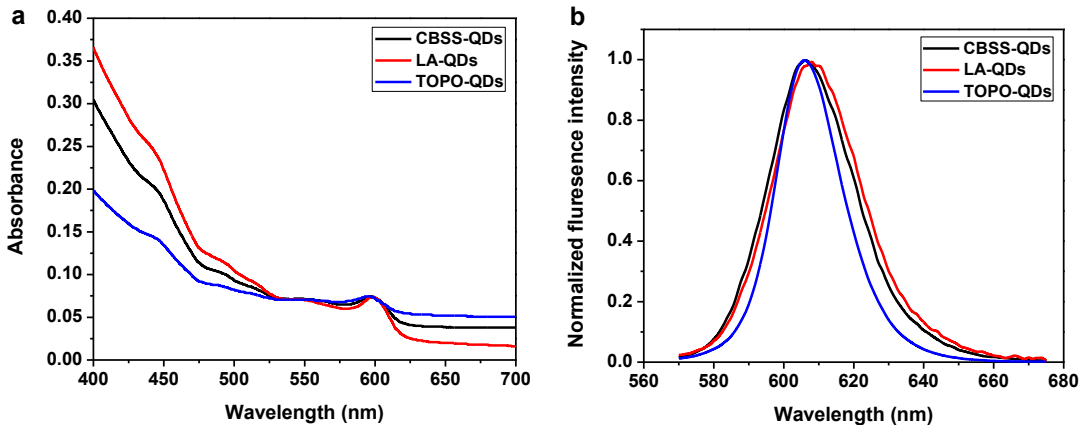

Figure 7.1 Fluorescence and absorbance spectra of CBSS- and LA-QDs in PBS and TOPO-QDs in chloroform. Fluorescence spectrum was measured at excitation of 450 nm.

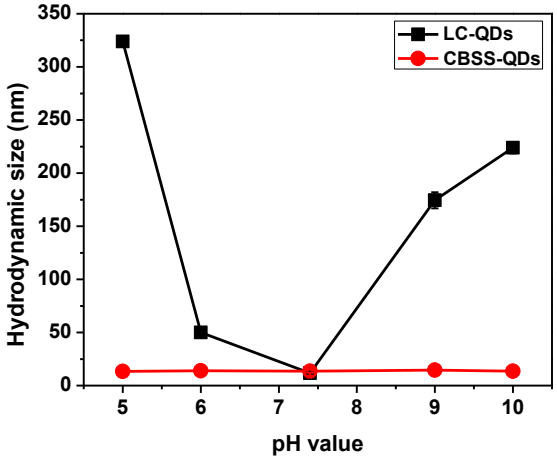

Figure 7.2 Hydrodynamic sizes of LA- and CBSS-QDs over a pH range from 5 to 10.

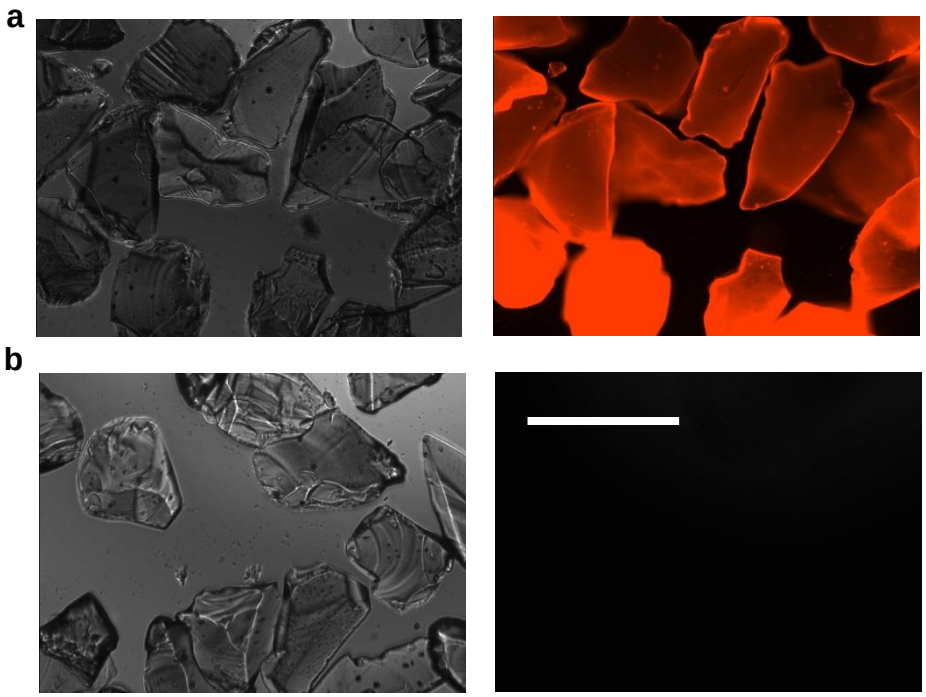

Figure 7.3 Nonspecific adsorptions of LA- and CBSS-QDs on BSA coated glass beads. (a) and (b), Typical images of LA-QDs and CBSS-QDs under bright field (left) and fluorescence (right), respectively. (Magnification: 20 ×, Scale bar:100 μm).

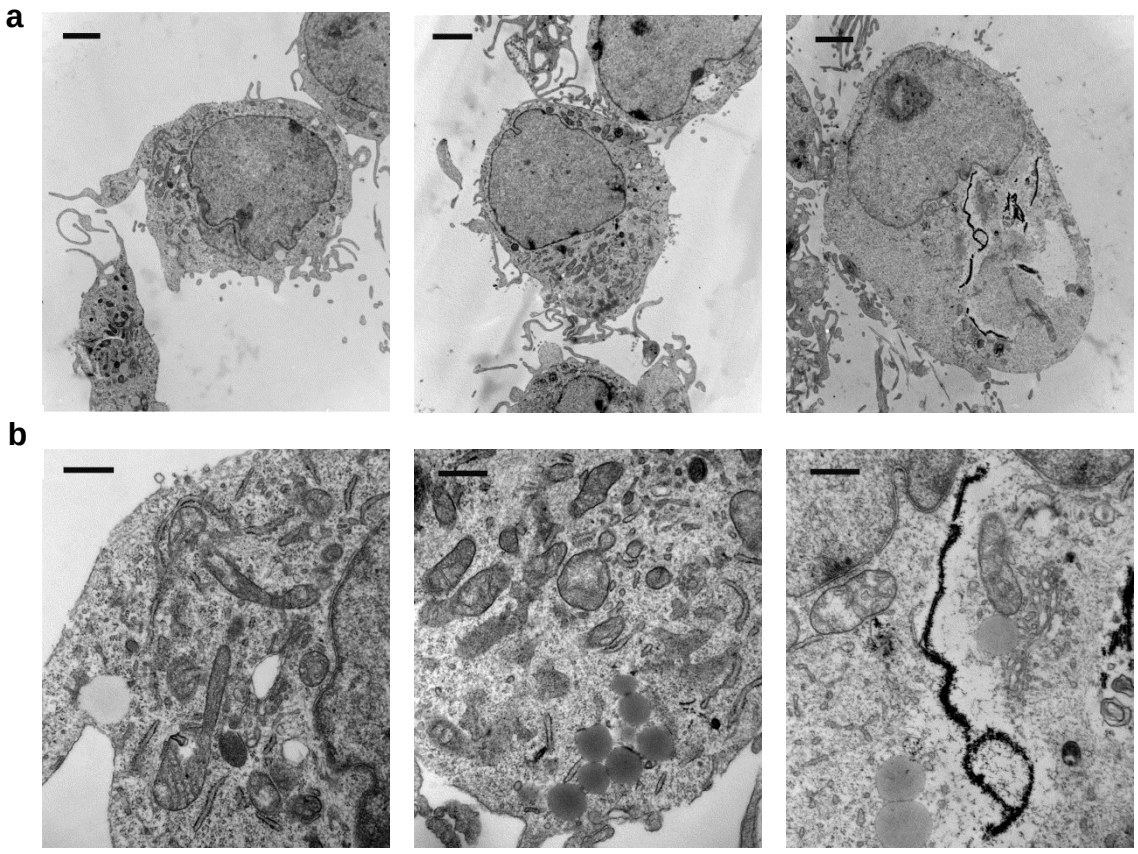

Figure 7.4 Intracellular localizations of LA- (right) and CBSS-QDs (middle) in COS-7 cells (left). (a) Magnification: 8000×, Scale bar: 2 μm. (b) Magnification: 40000×, Scale bar: 500 nm.

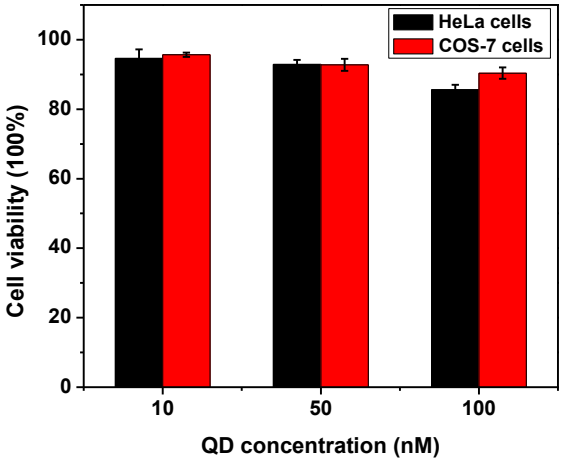

Figure 7.5 Cytotoxicity of CBSS-QDs to HeLa and COS-7 cells by MTT assay (n =3).

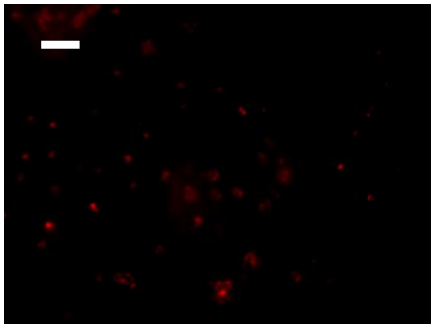

Figure 7.6 Specificity of functionalized QDs. Conjugated QDs-SA specifically bound silicon-biotin particles. (Magnification: 100×, Scale bar: 50 μm)

Chapter 8 Conclusions

Herein, zwitterionic PCB materials with different packing densities have been adapted to resist nonspecific protein adsorption in complex media for blood-contacting medical devices and nanoparticles. To achieve high immobilization and diffusion, a lightly crosslinked hydrogel was developed, in contrast to the conventional wisdom using a high packing density for surface coatings. To obtain a long circulation time and low immune response, PCB materials with a high packing density were used to modify nanoparticles. To maintain the stability of a thin coating, crosslinked CB or CB disulfide materials were developed with enhanced density to impede surface diffusion. Results show that PCB materials are able to prolong the lifetime of implantable devices, prevent an immune response and lengthen the circulation time of nanoparticles used for drug/gene delivery and diagnostics, and preserve the stability and imaging intensity of nanoparticles when a thin coating is required.

We first showed that a lightly crosslinked hydrogel composed of PCB moieties provides extraordinary performance in whole blood for a long period of time. This work proposes two unconventional points of view in materials and surface chemistry. First, it is generally believed that surface coatings with very high packing densities are a prerequisite to prevent biofouling in complex media. However, our results show that a lightly crosslinked hydrogel, the extreme opposite of high packing density surface coatings, also can work well. Second, it is generally believed that most hydrogels have a low level of fouling. However, it is shown in this work that simply low fouling is not

sufficient - “ultra-low fouling” is necessary for long-term applications in complex media such as whole blood. This work provides a new concept of surface chemistry that is easily adaptable for other medical devices beyond glucose sensors in order to realize long-term stability and high performance in whole blood.

Additionally, we demonstrated a platform with high packing density that minimizes the immunogenicity of NPs while maintaining a long circulation time and low accumulation in undesired organs, even after repeated injections. Our findings also emphasize the importance of ultra-low fouling, stealth PCB coatings at avoiding the ABC phenomenon, which is an essential issue often not addressed, or avoided, with most new injectable NPs. This PCB surface coating exhibits superior *in vivo* performance over its PEG counterpart, including extremely low levels of immune response along with a prolonged residence time in blood and low accumulation in tissues, thus demonstrating its tremendous potential as a robust drug delivery and diagnostics platform.

Finally, a functionalizable and stable surface platform containing CB (crosslinkable CB or CBSS) was developed to cap NPs (GNPs or QDs) via SAMs. It was shown that NPs modified with a SAM coating only one CB group thick are highly resistant to protein adsorption, and are stable at low pH and high temperature. In addition, bio-recognition elements such as streptavidin can be easily conjugated to CB SAMs via a NHS/EDC method and the subsequent efficient bioconjugation can be easily adjusted by controlling the ratios of functional ligands. This CB thiol holds tremendous potential for biomedical applications where stable and thin coatings are needed.

References

1. Ratner, B. D.; Hoffman, A. S.; Schoen, F. J.; Lemons, J. E., *Biomaterials Science, an Introduction to Materials in Medicine*. 2nd ed.; Elsevier: Amsterdam, 2004.
2. Ratner, B. D.; Bryant, S. J., Biomaterials: Where we have been and where we are going. *Annu. Rev. Biomed. Eng.* **2004,** 6, 41-75.
3. Prime, K. L.; Whitesides, G. M., Self-assembled organic monolayers-model systems for studying adsorption of proteins at surfaces. *Science* **1991,** 252, (5009), 1164-1167.
4. Langer, R., Perspectives: Drug delivery - Drugs on target. *Science* **2001,** 293, (5527), 58-59.
5. Knop, K.; Hoogenboom, R.; Fischer, D.; Schubert, U. S., Poly(ethylene glycol) in drug delivery: Pros and cons as well as potential alternatives. *Angew. Chem. Int. Ed.* **2010,** 49, (36), 6288-6308.
6. Li, L. Y.; Chen, S. F.; Jiang, S. Y., Protein interactions with oligo(ethylene glycol) (OEG) self-assembled monolayers: OEG stability, surface packing density and protein adsorption. *J. Biomater. Sci. Polym. Ed.* **2007,** 18, (11), 1415-1427.
7. Yang, W.; Chen, S. F.; Cheng, G.; Vaisocherova, H.; Xue, H.; Li, W.; Zhang, J. L.; Jiang, S. Y., Film thickness dependence of protein adsorption from blood serum and plasma onto poly(sulfobetaine)-grafted surfaces. *Langmuir* **2008,** 24, (17), 9211-9214.
8. Zhang, Z.; Chen, S. F.; Chang, Y.; Jiang, S. Y., Surface grafted sulfobetaine polymers via atom transfer radical polymerization as superlow fouling coatings. *J. Phys. Chem. B* **2006,** 110, (22), 10799-10804.
9. Mi, L.; Bernards, M. T.; Cheng, G.; Yu, Q. M.; Jiang, S. Y., pH responsive properties of non-fouling mixed-charge polymer brushes based on quaternary amine and carboxylic acid monomers. *Biomaterials* **2009,** 31, (10), 2919-2925.
10. Chen, S. F.; Zheng, J.; Li, L. Y.; Jiang, S. Y., Strong resistance of phosphorylcholine self-assembled monolayers to protein adsorption: Insights into nonfouling properties of zwitterionic materials. *J. Am. Chem. Soc.* **2005,** 127, (41), 14473-14478.
11. Keefe, A. J.; Jiang, S. Y., Poly(zwitterionic) protein conjugates offer increased stability without sacrificing binding affinity or bioactivity. *Nature Chem.* **2012,** 4, (1), 60-64.
12. Hetrick, E. M.; Prichard, H. L.; Klitzman, B.; Schoenfisch, M. H., Reduced foreign body response at nitric oxide-releasing subcutaneous implants. *Biomaterials* **2007,** 28, 4571-4580.
13. Ratner, B. D., Reducing capsular thickness and enhancing angiogenesis around implant drug release systems. *J. Control. Release* **2002,** 78, 211-218.
14. Anderson, J. M.; Rodriguez, A.; Chang, D. T., Foreign body reaction to biomaterials. *Semin. Immunol.***2008,** 20, 86-100.
15. Heo, Y. J.; Shibata, H.; Okitsu, T.; Kawanishi, T.; Takeuchi, S., Long-term in vivo glucose monitoring using fluorescent hydrogel fibers. *Proc. Natl. Acad. Sci. U. S. A.* **2011,** 108, (33), 13399-13403.
16. Wang, J., Electrochemical glucose biosensors. *Chem. Rev.* **2008,** 108, (2), 814-825.

17. Yu, B. Z.; Long, N.; Moussy, Y.; Moussy, F., A long-term flexible minimally-invasive implantable glucose biosensor based on an epoxy-enhanced polyurethane membrane. *Biosens. Bioelectron.* **2006,** 21, (12), 2275-2282.
18. Dobrovolskaia, M. A.; Aggarwal, P.; Hall, J. B.; McNeil, S. E., Preclinical studies to understand nanoparticle interaction with the immune system and its potential effects on nanoparticle biodistribution. *Mol. Pharm.* **2008,** 5, (4), 487-495.
19. Whitehead, K. A.; Langer, R.; Anderson, D. G., Knocking down barriers: advances in siRNA delivery. *Nature Rev. Drug Discov.* **2009,** 8, (2), 129-138.
20. Aggarwal, P.; Hall, J. B.; McLeland, C. B.; Dobrovolskaia, M. A.; McNeil, S. E., Nanoparticle interaction with plasma proteins as it relates to particle biodistribution, biocompatibility and therapeutic efficacy. *Adv. Drug Deliv. Rev.* **2009,** 61, (6), 428-437.
21. Ishida, T.; Kiwada, H., Accelerated blood clearance (ABC) phenomenon upon repeated injection of PEGylated liposomes. *Int. J. Pharm.* **2008,** 354, (1-2), 56-62.
22. Hu, C. M. J.; Zhang, L.; Aryal, S.; Cheung, C.; Fang, R. H.; Zhang, L. F., Erythrocyte membrane-camouflaged polymeric nanoparticles as a biomimetic delivery platform. *Proc. Natl. Acad. Sci. USA* **2011,** 108, (27), 10980-10985.
23. Yoo, J.-W.; Chambers, E.; Mitragotri, S., Factors that control the circulation time of nanoparticles in blood: Challenges, solutions and future prospects. *Curr. Pharm. Design* **2010,** 16, (21), 2298-2307.
24. Peer, D.; Karp, J. M.; Hong, S.; FaroKhzad, O. C.; Margalit, R.; Langer, R., Nanocarriers as an emerging platform for cancer therapy. *Nature Nanotech.* **2007,** 2, (12), 751-760.
25. Zhang, L.; Gu, F. X.; Chan, J. M.; Wang, A. Z.; Langer, R. S.; Farokhzad, O. C., Nanoparticles in medicine: Therapeutic applications and developments. *Clin. Pharmacol. Ther.* **2008,** 83, (5), 761-769.
26. Zhang, L.; Cao, Z. Q.; Li, Y. T.; Ella-Menye, J. R.; Bai, T.; Jiang, S. Y., Softer zwitterionic nanogels for longer circulation and lower splenic accumulation. *ACS Nano* **2012,** 6, (8), 6681-6686.
27. Gref, R.; Minamitake, Y.; Peracchia, M. T.; Trubetskoy, V.; Torchilin, V.; Langer, R., Biodegradable long-circulating polymer. *Science* **1994,** 263, (5153), 1600-1603.
28. Zhang, L.; Xue, H.; Gao, C. L.; Carr, L.; Wang, J. N.; Chu, B. C.; Jiang, S. Y., Imaging and cell targeting characteristics of magnetic nanoparticles modified by a functionalizable zwitterionic polymer with adhesive 3,4-dihydroxyphenyl-L-alanine linkages. *Biomaterials* **2010,** 31, (25), 6582-6588.
29. Ratner, B. D.; Hoffman, A. S.; Schoen, F. J.; Lemons, J. E., *Biomaterials Science, an Introduction to Materials in Medicine, 2nd ed.* Elsevier: Amsterdam: 2004.
30. Harris, J. M., *Poly(ethylene glycol) Chemistry : Biotechnical and Biomedical Applications* Plenum Press: New York and London: 1992.
31. Bailey, F. E.; Koleske, J. V., *Poly(ethylene Oxide)*. Academic Press: New York: 1976.
32. Li, L. Y.; Chen, S. F.; Jiang, S. Y., Protein interactions with oligo(ethylene glycol) (OEG) self-assembled monolayers: OEG stability, surface packing density and protein adsorption. *J. Biomater. Sci. Polym. Ed.* **2007,** 18, (11), 1415-1427.
33. Ostuni, E.; Chapman, R. G.; Holmlin, R. E.; Takayama, S.; Whitesides, G. M., A survey of structure-property relationships of surfaces that resist the adsorption of protein. *Langmuir* **2001,** 17, (18), 5605-5620.

34. Harder, P.; Grunze, M.; Dahint, R.; Whitesides, G. M.; Laibinis, P. E., Molecular conformation in oligo(ethylene glycol)-terminated self-assembled monolayers on gold and silver surfaces determines their ability to resist protein adsorption. *J. Phys. Chem. B* **1998,** 102, (2), 426-436.
35. Nederberg, F.; Watanabe, J.; Ishihara, K.; Hilborn, J.; Bowden, T., Biocompatible and biodegradable phosphorylcholine ionomers with reduced protein adsorption and cell adhesion. *J. Biomater. Sci. Polym. Ed.* **2006,** 17, (6), 605-614.
36. Feng, W.; Zhu, S. P.; Ishihara, K.; Brash, J. L., Protein resistant surfaces: Comparison of acrylate graft polymers bearing oligo-ethylene oxide and phosphorylcholine side chains. *Biointerphases* **2006,** 1, (1), 50-60.
37. Zhang, Z.; Chen, S. F.; Jiang, S. Y., Dual-functional biomimetic materials: Nonfouling poly(carboxybetaine) with active functional groups for protein immobilization. *Biomacromolecules* **2006,** 7, (12), 3311-3315.
38. Yang, W.; Xue, H.; Li, W.; Zhang, J. L.; Jiang, S. Y., Pursuing "zero" protein adsorption of poly(carboxybetaine) from undiluted blood serum and plasma. *Langmuir* **2009,** 25, (19), 11911-11916.
39. Chen, S. F.; Jiang, S. Y., A new avenue to nonfouling materials. *Adv. Mater.* **2008,** 20, (2), 335-338.
40. Tsai, W. B.; Shi, Q.; Grunkemeier, J. M.; McFarland, C.; Horbett, T. A., Platelet adhesion to radiofrequency glow-discharge-deposited fluorocarbon polymers preadsorbed with selectively depleted plasmas show the primary role of fibrinogen. *J. Biomater. Sci. Polym. Ed.* **2004,** 15, (7), 817-840.
41. Reach, G.; Wilson, G. S., Can continous glucose monitoring be used for the treatment of diabetes. *Anal. Chem.* **1992,** 64, (6), A381-A386.
42. Heller, A., Potentially implantable miniature batteries. *Anal. Bioanal. Chem.* **2006,** 385, (3), 469-473.
43. Yu, B. Z.; Wang, C. Y.; Ju, Y. M.; West, L.; Harmon, J.; Moussy, Y.; Moussy, F., Use of hydrogel coating to improve the performance of implanted glucose sensors. *Biosens. Bioelectron.* **2008,** 23, (8), 1278-1284.
44. Mano, N.; Fernandez, J. L.; Kim, Y.; Shin, W.; Bard, A. J.; Heller, A., Oxygen is electroreduced to water on a "wired" enzyme electrode at a lesser overpotential than on platinum. *J. Am. Chem. Soc.* **2003,** 125, (50), 15290-15291.
45. Heller, A.; Feldman, B., Electrochemical glucose sensors and their applications in diabetes management. *Chem. Rev.* **2008,** 108, (7), 2482-2505.
46. Henry, C., Getting under the skin: Implantable glucose sensors. *Anal. Chem.* **1998,** 70, (17), 594A-598A.
47. Wilson, G. S.; Gifford, R., Biosensors for real-time in vivo measurements. *Biosens. Bioelectron.* **2005,** 20, (12), 2388-2403.
48. Zhang, Z.; Cheng, G.; Carr, L. R.; Vaisocherova, H.; Chen, S. F.; Jiang, S. Y., The hydrolysis of cationic polycarboxybetaine esters to zwitterionic polycarboxybetaines with controlled properties. *Biomaterials* **2008,** 29, (36), 4719-4725.
49. Wang, J.; Chen, L.; Hocevar, S. B.; Ogorevc, B., One-step electropolymeric co-immobilization of glucose oxidase and heparin for amperometric biosensing of glucose. *Analyst* **2000,** 125, (8), 1431-1434.

50. Yang, Y.; Zhang, S. F.; Kingston, M. A.; Jones, G.; Wright, G.; Spencer, S. A., Glucose sensor with improved haemocompatibility. *Biosens. Bioelectron.* **2000,** 15, (5-6), 221-227.
51. Chen, C. Y.; Ishihara, K.; Nakabayashi, N.; Tamiya, E.; Karube, I., Multifunctional biocompatible membrane and its application to fabricate a miniaturized glucose sensor with potential for use in vivo. *Biomed. Microdevices* **1999,** 1, (2), 155-166.
52. Wu, Z. Y.; Wang, B. Q.; Dong, S. J.; Wang, E. K., Amperometric glucose biosensor based on lipid film. *Biosens. Bioelectron.* **2000,** 15, (3-4), 143-147.
53. Moussy, F.; Harrison, D. J.; Obrien, D. W.; Rajotte, R. V., Performance of subcutaneously implanted needle-type glucose sensors employing a novel trilayer coating. *Anal. Chem.* **1993,** 65, (15), 2072-2077.
54. Mignani, A.; Scavetta, E.; Guadagnini, L.; Tonelli, D., Comparative study of protective membranes for glucose biosensors based on electrodeposited hydrotalcites. *Sensor. Actuat. B Chem.* **2009,** 136, (1), 196-202.
55. Sasso, S. V.; Pierce, R. J.; Walla, R.; Yacynych, A. M., Electropolymerized 1,2-diaminobenzene as a means to prevent interferences and fouling and to stabilize immobilized enzyme in electrochemical biosensors. *Anal. Chem.* **1990,** 62, (11), 1111-1117.
56. Yasuzawa, M.; Matsuki, T.; Mitsui, H.; Kunugi, A.; Nakaya, T., Properties of glucose sensors prepared by the electropolymerization of pyrroles containing phosphatidylcholine (II). *Sensor. Actuat. B Chem.* **2000,** 66, (1-3), 25-27.
57. Peppas, N. A.; Hilt, J. Z.; Khademhosseini, A.; Langer, R., Hydrogels in biology and medicine: From molecular principles to bionanotechnology. *Adv. Mater.* **2006,** 18, (11), 1345-1360.
58. Hoffman, A. S., Hydrogels for biomedical applications. *Adv. Drug Deliver. Rev.* **2002,** 54, (1), 3-12.
59. Lee, K. Y.; Mooney, D. J., Hydrogels for tissue engineering. *Chem. Rev.* **2001,** 101, (7), 1869-1879.
60. Jeong, B.; Kim, S. W.; Bae, Y. H., Thermosensitive sol-gel reversible hydrogels. *Adv. Drug Deliver. Rev.* **2002,** 54, (1), 37-51.
61. Lin, C. C.; Metters, A. T., Hydrogels in controlled release formulations: Network design and mathematical modeling. *Adv. Drug Deliver. Rev.* **2006,** 58, (12-13), 1379-1408.
62. Zhang, Z.; Chao, T.; Liu, L. Y.; Cheng, G.; Ratner, B. D.; Jiang, S. Y., Zwitterionic hydrogels: an in vivo implantation study. *J. Biomater. Sci. Polym. Ed.* **2009,** 20, (13), 1845-1859.
63. Lee, K. Y.; Mooney, D. J., Hydrogels for tissue engineering. *Chem. Rev.* **2001,** 101, (7), 1869-1879.
64. Sirkar, K.; Pishko, M. V., Amperometric biosensors based on oxidoreductases immobilized in photopolymerized poly(ethylene glycol) redox polymer hydrogels. *Anal. Chem.* **1998,** 70, (14), 2888-2894.
65. Quinn, C. A. P.; Connor, R. E.; Heller, A., Biocompatible, glucose-permeable hydrogel for in situ coating of implantable biosensors. *Biomaterials* **1997,** 18, (24), 1665-1670.

66. Mano, N.; Yoo, J. E.; Tarver, J.; Loo, Y. L.; Heller, A., An electron-conducting cross-linked polyaniline-based redox hydrogel, formed in one step at pH 7.2, wires glucose oxidase. *J. Am. Chem. Soc.* **2007,** 129, (22), 7006-7007.
67. Ivekovic, D.; Milardovic, S.; Grabaric, B. S., Palladium hexacyanoferrate hydrogel as a novel and simple enzyme immobilization matrix for amperometric biosensors. *Biosens. Bioelectron.* **2004,** 20, (4), 872-878.
68. Jimenez, C.; Bartrol, J.; deRooij, N. F.; KoudelkaHep, M., Use of photopolymerizable membranes based on polyacrylamide hydrogels for enzymatic microsensor construction. *Anal. Chim. Acta* **1997,** 351, (1-3), 169-176.
69. Fernandez, E.; Lopez, D.; Lopez-Cabarcos, E.; Mijangos, C., Viscoelastic and swelling properties of glucose oxidase loaded polyacrylamide hydrogels and the evaluation of their properties as glucose sensors. *Polymer* **2005,** 46, (7), 2211-2217.
70. Brahim, S.; Narinesingh, D.; Guiseppi-Elie, A., Bio-smart hydrogels: co-joined molecular recognition and signal transduction in biosensor fabrication and drug delivery. *Biosens. Bioelectron.* **2002,** 17, (11-12), 973-981.
71. Brahim, S.; Narinesingh, D.; Giuseppi-Elie, A., Interferent suppression using a novel polypyrrole-containing hydrogel in amperometric enzyme biosensors. *Electroanalysis* **2002,** 14, (9), 627-633.
72. Carr, L. R., Functionalizable and Nonfouling Zwitterionic Carboxybetaine Hydrogels with a Carboxybetaine Dimethacrylate Crosslinker. *Biomaterials* **2010**.
73. Yang, W.; Zhang, L.; Wang, S. L.; White, A. D.; Jiang, S. Y., Functionalizable and ultra stable nanoparticles coated with zwitterionic poly(carboxybetaine) in undiluted blood serum. *Biomaterials* **2009,** 30, (29), 5617-5621.
74. Park, K.; Shalaby, W.; Park, H., *Biodegradable Hydrogels for Drug Delivery*. Technomic Publishing Company: Lancaster, PA, USA, 1993.
75. Jimenez, C.; Bartrol, J.; deRooij, N. F.; KoudelkaHep, M., Use of photopolymerizable membranes based on polyacrylamide hydrogels for enzymatic microsensor construction. *Anal. Chim. Acta* **1997,** 351, (1-3), 169-176.
76. Martin, S. M.; Ganapathy, R.; Kim, T. K.; Leach-Scampavia, D.; Giachelli, C. M.; Ratner, B. D., Characterization and analysis of osteopontin-immobilized poly(2-hydroxyethyl methacrylate) surfaces. *J. Biomed. Mater. Res. A* **2003,** 67A, (1), 334-343.
77. Smetana, K.; Lukas, J.; Paleckova, V.; Bartunkova, J.; Liu, F. T.; Vacik, J.; Gabius, H. J., Effect of chemical structure of hydrogels on the adhesion and phenotypic characteristics of human monocytes such as expression of galectins and other carbohydrate-binding sites. *Biomaterials* **1997,** 18, (14), 1009-1014.
78. Zhang, Z.; Zhang, M.; Chen, S. F.; Horbetta, T. A.; Ratner, B. D.; Jiang, S. Y., Blood compatibility of surfaces with superlow protein adsorption. *Biomaterials* **2008,** 29, (32), 4285-4291.
79. Cheng, G.; Li, G. Z.; Xue, H.; Chen, S. F.; Bryers, J. D.; Jiang, S. Y., Zwitterionic carboxybetaine polymer surfaces and their resistance to long-term biofilm formation. *Biomaterials* **2009,** 30, (28), 5234-5240.
80. Harris, J. M., *Poly(ethylene glycol) Chemistry: Biotechnical and Biomedical Applications*. Plenum Press: New York, 1992.
81. Ishihara, K.; Ziats, N. P.; Tierney, B. P.; Nakabayashi, N.; Anderson, J. M., Protein adsrption from human plasma is reduced on phopholipid polymers. *J. Biomed. Mater. Res.* **1991,** 25, (11), 1397-1407.

82. Lewis, A. L., Phosphorylcholine-based polymers and their use in the prevention of biofouling. *Colloids Surf. B* **2000,** 18, (3-4), 261-275.
83. Wichterle, O.; Lim, D., Hydrophilic gels for biological use. *Nature* **1960,** 185, (4706), 117-118.
84. Yang, W.; Xue, H.; Carr, L. R.; Wang, J.; Jiang, S. Y., Zwitterionic poly(carboxybetaine) hydrogels for glucose biosensors in complex media. *Biosens. Bioelectron.* **2011,** 26, (5), 2454-2459.
85. Moretti, S.; Tschuor, F.; Osto, M.; Franchini, M.; Wichert, B.; Ackermann, M.; Lutz, T. A.; Reusch, C. E.; Zini, E., Evaluation of a novel real-time continuous glucose-monitoring system for use in cats. *J. Vet. Intern. Med.* **2010,** 24, (1), 120-126.
86. Gross, T. M.; Mastrototaro, J. J., Efficacy and reliability of the continuous glucose monitoring system. *Diabetes Technol. Ther.* **2000,** 2, S19-S26.
87. Feldman, B.; Brazg, R.; Schwartz, S.; Weinstein, R., A continuous glucose sensor based on wired enzyme™ technology - Results from a 3-day trial in patients with Type 1 diabetes. *Diabetes Technol. Ther.* **2003,** 5, (5), 769-779.
88. Vaisocherova, H.; Yang, W.; Zhang, Z.; Cao, Z. Q.; Cheng, G.; Piliarik, M.; Homola, J.; Jiang, S. Y., Ultralow fouling and functionalizable surface chemistry based on a zwitterionic polymer enabling sensitive and specific protein detection in undiluted blood plasma. *Anal. Chem.* **2008,** 80, (20), 7894-7901.
89. Vaisocherova, H.; Zhang, Z.; Yang, W.; Cao, Z. Q.; Cheng, G.; Taylor, A. D.; Piliarik, M.; Homola, J.; Jiang, S. Y., Functionalizable surface platform with reduced nonspecific protein adsorption from full blood plasma-Material selection and protein immobilization optimization. *Biosens. Bioelectron.* **2009,** 24, (7), 1924-1930.
90. Carr, L. R.; Xue, H.; Jiang, S. Y., Functionalizable and nonfouling zwitterionic carboxybetaine hydrogels with a carboxybetaine dimethacrylate crosslinker. *Biomaterials* **2011,** 32, (4), 961-968.
91. Chen, S. F.; Jiang, S. Y., A new avenue to nonfouling materials. *Adv. Mater.* **2008,** 20, (2), 335-338.
92. Vianello, F.; Bortoluzzi, S.; Zennaro, L.; Rigo, A., Determination of glucose oxidase immobilised as monolayer onto a flat surface. *J. Biochem. Bioph. Methods* **2002,** 51, (3), 263-271.
93. Bhatia, S. R.; Khattak, S. F.; Roberts, S. C., Polyelectrolytes for cell encapsulation. *Curr. Opin. Colloid Interface Sci.* **2005,** 10, (1-2), 45-51.
94. Ge, J.; Lu, D. N.; Wang, J.; Yan, M.; Lu, Y. F.; Liu, Z., Molecular fundamentals of enzyme nanogels. *J. Phys. Chem. B* **2008,** 112, (45), 14319-14324.
95. Peng, Y.; Jiang, D. L.; Su, L.; Zhang, L.; Yan, M.; Du, J. J.; Lu, Y. F.; Liu, Y. N.; Zhou, F. M., Mixed monolayers of ferrocenylalkanethiol and encapsulated horseradish peroxidase for sensitive and durable electrochemical detection of hydrogen peroxide. *Anal. Chem.* **2009,** 81, (24), 9985-9992.
96. Dobrovolskaia, M. A.; McNeil, S. E., Immunological properties of engineered nanomaterials. *Nature Nanotech.* **2007,** 2, (8), 469-478.
97. Kontos, S.; Hubbell, J. A., Drug development: longer-lived proteins. *Chem. Soc. Rev.* **2012,** 41, 2686-2695.
98. Armstrong, J. K.; Hempel, G.; Koling, S.; Chan, L. S.; Fisher, T.; Meiselman, H. J.; Garratty, G., Antibody against poly(ethylene glycol) adversely affects PEG-

asparaginase therapy in acute lymphoblastic leukemia patients. *Cancer* **2007,** 110, (1), 103-111.
99. Mitragotri, S.; Lahann, J., Physical approaches to biomaterial design. *Nature Mater.* **2009,** 8, (1), 15-23.
100. Owens, D. E.; Peppas, N. A., Opsonization, biodistribution, and pharmacokinetics of polymeric nanoparticles. *Int. J. Pharm.* **2006,** 307, (1), 93-102.
101. Jiang, S. Y.; Cao, Z. Q., Ultralow-fouling, functionalizable, and hydrolyzable zwitterionic materials and their derivatives for biological applications. *Adv. Mater.* **2010,** 22, (9), 920-932.
102. Holmlin, R. E.; Chen, X. X.; Chapman, R. G.; Takayama, S.; Whitesides, G. M., Zwitterionic SAMs that resist nonspecific adsorption of protein from aqueous buffer. *Langmuir* **2001,** 17, (9), 2841-2850.
103. Jones, D. M.; Brown, A. A.; Huck, W. T. S., Surface-initiated polymerizations in aqueous media: Effect of initiator density. *Langmuir* **2002,** 18, (4), 1265-1269.
104. Brust, M.; Walker, M.; Bethell, D.; Schiffrin, D. J.; Whyman, R., Synthesis of thiol-derivatized gold nanoparticles in a 2-phase liquid-liquid system. *J. Chem. Soc., Chem. Commun.* **1994**, (7), 801-802.
105. Dong, H. C.; Zhu, M. Z.; Yoon, J. A.; Gao, H. F.; Jin, R. C.; Matyjaszewski, K., One-pot synthesis of robust core/shell gold nanoparticles. *J. Am. Chem. Soc.* **2008,** 130, (39), 12852-12853.
106. Maye, M. M.; Zheng, W. X.; Leibowitz, F. L.; Ly, N. K.; Zhong, C. J., Heating-induced evolution of thiolate-encapsulated gold nanoparticles: A strategy for size and shape manipulations. *Langmuir* **2000,** 16, (2), 490-497.
107. Choi, H. S.; Liu, W.; Misra, P.; Tanaka, E.; Zimmer, J. P.; Ipe, B. I.; Bawendi, M. G.; Frangioni, J. V., Renal clearance of quantum dots. *Nature Biotechnol.* **2007,** 25, (10), 1165-1170.
108. Moghimi, S. M.; Hunter, A. C.; Murray, J. C., Long-circulating and target-specific nanoparticles: Theory to practice. *Pharmacol. Rev.* **2001,** 53, (2), 283-318.
109. Dams, E. T. M.; Laverman, P.; Oyen, W. J. G.; Storm, G.; Scherphof, G. L.; Van der Meer, J. W. M.; Corstens, F. H. M.; Boerman, O. C., Accelerated blood clearance and altered biodistribution of repeated injections of sterically stabilized liposomes. *J. Pharmacol. Exp. Ther.* **2000,** 292, (3), 1071-1079.
110. Merkel, T. J.; Jones, S. W.; Herlihy, K. P.; Kersey, F. R.; Shields, A. R.; Napier, M.; Luft, J. C.; Wu, H. L.; Zamboni, W. C.; Wang, A. Z.; Bear, J. E.; DeSimone, J. M., Using mechanobiological mimicry of red blood cells to extend circulation times of hydrogel microparticles. *Proc. Natl. Acad. Sci. USA* **2011,** 108, (2), 586-591.
111. Ishida, T.; Wang, X.; Shimizu, T.; Nawata, K.; Kiwada, H., PEGylated liposomes elicit an anti-PEG IgM response in a T cell-independent manner. *J. Control. Release* **2007,** 122, (3), 349-355.
112. Sroda, K.; Rydlewski, J.; Langner, M.; Kozubek, A.; Grzybek, M.; Sikorski, A. F., Repeated injections of PEG-PE liposomes generate anti-PEG antibodies. *Cell. Mol. Biol. Lett.* **2005,** 10, (1), 37-47.
113. Fang, R. H.; Hu, C. M. J.; Zhang, L. F., Nanoparticles disguised as red blood cells to evade the immune system. *Expert Opin. Biol. Ther.* **2012,** 12, (4), 385-389.
114. Veronese, F. M.; Pasut, G., PEGylation, successful approach to drug delivery. *Drug Discov. Today* **2005,** 10, (21), 1451-1458.

115. Hu, C. M. J.; Fang, R. H.; Luk, B. T.; Zhang, L. F., Nanoparticle-detained toxins for safe and effective vaccination. *Nature Nanotech.* **2013,** 8, (12), 933-938.
116. Yang, W.; Liu, S. S.; Bai, T.; Keefe, A. J.; Zhang, L.; Ella-Menye, J. R.; Li, Y. T.; Jiang, S. Y., Poly(carboxybetaine) nanomaterials enable long circulation and prevent polymer-specific antibody production. *Nano Today* **2014,** 9, 10-16.
117. Ishida, T.; Ichihara, M.; Wang, X. Y.; Kiwada, H., Spleen plays an important role in the induction of accelerated blood clearance of PEGylated liposomes. *J. Control. Release* **2006,** 115, (3), 243-250.
118. Richter, A. W.; Akerblom, E., Antibodies against polyethylene glycol produced in animals by immunization with monomethoxy polyethylene glycol modified proteins. *Int. Arch. Allergy. Appl. Immunol.* **1983,** 70, 124-131.
119. Sherman, M. R.; Williams, L. D.; Sobczyk, M. A.; Michaels, S. J.; Saifer, M. G. P., Role of the Methoxy Group in Immune Responses to mPEG-Protein Conjugates. *Bioconjugate Chem.* **2012,** 23, (3), 485-499.
120. Richter, A. W.; Akerblom, E., Polyethylene glycol reactive antibodies in man: Titer distribution in allergic patients treated with monomethoxy polyethylene glycol modified allergens or placebo, and in healthy blood donors. *Int. Arch. Allergy Appl. Immunol.* **1984,** 74, 36-39.
121. Meng, J.; Ji, Y. L.; Liu, J.; Cheng, X. L.; Guo, H.; Zhang, W. Q.; Wu, X. C.; Xu, H. Y., Using gold nanorods core/silver shell nanostructures as model material to probe biodistribution and toxic effects of silver nanoparticles in mice. *Nanotoxicology* **2014,** 8, (6), 686-696.
122. Schuijt, T. J.; Coumou, J.; Narasimhan, S.; Dai, J. F.; DePonte, K.; Wouters, D.; Brouwer, M.; Oei, A.; Roelofs, J.; van Dam, A. P.; van der Poll, T.; van't Veer, C.; Hovius, J. W.; Fikrig, E., A tick mannose-binding lectin inhibitor interferes with the vertebrate complement cascade to enhance transmission of the lyme disease agent. *Cell Host Microbe* **2011,** 10, (2), 136-146.
123. Ohno, K.; Akashi, T.; Tsujii, Y.; Yamamoto, M.; Tabata, Y., Blood clearance and biodistribution of polymer brush-afforded silica particles prepared by surface-initiated living radical polymerization. *Biomacromolecules* **2012,** 13, (3), 927-936.
124. Koide, H.; Asai, T.; Hatanaka, K.; Akai, S.; Ishii, T.; Kenjo, E.; Ishida, T.; Kiwada, H.; Tsukada, H.; Oka, N., T cell-independent B cell response is responsible for ABC phenomenon induced by repeated injection of PEGylated liposomes. *Int. J. Pharm.* **2010,** 392, 218-223.
125. Ishida, T.; Ichihara, M.; Wang, X. Y.; Yamamoto, K.; Kimura, J.; Majima, E.; Kiwada, H., Injection of PEGylated liposomes in rats elicits PEG-specific IgM, which is responsible for rapid elimination of a second dose of PEGylated liposomes. *J. Control. Release* **2006,** 112, 15-25.
126. Laverman, P.; Carstens, O. C.; Carstens, M. G.; Boerman, O. C.; Dams, E. T.; Oyen, W. J.; van Rooijen, N.; Corstens, F. H.; Storm, G., Factors affecting the accelerated blood clearance of polyethylene glycol-liposomes upon repeated injection. *J. Pharmacol. Exp. Ther.* **2001,** 298, 607-612.
127. Semmler-Behnke, M.; Kreyling, W. G.; Lipka, J.; Fertsch, S.; Wenk, A.; Takenaka, S.; Schmid, G.; Brandau, W., Biodistribution of 1.4-and 18-nm Gold Particles in Rats. *Small* **2008,** 4, (12), 2108-2111.

128. Liu, X. S.; Cao, J. M.; Li, H.; Li, J. Y.; Jin, Q.; Ren, K. F.; Ji, J., Mussel-inspired polydopamine: A biocompatible and ultrastable coating for nanoparticles in vivo. *ACS Nano* **2013,** 7, (10), 9384-9395.
129. Cho, W. S.; Cho, M. J.; Jeong, J.; Choi, M.; Cho, H. Y.; Han, B. S.; Kim, S. H.; Kim, H. O.; Lim, Y. T.; Chung, B. H., Acute toxicity and pharmacokinetics of 13 nm-sized PEG-coated gold nanoparticles. *Toxicol. Appl. Pharm.* **2009,** 236, (1), 16-24.
130. Moghimi, S. M.; Szebeni, J., Stealth liposomes and long circulating nanoparticles: critical issues in pharmacokinetics, opsonization and proteinbinding properties. *Prog. Lipid Res.* **2003,** 42, 463-478.
131. Petros, R. A.; DeSimone, J. M., Strategies in the design of nanoparticles for therapeutic applications. *Nature Rev.* **2010,** 9, 615-627.
132. Zhang, L.; Xue, H.; Gao, C. L.; Carr, L. R.; Wang, J. N.; Chu, B. C.; Jiang, S. Y., Imaging and cell targeting characteristics of magnetic nanoparticles modified by a functionalizable zwitterionic polymer with adhesive 3,4-dihydroxyphenyl-l-alanine linkages. *Biomaterials* **2010,** 31, 6582-6588.
133. Cao, Z. Q.; Jiang, S. Y., Super-hydrophilic zwitterionic poly(carboxybetaine) and amphiphilic non-ionic poly(ethylene glycol) for stealth nanoparticles. *Nano Today* **2012,** 7, (5), 404-413.
134. Chan, Y. H.; Lin, J. T.; Chen, I. W. P.; Chen, C. H., Monolayers of diphenyldiacetylene derivatives: Tuning molecular tilt angles and photopolymerization efficiency via electrodeposited Ag interlayer on Au. *J. Phys. Chem. B* **2005,** 109, (41), 19161-19168.
135. Zhou, H. S.; Wada, T.; Sasabe, H., Enhanced photopolymerization of diacetylene in colloidal gold solution. *J. Chem. Soc. Chem. Commun.* **1995**, (15), 1525-1526.
136. Sarkar, A.; Okada, S.; Matsuzawa, H.; Matsuda, H.; Nakanishi, H., Novel polydiacetylenes for optical materials: beyond the conventional polydiacetylenes. *J. Mater. Chem.* **2000,** 10, (4), 819-828.
137. Chan, K. C.; Kim, T.; Schoer, J. K.; Crooks, R. M., Polymeric self-assembled monolayors. 3. Pattern transfer by use of photolithography, electrochemical methods, and an ultrthin, self-assembled diacetylenic resist. *J. Am. Chem. Soc.* **1995,** 117, (21), 5875-5876.
138. Warman, J. M.; de Haas, M. P.; Dicker, G.; Grozema, F. C.; Piris, J.; Debije, M. G., Charge mobilities in organic semiconducting materials determined by pulse-radiolysis time-resolved microwave conductivity: pi-bond-conjugated polymers versus pi-pi-stacked discotics. *Chem. Mater.* **2004,** 16, (23), 4600-4609.
139. Patel, M.; Vivien, E.; Hauchecorne, M.; Oudrhiri, N.; Ramasawmy, R.; Vigneron, J. P.; Lehn, P.; Lehn, J. M., Efficient gene transfection by bisguanylated diacetylene lipid formulations. *Biochem. Biophys. Res. Commun.* **2001,** 281, (2), 536-543.
140. Alloisio, M.; Demartini, A.; Cuniberti, C.; Muniz-Miranda, M.; Giorgetti, E.; Giusti, A.; Dellepiane, G., Photopolymerization of diacetylene-capped gold nanoparticles. *Phys. Chem. Chem. Phys.* **2008,** 10, (16), 2214-2220.
141. Ahn, D. J.; Chae, E. H.; Lee, G. S.; Shim, H. Y.; Chang, T. E.; Ahn, K. D.; Kim, J. M., Colorimetric reversibility of polydiacetylene supramolecules having enhanced hydrogen-bonding under thermal and pH stimuli. *J. Am. Chem. Soc.* **2003,** 125, (30), 8976-8977.

142. Mosley, D. W.; Sellmyer, M. A.; Daida, E. J.; Jacobson, J. M., Polymerization of diacetylenes by hydrogen bond templated adlayer formation. *J. Am. Chem. Soc.* **2003,** 125, (35), 10532-10533.
143. Cai, M.; Mowery, M. D.; Menzel, H.; Evans, C. E., Fabrication of extended conjugation length polymers within diacetylene monolayers on Au surfaces: Influence of UV exposure time. *Langmuir* **1999,** 15, (4), 1215-1222.
144. Song, Y.; Klivansky, L. M.; Liu, Y.; Chen, S. W., Enhanced stability of Janus nanoparticles by covalent cross-linking of surface ligands. *Langmuir* **2011,** 27, (23), 14581-14588.
145. Bartczak, D.; Kanaras, A. G., Diacetylene-containing ligand as a new capping agent for the preparation of water-soluble colloidal nanoparticles of remarkable stability. *Langmuir* **2010,** 26, (10), 7072-7077.
146. Ladd, J.; Zhang, Z.; Chen, S. F.; Hower, J. C.; Jiang, S. Y., Zwitterionic polymers exhibiting high resistance to nonspecific protein adsorption from human serum and plasma. *Biomacromolecules* **2008,** 9, 1357-1361.
147. Kim, D.; Park, S.; Lee, J. H.; Jeong, Y. Y.; Jon, S., Antibiofouling polymer-coated gold nanoparticles as a contrast agent for in vivo x-ray computed tomography imaging. *J. Am. Chem. Soc.* **2007,** 129, (24), 7661-7665.
148. Iyer, A. K.; Khaled, G.; Fang, J.; Maeda, H., Exploiting the enhanced permeability and retention effect for tumor targeting. *Drug Discov. Today* **2006,** 11, 812-818.
149. Mirkin, C. A.; Letsinger, R. L.; Mucic, R. C.; Storhoff, J. J., A DNA-based method for rationally assembling nanoparticles into macroscopic materials. *Nature* **1996,** 382, (6592), 607-609.
150. Simpson, C. A.; Agrawal, A. C.; Balinski, A.; Harkness, K. M.; Cliffel, D. E., Short-Chain PEG Mixed Monolayer Protected Gold Clusters Increase Clearance and Red Blood Cell Counts. *ACS Nano* **2011,** 5, (5), 3577-3584.
151. Miyamoto, D.; Oishi, M.; Kojima, K.; Yoshimoto, K.; Nagasaki, Y., Completely dispersible PEGylated gold nanoparticles under physiological conditions: Modification of gold nanoparticles with precisely controlled PEG-b-polyamine. *Langmuir* **2008,** 24, 5010-5017.
152. Storhoff, J. J.; Elghanian, R.; Mucic, R. C.; Mirkin, C. A.; Letsinger, R. L., One-pot colorimetric differentiation of polynucleotides with single base imperfections using gold nanoparticle probes. *J. Am. Chem. Soc.* **1998,** 120, 1959-1964.
153. Menzel, H.; Mowery, M. D.; Cai, M.; Evans, C. E., Vertical Positioning of Internal Molecular Scaffolding within a Single Molecular Layer. *J. Phys. Chem. B* **1998,** 102, 9550-9556.
154. Bain, C. D.; Troughton, E. B.; Tao, Y. T.; Evall, J.; Whitesides, G. M.; Nuzzo, R. G., Formation of monolayor films by the spontaneous assembly of organic thiols from solution onto gold. *J. Am. Chem. Soc.* **1989,** 111, 321-335.
155. Yoo, M.; Kim, S.; Lim, J.; Kramer, E. J.; Hawker, C. J.; Kim, B.; Bang, J., Facile synthesis of thermally stable core-shell gold nanoparticles via photo-cross-linkable polymeric ligands. *Macromolecules* **2010,** 43, 3570-3575.
156. Park, J.; Nam, J.; Won, N.; Jin, H.; Jung, S.; Cho, S. H.; Kim, S., Compact and stabel quantum dots with positive, negative, or zwitterionic surface: Specific cell

Interactions and non-specific adsorptions by the surface charges. *Adv. Funct. Mater.* **2011,** 21, (9), 1558-1566.
157. Susumu, K.; Uyeda, H. T.; Medintz, I. L.; Pons, T.; Delehanty, J. B.; Mattoussi, H., Enhancing the stability and biological functionalities of quantum dots via compact multifunctional ligands. *J. Am. Chem. Soc.* **2007,** 129, (45), 13987-13996.
158. Liu, W.; Howarth, M.; Greytak, A. B.; Zheng, Y.; Nocera, D. G.; Ting, A. Y.; Bawendi, M. G., Compact biocompatible quantum dots functionalized for cellular imaging. *J. Am. Chem. Soc.* **2008,** 130, (4), 1274-1284.
159. Mattoussi, H.; Mauro, J. M.; Goldman, E. R.; Anderson, G. P.; Sundar, V. C.; Mikulec, F. V.; Bawendi, M. G., Self-assembly of CdSe-ZnS quantum dot bioconjugates using an engineered recombinant protein. *J. Am. Chem. Soc.* **2000,** 122, (49), 12142-12150.
160. Muro, E.; Pons, T.; Lequeux, N.; Fragola, A.; Sanson, N.; Lenkei, Z.; Dubertret, B., Small and stable sulfobetaine zwitterionic quantum dots for functional live-cell imaging. *J. Am. Chem. Soc.* **2010,** 132, (13), 4556-4557.
161. Ohyanagi, T.; Nagahori, N.; Shimawaki, K.; Hinou, H.; Yamashita, T.; Sasaki, A.; Jin, T.; Iwanaga, T.; Kinjo, M.; Nishimura, S. I., Importance of sialic acid residues illuminated by live animal imaging using phosphorylcholine self-assembled monolayer-coated quantum dots. *J. Am. Chem. Soc.* **2011,** 133, (32), 12507-12517.
162. Liu, W.; Choi, H. S.; Zimmer, J. P.; Tanaka, E.; Frangioni, J. V.; Bawendi, M., Compact cysteine-coated CdSe(ZnCdS) quantum dots for in vivo applications. *J. Am. Chem. Soc.* **2007,** 129, (47), 14530-14531.
163. Medintz, I. L.; Uyeda, H. T.; Goldman, E. R.; Mattoussi, H., Quantum dot bioconjugates for imaging, labelling and sensing. *Nature Mater.* **2005,** 4, (6), 435-446.
164. Ohyanagi, T.; Nagahori, N.; Shimawaki, K.; Hinou, H.; Yamashita, T.; Sasaki, A.; Jin, T.; Iwanaga, T.; Kinjo, M.; Nishimura, S. I., Importance of sialic acid residues illuminated by live animal imaging using phosphorylcholine self-assembled monolayer-coated quantum dots. *J. Am. Chem. Soc.* **2011,** 133, (32), 12507-12517.

Curriculum Vitae

Wei Yang was born and raised in Baoding, Hebei Province, China. Upon receiving her Master of Science degree (2006) in Chemical Technology from Tianjin University, she went to the University of Washington as a visiting student. In 2009, she joined the University of Washington as a Ph. D candidate and received her Doctor of Philosophy in Chemical Engineering in June of 2014.

Publications:

1. **W. Yang**, J. R. Ella-Menye, Y. Wang, S. Liu, T. Bai, and S. Y. Jiang, Zwitterionic Polymer Surface Evades the Immune System and Enables Long Circulation, in preparation, 2014.

2 **W. Yang**, J. R. Ella-Menye, S. Y. Jiang, Stable Quantum Dots with Zwitterionic Modification, in preparation, 2014.

3. W. Yang, S. Liu, T. Bai, A. J. Keefe, J. R. Ella-Menye, Y. T. Li, and S. Y. Jiang, Poly(carboxybetaine) nanomaterials enable long circulation and prevent polymer-specific antibody production, *Nano Today*, **2014**, 9, 10-16.

4. **W. Yang**, J. R. Ella-Menye, Y. T. Li, and S. Y. Jiang, Crosslinked Carboxybetaine SAMs Enable Nanoparticles with Remarkable Stability in Complex Media, *Langmuir*, 2014, 30, 2522-2529.

5. **W. Yang**, T. Bai, L. R. Carr, A. J. Keefe, J. J. Xu, H. Xue, C. A. Irvin, S. F. Chen, J. Wang, and S. Y. Jiang, The effect of lightly crosslinked poly(carboxybetaine) hydrogel coating on the performance of sensors in whole blood, *Biomaterials*, 2012, 33, 7945.

6. **W. Yang**, H. Xue, L. R. Carr, J. Wang, S. Y. Jiang, Zwitterionic poly(carboxybetaine) hydrogels for glucose biosensors in complex Media, *Biosensors and Bioelectronics*, 2011, 26, 2454,

7. G. Mahmud, S. Huda, **W. Yang**, K. Kandere-Grzybowska, D. Pilans, S. Y. Jiang, B. A. Grzybowski, Carboxybetaine Methacrylate Polymers Offer Robust, Long-Term Protection against Cell Adhesion, *Langmuir*, 27, 10800, 2011;

8 C. L. Gao, G. Z. Li, H. Xue, **W. Yang**, F. B. Zhang, S. Y. Jiang, Functionalizable and ultra-low fouling zwitterionic surfaces via adhesive mussel mimetic linkages, *Biomaterials*, 31, 1486, 2011.